Avşar, Ö., Avşar, U., Arslan, Ş., Kurtuluş, B., Niedermann, S., Güleç, N. (2017): Subaqueous hot springs in Köyceğiz Lake, Dalyan Channel and Fethiye-Göcek Bay (SW Turkey): Locations, chemistry and origins. - *Journal of Volcanology and Geothermal Research*, *345*, pp. 81—97.

DOI: http://doi.org/10.1016/j.jvolgeores.2017.07.016

Subaqueous hot springs in Köyceğiz Lake, Dalyan Channel and Fethiye-Göcek Bay (SW Turkey): locations, chemistry and origins

Özgür Avşar[1*], Ulaş Avşar[2,3], Şebnem Arslan[4], Bedri Kurtuluş[1], Samuel Niedermann[5], Nilgün Güleç[2]

[1]Muğla Sıtkı Koçman University, Department of Geological Engineering, Muğla, Turkey

[2]Middle East Technical University, Department of Geological Engineering, TR-06531, Ankara, Turkey

[3]King Abdullah University of Science and Technology (KAUST), Physical Science and Engineering Division (PSE), Thuwal, Saudi Arabia

[4]Ankara University, Faculty of Engineering, Department of Geological Engineering, TR-06100, Tandoğan, Ankara, Turkey

[5]Deutsches GeoForschungsZentrum GFZ, Telegrafenberg, D-14473 Potsdam, Germany

*Corresponding Author: Muğla Sıtkı Koçman University, Department of Geological Engineering, TR-48000, Kötekli, Muğla, Turkey

Tel (work): +90 252 2113156

Tel (mobile): +90 532 332 9008

Fax: +90 252 211 1912

e-mail: ozguravsar@mu.edu.tr ; ozguravsar@gmail.com

ABSTRACT

In this study, horizontal temperature measurements along organized grids have been used to detect subaqueous hot springs. The study area, located in the southwest of Turkey and comprised of Köyceğiz Lake, Dalyan Channel and Fethiye-Göcek Bay, was scanned by measuring temperatures horizontally, 2-3 meters above the bottom of the lake or sea. After analyzing the temperature data along the grids, the locations with anomalous temperature values were detected, and divers headed here for further verification. Accordingly, among these anomalies, the divers confirmed seven of them as subaqueous hot springs. Three of these hot springs are located in the Köyceğiz Lake, three of them are located in the Dalyan Channel and one hot spring is located in the Fethiye-Göcek Bay. At the locations where temperature anomalies were detected, the divers collected samples directly from the subaqueous hot spring using a syringe-type sampler. We evaluated these water samples together with samples collected from hot and cold springs on land and from local rivers, lakes and the sea, with an aim to generate a conceptual hydrogeochemical model of the geothermal system in the study area. This model predicts that rainwater precipitating in the highlands percolates through fractures and faults into the deeper parts of the Earth's crust, here it is heated and ascends through the sea bottom via buried faults. Pervious carbonate nappes that are underlain and overlain by impervious rocks create a confined aquifer. The southern boundary of the Carbonate-Marmaris nappes is buried under alluvium and/or sea/lake water bodies and this phenomenon determines whether hot springs occur on land or subaqueous. The chemical and isotopic properties of the hot springs point to seawater mixing at deep levels. Thus, the mixing most probably occurs while the water is ascending through the faults and fractures. The gas geochemistry results reveal that the lowest mantle He contributions occur in the samples from Köycegiz Lake, whereas the highest ones are found in samples from the Dalaman plain. For the first time, we made use of the micro-XRF sediment core scanning (ITRAX Scanner) for exploring the relation between subaqueous geothermal occurrence and chemical properties of the

surrounding sediments. The spatial elemental distribution of sea/lake bottom sediments suggests that depending on the surrounding rock units and the temperature of the hot spring, the sediments around the spring can be enriched with certain elements.

Key words: Water chemistry, Mixing, Gas geochemistry, ITRAX analysis, Saturation index, Conceptual model

1. Introduction

The world's energy demands are increasing (IEA, 2012) along with the global population and resulting rise in consumption, which in turn leads to further exploration of alternative and renewable energy sources by investors, researchers, and governments. Geothermal energy production has become popular since it is environmentally friendly when compared to stock-limited fossil fuels and the emissions of greenhouse gases associated with their burning. Along with the limited environmental concerns associated with geothermal energy, its sustainability will likely make it an indispensable energy source in the future.

Most of the on-land geothermal sites in Turkey are well studied. For example, there were a number of comprehensive studies carried out about the hydrogeochemistry of Turkish on-land geothermal sites (İlkışık, 1995; Balderer and Synal, 1997; Mutlu and Güleç, 1998; Vengosh et al., 2002; Tarcan, 2005; Süer et al., 2008; Baba and Sözbilir, 2012; Bundschuh et al., 2013; Karakuş and Şimşek, 2013; Özgür and Çalışkan, 2013). In addition, there exists an inventory of the geothermal sites issued by the General Directorate of Mineral Research and Exploration (MTA) in 2005. Tüfekçi et al. (2010) used this inventory together with the publicly available magnetic anomaly, Bouguer gravity anomaly, earthquake epicenter and lineament datasets and statistically showed the spatial distribution of potential geothermal occurrences in western Anatolia.

Geothermal energy started gaining popularity in Turkey after a geothermal law was passed in 2007. Accordingly, geothermal investments in electrical power generation increased by 336% (Bertani, 2015), and the direct utilization of geothermal energy increased by 38% over the last five years (Mertoğlu et al., 2010; Mertoğlu et al., 2015). Moreover, the purchasing guarantee issued by the Turkish Government at a rate of 0.105 USD/kWh has provided the sector with a great incentive for investment. Mertoğlu et al. (2015) reported that there are over 2000 hot and mineral water sources, and 227 geothermal sites in Turkey, 70-80% of which are located in western Anatolia.

Not only in Turkey but also throughout the world, on-land geothermal sources have witnessed extensive exploration through geochemical, mineralogical, and hydrogeochemical investigations as well as expensive geophysical prospecting methods such as seismic stratigraphical methods. However, explorations for subaqueous geothermal resources have not yet had their deserved attention. There have been efforts to estimate the earth's heat loss and to assess shallow hydrothermal activity. For example, Williams (1976) stated that approximately 2×10^{12} cal/s (=8.37×10^{12} W) of heat (20% of the earth's heat loss) is released through 1% of the Earth's surface area. This release is in the form of hydrothermal discharge from young rocks near active seafloor-spreading areas and submarine volcanoes. This amount of energy was roughly equal to the world's total energy consumption at that time (1976). Similarly, Prol-Ledesma et al. (2005) described "shallow hydrothermal activity" as an interesting but not-as-yet well-studied phenomenon, where shallow means a water depth less than 200 m, and they stated "Shallow-water vents provide accessible geological and chemical settings for studying the interaction of hydrothermal fluids with unconsolidated sediments, seawater, and basement rocks". More recently, Suarez-Arriaga et al. (2014) declared that submarine geothermal resources have not been sufficiently used and studied yet, but they could cover the world's

considerable energy demand of in an environmentally friendly way by integrating on-land geothermal prospecting experience and offshore hydrocarbon exploitation technology.

Although submarine and sub-lacustrine hydrothermal systems are not as well studied as on-land geothermal sources, recent technological developments have drawn many researchers to undertake studies on subaqueous hydrothermal systems. These studies include the ones carried out in lakes (Michel et al., 2001; Remsen et al., 2002; Ronde et al., 2002; De Batist et al., 2002; Duchkov et al., 2009), and in different parts of the world including Greece, Italy, Japan, the Antilles, Galapagos rift zone, Iceland, Mexico, the Pacific Ocean, Papua New Guinea, and Turkey (Williams et al., 1974; Corliss et al., 1979; Italiano and Nuccio, 1991; McMurtry et al., 1993; Michard et al., 1993; Fitzsimons et al., 1997; Hannington et al., 2001; Glasby and Notsu, 2003; Prol-Ledesma, 2003; Prol-Ledesma et al., 2004; McCarthy et al., 2005; Pichler, 2005; Valsami-Jones et al., 2005; Esposito et al., 2006; Koschinsky et al., 2007; Pekçetinöz et al., 2009; Arango-Galván et al., 2011; Yamanaka et al., 2013). However, most of the hydrothermal systems in these studies were either discovered by chance or identified by local people.

This study presents the results of the exploratory research of subaqueous thermal systems that were expected to occur at the bottom of Fethiye-Göcek Bay as well as the Köyceğiz, Alagöl, Sülüngür and Kocagöl lakes (Fig. 1), according to the measurements of water temperature along horizontal lines taken to detect temperature anomalies. In addition, a hydrogeochemical conceptual model of the region was constructed by using water, gas and sediment geochemistry. The study area is located in southwestern Anatolia, which is a seismically active region. Additionally, the Fethiye-Göcek shoreline is located along one of the main fault zones of SW Anatolia, namely, the Fethiye-Burdur fault zone (on land continuation of Pliny-Strabo fault zone) (Fig. 1). There are lineations recorded by Yağmurlu et al. (2005), Ocakoğlu (2011) and faults recorded by Hall et al. (2014) in the south of continental shelf of Fethiye-Göcek Bay. Findings of these researches favor the idea that there are submarine buried faults at the bottom

of the Fethiye-Göcek Bay, these may enable submarine geothermal systems, making the Fethiye-Göcek Bay a potential site to investigate for submarine hot springs.

2. Geological setting

The Menderes Massif, the Beydağları Autochthon and the Lycian nappes are the main tectonic units of SW Anatolia (Fig. 1). The study area is located mainly on the Lycian nappes; the Beydağları Autochthon crops out in the region as tectonic windows. The Beydağları Autochthon is composed of Upper Cretaceous carbonate rocks and is the base rock in the region. The Lycian nappes are thrusting over the Beydağları Autochthon tectonically. Although there are many categorizations for the Lycian nappes, in this study we mainly use the one of Şenel (1997a; 1997b) where the nappes are divided into 5 main units: the Yeşilbarak, Tavas, Bodrum, Gülbahar, and Marmaris Nappes from the bottom to the top (Fig. 1).

The Late Lutetian-Early Burdigalian aged Yeşilbarak nappe is composed of shales and sandstones and located between the Beydağları Autochthon and the overlying Lycian nappe units. The overlying Tavas, Bodrum and Gülbahar nappes are composed of carbonate units and presented together (without differentiating) in the geological map as their hydrogeological properties are similar in the region. The Lower Cretaceous Marmaris nappe comprising peridotites overlies all rock units in the region and crops out as a NW-SE trending strip. The impervious to semi-pervious character of this unit greatly affects the hydrogeology, and consequently the geothermal system of the region. This subject matter will be discussed in the Hydrogeochemical Model section (Section 4.4.4) in detail.

3. Materials and methods

In order to detect the temperature anomalies, we measured the temperature of the water together with electrical conductivity (EC) and pH along horizontal linear routes. Where temperature

anomalies were detected, divers were sent to these localities to seek and confirm the presence of the hot springs. If there was a hot spring, water samples were taken, to be analyzed chemically. Together with the subaqueous samples, on-land hot and cold springs, stream water, seawater, lake water and channel water were sampled and chemically analyzed. The results of these chemical analyses were used to develop a hydrogeochemical model. Along with water chemistry, we also studied gas and sediment geochemistry. The following subsections present further details.

3.1 Subaqueous hot spring exploration/prospecting

In order to explore subaqueous hot springs in the study area, a total of about 900 km of cruising was carried out (Fig. 2), using a boat equipped with a sonar-mounted Global Positioning System (GPS) device (Garmin GPSmap 421s) and a multi-parameter conductivity-temperature-depth (CTD) sonde (YSI 6600), which allowed simultaneous real-time measurements of geographical coordinates, water depth and temperature. During the cruising, based on the water depth information from the sonar, the CTD was lowered down to a certain height above the sediment/water interface (2-3 m), and its depth was modified with respect to the bathymetrical changes. In this way, we ensured that we measured the water temperature as close as possible to the probable subaqueous hot springs while preventing the CTD from crashing to the ground. By setting the cruise speed to ca. 7 km/h and the devices to perform measurements every two seconds, we also ensured that the CTD and GPS measurements were done every 4 meters along the cruising routes. As a preliminary approach, the routes were designed in order to cover the complete target area of the bay and lakes. After analyzing the data, promising sites were identified, and more detailed measurements were done around these locations via fine grid routes.

In order to detect water temperature anomalies, which could be related to subaqueous hot springs, the datasets from the CTD and GPS were merged and synchronized to obtain temperature vs. time plots. Careful inspection of those plots allowed the determination of the approximate locations of the "potential" subaqueous hot springs. Afterwards, more detailed exploratory cruises with denser survey grids were conducted at the "potential" locations in order to confirm the anomalies and to provide the divers with more precise coordinates for water sampling. While measuring the temperature, EC and pH, sonar profiles were taken by the GPS. These sonar profiles were recorded by taking screenshots from the GPS device, and they were investigated and used as a tool to detect subaqueous hot springs. Moreover, some topographic anomalies, which may be related to the faults, were detected using the detailed bathymetric data generated by sonar GPS measurements. The CTD measurements were concentrated around these locations by designing a finer cruise grid.

3.2 Hydrochemistry

Whenever the divers confirmed the presence of a hot spring, they collected water samples with syringe-type samplers, measured the temperature of the spring water by putting the CTD at the outlet of the hot spring, and took photos as well as videos. The water samples were collected directly from the outlet of the spring to avoid or minimize mixing with sea/lake water. The water samples in the syringes were transferred into three different polyethylene bottles (100 ml each) for stable isotope, cation+trace element, and anion analyses, respectively.

Samples collected for cation and anion analyses passed through a 0.45 μm filter, and the former ones were acidified to 1% HNO_3 after filtering. Along with subaqueous hot spring samples, five on-land fresh water springs were also sampled (Fig. 1). In addition, three water samples were taken from the sea surface in order to delineate the chemical and isotopic properties of the seawater (Table 1). The water samples were kept refrigerated (4 °C) and immediately sent to

dedicated laboratories. Major ion and trace element analyses were carried out at the Hacettepe University Water Chemistry and Environmental Tritium Laboratory (Ankara, Turkey), and stable isotope analyses were carried out at the Hacettepe University International Karst Water Resources Application and Research Center Stable Isotope Laboratory (UKAM, Ankara, Turkey). The titration technique was used to determine carbonate (CO_3^{2-}) and bicarbonate (HCO_3^-) ion concentrations. Fluoride (F^-), chloride (Cl^-), nitrite (NO_2^-), bromide (Br^-), nitrate(NO_3^-), phosphate (PO_4^{3-}), sulfate (SO_4^{2-}), lithium (Li^+), sodium(Na^+), ammonium (NH_4^+), potassium (K^+), magnesium (Mg^{2+}), and calcium (Ca^{2+}) ion concentrations were determined by using a high performance ion chromatography device (DIONEX LC25, ICS-1000 Ion Chromatography system) and a conductivity detector. The spectrophotometric method (aT60U Spectrometer) was used to determine SiO_2 and boron concentrations. Trace element (Ag, Al, As, Au, Ba, Be, Cd, Ce, Co, Cr, Cs, Cu, Dy, Er, Eu, Fe, Ga, Gd, Ge, Hf, Hg, Ho, Ir, La, Lu, Mn, Mo, Nb, Nd, Ni, Pb, Pd, Pr, Pt, Rb, Re, Rh, Ru, Sb, Se, Sm, Sn, Sr, Ta, Tb, Te, Th, Ti, Tl, Tm, U, V, W, Y, Yb, Zn, Zr) concentrations were measured in a Thermo Electron X7 model ICP-MS (Inductively Coupled Plasma–Mass Spectrometer) and the detection limits range between 0.001 ppt to 0.3 ppb. Chemical analyses of the waters were conducted in compliance with Clesceri et al. (1989). Stable isotope analyses were conducted by using laser spectroscopic methods, where the reference standard was Vienna Standard Mean Ocean Water (VSMOW). The analytical precisions are 0.2‰ and 1‰ for $\delta^{18}O$ and δD, respectively.

Helium analyses of eleven samples were conducted at the GFZ Potsdam noble gas laboratory in Germany. Four of those samples were collected from subaqueous springs, and seven of them from on-land springs. At seven locations, including the subaqueous spring SUBC-2, free gas bubbling through the water was collected in glass flasks by means of a funnel, while at four locations spring water was sampled in 1 cm outer diameter, 50 cm long copper tubes sealed by steel clamps. During sampling, special care was taken to avoid atmospheric contamination.

Except for the gas sample SUBC-2 (see above), the other subaqueous springs were sampled by installing a small water pump at the outlet of the spring. In the lab, total gas analyses were carried out for the free gas samples using a Pfeiffer Omnistar quadrupole mass spectrometer. Detection limits in these analyses are ~10 ppmv for N_2, O_2, CO_2, and ~1 ppmv for H_2 and Ar (Wiersberg et al., 2011). The glass flasks were then attached to the noble gas line, and appropriate volume splits were analyzed for noble gas concentrations and isotopic compositions. Water samples from copper tubes were discharged into a glass bulb and degassed in an ultrasonic bath, and the gases were transferred to a cold trap by means of a laminar flow of gaseous H_2O (evaporated from the liquid water sample) through a connecting capillary. Again, appropriate splits were transferred to the noble gas line. There, chemically active gases were removed using another cold trap, two Ti sponge getters, and two SAES (Zr-Al) getters, and the noble gases were adsorbed to a stainless steel frit or activated charcoal in two cryostatic cold heads in order to separate them from each other for the measurement in a VG5400 noble gas mass spectrometer. Further details about experimental procedures and data reduction methods can be found in Niedermann et al. (1997).

3.3 Sediment geochemistry

In order to spatially evaluate the geochemical composition of the bottom sediments, and therefore in order to detect the possible geochemical effects of subaqueous hydrothermal fluid emissions on sedimentation, gravity cores were collected and analyzed by an ITRAX μXRF core scanner. For an unbiased spatial comparison, it is crucial to do the geochemical analyses for the same stratigraphical horizon (i.e., on the sediments that were deposited in the same time window). For this reason, this study targeted the sediments at the water/sediment interface. Accordingly, rather than using an Ekman sampler that may significantly mix and disturb sediments, we used a gravity corer with a messenger-triggered vacuum system. Moreover, this

method helped to achieve minimum sediment loss and disturbance at the water/sediment interface.

A total of 233 gravity cores, 30-50 cm long, with a diameter of 7.5 cm, were collected (99 from Fethiye-Göcek Bay, 105 from Köyceğiz Lake, and 29 from Dalyan Channel). The cores were collected in two groups: 1) Cold Location Cores (CLC), which were almost uniformly distributed within the study areas to reveal the general characteristics of sediments, and 2) Hot Location Cores (HLC), which were collected in the vicinity of the detected subaqueous hot springs. The geochemical data from the CLCs and HLCs were then compared to investigate the possible effects of subaqueous hot springs on the chemical composition of sediments.

Since splitting and scanning 233 cores one by one would require a significant amount of labor and time, only the top 3-5 cm of each gravity core were sampled by using 2 cm diameter syringes, and put successively in PVC half pipes. In this way, ten artificial cores, being approximately 1 m long and containing sediments from 20-30 locations each, were prepared and sent to the GEOPOLAR Laboratory of the University of Bremen for ITRAX μXRF scanning to obtain geochemical data as well as optical and radiographic images.

Along the artificial cores, radiographic scanning was done at 200 μm resolution. XRF scanning, on the other hand, was carried out with a Mo-tube at 1 mm increments for the Fethiye-Göcek cores, and at 2 mm increments for the Köyceğiz and Dalyan cores, with an exposure time of 12 seconds. As a result of the XRF scanning, semi-quantitative distributions of 19 elements (Si, S, Cl, K, Ca, Ti, Cr, Mn, Fe, Ni, Zn, As, Se, Br, Rb, Sr, Y, Zr, and Pb) were obtained in units of kilo counts per second (kcps). For each element, average values for all sampling locations were calculated. In order to achieve comparable scales among the elements for spatial evaluation, average kcps values were standardized separately for the three study sites, which have different sedimentological environments.

Since ITRAX μXRF scanning is performed on bulk sediments, the scanning results are also influenced by the physical properties of the sediments, such as grain-size distribution, water, and organic matter contents. In order to minimize these effects and to better reveal the geochemical signal, inter-element ratios are used (e.g., Croudace et al., 2006; Kylander et al., 2011). As a first step, all possible inter-element ratios (i.e., 380 for 19 elements) were calculated for each location and their spatial distribution maps were prepared. However, visual inspection of spatial distribution maps does not always reveal the difference between the HLCs and CLCs. For this reason, the mean values of inter-element ratios from the two groups of cores (i.e., HLCs and CLCs) were determined and compared. Finally, those inter-element ratios of the HLCs that significantly deviated from the means of the CLCs were detected and were attributed to the effect of subaqueous hot springs on the chemical composition of the sediments.

4. Results and discussions

4.1. Subaqueous hot spring exploration/prospecting

The measurement routes and the bathymetric maps are shown in Fig. 2. Along with the temperature measurements, EC and pH values were also measured. As a result of these physicochemical measurements, on first inspection of the data, over one hundred temperature anomaly indications were detected (some of the selected anomalies can be seen in time vs. temperature plots provided in Supplementary Fig. 1). At several of these locations, detailed physicochemical measurements were performed by tracking along a finer mesh of routes (Fig. 2a and b). As a result, divers were sent to 49 potential hot spring locations for confirmation of the presence of subaqueous hot springs. Among the 49 locations, they confirmed seven subaqueous hot springs: three in Köyceğiz Lake, three in the Dalyan Channel, and one in the Fethiye-Göcek Bay (Fig. 1). The temperature of the subaqueous hot springs in the Köyceğiz Lake ranges between 26.17 and 29.47 °C (Table 1). The discharge temperatures of the Dalyan

subaqueous springs are around 27-28 °C. The water depth and temperature of the subaqueous hot spring in the Fethiye-Göcek Bay was 19 m and 27.19 °C, respectively (VIDEO). No temperature anomalies were found at the bottom of the Alagöl, Sülüngür and Kocagöl lakes.

The other aid used in detecting hot springs were the sonar profiles. SUB-2 and SUB-3 springs in Köyceğiz Lake were detected by considering the lineations on the sonar profile as an indication of a subaqueous hot spring. These locations were also marked as anomalies, and divers were sent there in order to search for the hot springs under water. Bathymetry maps of Köyceğiz Lake and the Fethiye-Göcek Bay were prepared by using the sonar GPS data (Fig. 2c and d). Köyceğiz lake has two troughs in the north and the south and the deepest points are 25 m and 32 m respectively. In the Fethiye-Göcek Bay the shelf is located around 125 m from the shoreline, and the water depth reaches 500 m in the outer shelf. Some lineations were detected in the bay through detailed investigation of the bathymetry map; they may be inferred as the faults at the bottom of the sea. Temperature anomalies that were detected at the nearshore section of these lineations made these areas potential subaqueous hot spring sites, so it was worth studying them in detail (Fig. 2b). Except for İnlice Bay, there were, however, no hot springs found at the remaining three locations.

4.2 Sediment geochemistry

ITRAX μXRF scanning on basin-wide sediment samples allowed detection of the geochemical traces of subaqueous hot springs on the sediments. The locations of the cores collected in this study are presented in Fig. 3. The optical and radiographic images of the artificial cores, which are composed of the top 3-5 cm of sediment from 233 gravity cores, are shown in Supplementary Fig. 2. Along the radiographic images, especially, the boundaries between different cores can be clearly seen as horizontal white lines, which correspond to mm-scale low-density gaps. Before calculating the average “kcps” values for each element at coring locations,

several measurement points above and below these boundaries are excluded from the XRF dataset since they can be erroneous. After data purging, the average "kcps" values were standardized for each element in the three study sites separately (Köyceğiz Lake, Supplementary Table 1; Dalyan Channel, Supplementary Table 2; and Fethiye-Göcek Bay, Supplementary Table 3).

All possible elemental ratios derived from the standardized "kcps" values are plotted separately for the cold and hot locations of each site (Supplementary Fig. 3). In addition, these ratios are interpolated over the study areas to visualize their spatial distribution (Supplementary Fig. 4). Fig. 5 illustrates the Sr/Ti ratios at the coring locations in the Fethiye-Göcek Bay. The cores are sorted along the x-axis in the way that the 12 HLCs are plotted far-left in the graph and the CLCs in the order roughly from west to east (Fig. 4a). It is clear from the plot that the mean Sr/Ti ratio of the HLCs significantly deviates from the CLCs and is almost 4σ higher than the mean of the CLCs. The spatial distribution map of the same ratio, on the other hand, enables visualization and can pinpoint the highest values of the HLCs (Fig. 4b). This observation implies that the sediments around the subaqueous hot spring in İnlice Bay are enriched in Sr. It should also be noted that the high Sr/Ti ratio of the F-71 core, which was classified as CLC, may indicate another hot spring location in the vicinity of that core. Unfortunately, water sampling could not be done at this location since the depth is around 40 m there, which exceeds the safe diving limit.

Similar to the Sr enrichments illustrated in Fig. 4, other elemental enrichments were also detected. In order to find out which elements are more prominent, the deviations of the HLCs from the CLCs for all possible elemental ratios are presented in matrix form for the three study sites separately (Fig. 5). The colors of the cells represent the magnitude of deviation between the means of CLCs and HLCs. For instance, in Köyceğiz Lake, the means of the ratios of Cl to

almost all other elements for HLCs are higher by 2σ than the mean of the same ratios for CLCs. It can be deduced, accordingly, that the sediments around the Köyceğiz subaqueous hot springs are enriched in S, Cl, and Br, while they are depleted in Mn (Fig. 5a). Similarly, in the Fethiye-Göcek Bay, the sediments around the subaqueous hot spring in İnlice Bay are enriched in S, Cl, Ca, and Sr (Fig. 5c). No significant elemental enrichment related to subaqueous hot springs is detected in the Dalyan Channel (Fig. 5b). The plots and some of the representative spatial distribution maps for the above-mentioned elements are presented for Köyceğiz Lake and Fethiye-Göcek Bay in Fig. 6. In Köyceğiz Lake, not only the HLCs but also the CLCs in the southern basin show similar anomalies, which implies that the subaqueous hot springs affect the sedimentation throughout the southern basin. This can be attributed to the lack of significant tributaries in the southern basin, which may cause subaqueous hot springs to dominate the water chemistry in the basin.

Although some elemental ratios show significant anomalies in the Köyceğiz Lake and the Fethiye–Göcek Bay, no prominent elements could be determined for the Dalyan Channel. The absence of any elemental enrichment in the Dalyan Channel can be due to water currents in the channel, which may hinder regular sedimentation, thereby preventing any archive of sedimentary traces of subaqueous hot springs on the channel's bottom sediments.

4.3 Hydrogeochemistry

4.3.1 Water chemistry

For a better understanding of the origin of natural waters, it is crucial to characterize their chemical properties in detail. Major and minor ion concentrations of the waters are given in Table 2 and Table 3, respectively. According to the results, inland cold waters and stream waters are of the Mg or Ca – HCO_3 type (Fig. 7). The other samples (subaqueous, lake, channel etc.) are Na-Cl type waters. This is an expected result because a seawater contribution to the lake

363 waters and geothermal waters in the Köyceğiz-Dalaman region was reported by previous
364 studies (Bayarı et al., 1995; Gökgöz and Tarcan, 2006; Avşar et. al., 2016). The total dissolved
365 solids (TDS) of the waters range from 302 to 41528 ppm. When the Cl ion concentration and
366 TDS are compared, it is obvious that the TDS of the waters are dominated by the Cl
367 concentration (Fig. 8). The Cl content of the waters may be considered as seawater contribution.
368 Accordingly, it is obvious that all the waters (including subaqueous springs) are mixtures of
369 fresh and seawater, and the seawater contribution (Cl concentration) correlates with the distance
370 to the sea. This phenomenon will be the key point of the hydrogeochemical model, which will
371 be discussed in the following sections.

372 In order to find out the possible impacts of temperature on mineralization, Saturation Indices
373 (SI) were calculated by changing the temperature from 20 to 165 °C with the help of the
374 computer program PHREEQC (Parkhurst and Appelo, 1999). The results for SUB-1 and SUB-7
375 are presented as temperature vs SI graphs in Fig. 9. In the Fethiye-Göcek Bay, the calculated
376 SI of the SUB-7 hot spring in İnlice Bay reveals that aragonite, calcite, dolomite, and fluorite
377 are highly saturated (positive SI) at the discharge temperature of the hot spring (i.e., 28 °C)
378 (Fig. 9a). Hence, the Ca enrichments at this spot can be attributed to precipitation of the above-
379 mentioned minerals from SUB-7 hot spring water. Sr has similar chemical properties as Ca, and
380 thus it can replace Ca within the crystalline structure of the above-mentioned minerals (Hem,
381 1985). Sr is a trace element and is not as abundant in nature as Ca. Yet, given their chemical
382 similarities, it is not unusual to observe Sr anomalies in a system with Ca anomalies. The
383 mineral anhydrite, the presence of which could be a possible explanation for high S values in
384 İnlice Bay sediments, has positive SI values at temperatures higher than 80 °C. Given the
385 discharge temperature of 28 °C, the SI of anhydrite for the İnlice Bay hot spring is negative,
386 which eliminates the possibility of S-enrichment due to anhydrite precipitation. The presence
387 of S and Sr anomalies may also be due to celestite precipitation; however, its SI is also negative

388 at all temperatures and hence, it is not likely that the high abundances of these elements are
389 related to this mineral. Although the present chemical composition of the İnlice Bay hot spring
390 does not seem suitable for anhydrite and celestite precipitation, it might have been different in
391 the recent past. Given that the elemental results are the average values of the top 3-5 cm of the
392 sediments, which represents ca. 15-20 years of sedimentation, S and Sr enrichments may
393 indicate that the chemical composition of the İnlice Bay hot spring was possibly different and
394 was suitable for anhydrite and celestite precipitation in the past.

395 It is well known that the Cl ion is highly soluble, thus it is almost impossible for Cl to make a
396 bond with a cation and precipitate as a mineral once it enters the solution as an anion. Hence,
397 highly negative saturation values of sylvite and celestite are not surprising in this study. To
398 explain Cl enrichments in the sediments, a more extended and comprehensive study focusing
399 on geochemistry is required.

400 Cl and Br enrichments in the sediments around the Köyceğiz subaqueous spring cannot be
401 explained by halite or sylvite precipitation since their saturation index values are highly
402 negative (Fig. 9b). In order to find out the reason for Cl and Br-enriched sediments, more
403 detailed investigations and analyses such as pore water chemistry analyses are required in this
404 area.

405 ***4.3.2 O- and H-isotope compositions***

406 Stable isotope ratios are useful to understand the origin of the waters and delineate the
407 subsurface processes that affect their chemical composition. In this study, two campaigns of
408 sampling were conducted for stable isotope analyses; 1) in September 2013 (dry season) and 2)
409 in May 2014 (wet season) (Table 4). Highly negative δD and $\delta^{18}O$ values of on-land fresh
410 waters are an indication of recharge from inland and high altitudes (Fig. 10a and b). The on-
411 land fresh waters seem to be of meteoric origin. However, a seawater effect is obvious where

412 the $\delta^{18}O$ and δD values of the affected waters plot on a line that connects fresh water and
413 seawater instead of the meteoric water lines (Fig. 10 a and b). This line may be interpreted as a
414 mixing line between the freshwater and the seawater in the study region.

415 Another point that should be mentioned here is the role of the geographic position of the
416 sampling locations (waters) with regard to seawater contribution. The closer the sampling
417 location is to the sea, the more positive the isotope ratio becomes. As mentioned above, the
418 mixing phenomenon was inferred from the chemical composition (Cl concentration) of the
419 waters, and the distance to the sea affects the amount of seawater contribution and thus the Cl
420 concentrations. The waters from close to the sea are also enriched with heavy isotopes, while
421 the distant ones mostly show properties similar to fresh waters and are enriched in light isotopes.

422 The seasonal variations in the stable isotope ratios are also an important point to be taken into
423 account. The water samples are generally, slightly enriched in light isotopes of O and H during
424 the wet season (Fig. 10a). The most probable reason for this is a dilution effect due to the
425 contribution of rainwater, which is enriched in light isotopes. On the other hand, during the dry
426 season the waters are enriched in heavy isotopes of O and H, most probably due to evaporation.
427 There are two samples which do not follow the seasonal variation trend: 1) Sülüngür Lake water
428 and 2) sample DAL-2 from the Dalyan Channel (Table 4, Fig. 10b). The Dalyan Channel and
429 Sülüngür Lake are known to be connected to the sea. A heavy isotope enrichment (seawater
430 effect) in these waters in the wet season, in spite of the diluting effect of rainwaters, may be due
431 to a water current that occurs in the wet season from the sea to the lake and channel. Although
432 Alagöl Lake is also connected to the sea in the same way, a light isotope enrichment in this
433 lake's waters in the wet season is compatible with the other waters. This indicates that although
434 Alagöl Lake is very close to the sea and connected to it by a channel like Sülüngür Lake, for
435 some reason, it is physically more isolated.

4.3.3 Gas geochemistry

The geothermal potential is generally high in areas where there is recent magmatic or tectonic activity like volcanism, extension, or fluid transport through fault-hosted deep pathways. The most sensitive indicator of such activity is the isotopic composition of helium ($^3He/^4He$) (e.g. Kennedy and van Soest, 2007). Variations in helium isotope ratios of the fluids give researchers clues about the origin of these fluids and provide evidence for the presence of mantle-derived volatiles in geothermal systems. Helium in geothermal waters is derived from two terrigenous components with distinct isotopic composition (crustal He and mantle He). The continental crust is dominated by isotopically heavy helium (^4He) that has been produced in situ by nuclear reactions (^4He by radioactive decay of uranium and thorium, ^3He by thermal and epithermal neutron capture of lithium) in crustal rocks and minerals. This crustal component has a $^3He/^4He$ ratio of $\sim 2\times10^{-8}$ (Mamyrin and Tolstikhin, 1984; Andrews, 1985). In contrast, the Earth's mantle contains He enriched in the light isotope ^3He that has been inherited from planet formation. The convective mantle as sampled by mid-ocean ridge basalts (MORB) has a $^3He/^4He$ ratio of $\sim 1.1\times10^{-5}$ (Mamyrin and Tolstikhin, 1984; Ozima and Podosek, 2002), though other mantle domains may have higher or lower $^3He/^4He$ ratios. $^3He/^4He$ ratios are often expressed as a multiple of the present-day atmospheric $^3He/^4He$ ratio, R_a, which is 1.39×10^{-6}. Thus, the $^3He/^4He$ ratio of the atmosphere is 1 R_a, that of the crust may vary between ~0.01 and 0.1 R_a, and typical mantle values are ~8 R_a. In the vicinity of the study area, a mantle $^3He/^4He$ ratio of 7.7 R_a has recently been measured in olivines from the Kula volcanic field (Heineke et al., 2016).

In addition to $^3He/^4He$ ratios, $CO_2/^3He$ ratios are also used to recognize mixing of mantle and crustal fluids (Barry et al., 2013; Karakuş and Şimşek, 2013). Mantle-derived CO_2 gases usually have a $CO_2/^3He$ ratio of approximately 2×10^9 (Marty and Jambon, 1987), which will be

460 preserved unless mixing or fractionation occur during the journey of the mantle gases through
461 the lithosphere (O'Nions and Oxburgh, 1988; Wiersberg et al., 2011; Karakuş and Şimşek,
462 2013).

463 In this study, to contribute to the hydrogeochemical conceptual modeling of the geothermal
464 system in the study area, gas geochemistry analyses and helium isotope data were evaluated
465 accordingly. For springs where free gases could be sampled, the total gas compositions are
466 presented in Table 5 together with the helium isotope, $^{4}He/^{20}Ne$ and $CO_2/^{3}He$ ratios. Water
467 samples degassed in the lab were only analyzed for noble gases, therefore no total gas
468 compositions and $CO_2/^{3}He$ ratios are available for them. Air-corrected $^{3}He/^{4}He$ ratios
469 ($(^{3}He/^{4}He)_c$) were calculated according to Craig et al. (1978) and are also given in the same
470 table. According to Table 5, the majority of the gas samples are composed mainly of nitrogen
471 (N_2) with variable amounts of CO_2, Ar, O_2, CH_4, H_2 and He, except for one sample collected
472 from Köyceğiz Lake (SUB-2) in which the major contribution is from CH_4 with considerable
473 contributions of H_2 and O_2. N_2/Ar ratios of the gas samples are up to 119 and are close to the
474 atmospheric value (83). The gas compositions reported here are distinctly different from those
475 reported by Wiersberg et al. (2011) for the Büyük Menderes Graben, where the majority of the
476 samples have CO_2 concentrations > 95%.

477 The $^{4}He/^{20}Ne$ ratios of the samples range from 0.35 to 130, indicating that contributions from
478 atmospheric He are significant in some samples, but negligible in others when compared to the
479 $^{4}He/^{20}Ne$ ratios of air (~0.319; Sano and Wakita, 1985) or air-saturated water (0.274 at 25 °C;
480 e.g. Ozima and Podosek, 2002) (Table 5). The atmospheric contribution is highest in samples
481 collected from Köyceğiz Lake, where $^{4}He/^{20}Ne$ ratios are close to the ones reported for air,
482 which might be due to admixing of lake water during sampling.

The $(^3He/^4He)_c$ of all samples are above the crustal value (~0.05 R_a), indicating a contribution of mantle origin. A mantle helium component has been reported in Western Anatolia by previous researchers (Güleç, 1988; Güleç and Hilton, 2006; Karakuş and Şimşek, 2013). In fact, Güleç (1988) stated that mantle helium could be observed in a large area in Western Anatolia depending on the distribution of fault systems related to the extensional regime. By using $(^3He/^4He)_c$, which corrects for atmospheric helium contributions, relative fractions of mantle and crustal helium can be calculated using a simple mixing model between mantle and crustal endmembers (Equation 1):

$$\text{Mantle He (\%)} = 100\times [(^3He/^4He)_c - (^3He/^4He)_{crust}] / [(^3He/^4He)_{mantle} - (^3He/^4He)_{crust}]$$

Equation 1

Assuming $(^3He/^4He)_{crust}$ = 0.02 R_a and $(^3He/^4He)_{mantle}$ = 8 R_a, mantle He percentages between 2% and 17% are obtained (Table 5). The lowest mantle He contributions were found in the samples from Köyceğiz Lake, whereas the highest ones were observed in springs located on-land in the Dalaman plain near the Mediterranean Sea (THER, MUS, CUR, KAP-2). Small mantle He contributions also occur in on-land springs located near Köyceğiz Lake and the Dalyan Channel (SUL-2, KEL, DEL). The different helium contributions from air, crust and mantle in all samples are visualized in a $^3He/^4He$ vs. $^4He/^{20}Ne$ graph (Fig. 11). For instance, the Köyceğiz Lake samples with the highest atmospheric He contributions plot near air/ASW on the mixing line between ASW and crustal He endmembers (Fig. 11). Likewise, samples with a high crustal He contribution plot near the ASW-crustal He mixing line (Fig. 11). On the other hand, those samples with the highest mantle He contribution are located closer to the mixing line between ASW and mantle He. A relatively high contribution of mantle He in the Dalaman plain suggests that the faults of extensional tectonics in the area promote the escape of gases

originating from the deeper parts of the Earth through the brittle parts of the crust, and this affects the geothermal system.

Examining the differences in mantle helium contributions of subaqueous (SUB-2, 3, 4 and SUBC-2) and on-land (SUL-2, KEL, DEL) Köyceğiz Lake samples with the Dalaman plain samples (CUR, MUS, THER, KAP-2) indicates that these samples are products of two different geothermal systems. Köyceğiz Lake on-land samples have relatively high discharge temperatures (between 37 and 40 °C) when compared to Dalaman plain samples (26-30 °C). The $CO_2/^3He$ ratios in free gas samples range from 0.05×10^9 to 1.097×10^9. These ratios are lower than the average ratio reported for the upper mantle ($2x10^9$) (Marty and Jambon, 1987). Moreover, these ratios are much lower than the ones reported by Mutlu et al. (2008), Wiesberg et al. (2011) and Karakuş and Şimşek (2013). This probably reflects the effects of gas fractionation processes (such as degassing and/or dissolution) in the hydrothermal system, which modified the He-CO_2 systematics. A sound discussion of He-CO_2 systematics, however, would require $\delta^{13}C$ data in addition and is beyond the scope of the present study.

4.3.4 Hydrogeochemical model

Our findings from this study enable us to construct a conceptual model (Fig. 12), which shows that fresh water percolates from the fractures, joints, and faults and is heated at depth along the geothermal gradient of the earth. While ascending to the surface from either the sea or lake bottom or on-land via active faults, the waters appear to be mixed with seawater below the sea or lake bottom.

The study area is located on the Lycian nappes (Fig. 1), where rock packages are overlain by thrust faults. Generally, faults dip southward. The key point is that the carbonate rocks are pervious, and these rocks are underlain and overlain by the impervious Yeşilbarak nappe and Marmaris nappe, respectively. The southward-dipping nappes force groundwater to flow from

north to south (to the Mediterranean). The Yeşilbarak nappe is located at the bottom of all other nappes tectonically; and since it is buried, it crops out in only a very limited area in the study region (Fig. 1). This makes it an impervious mat lying at the bottom of the Lycian nappes. The Marmaris nappe is tectonically the uppermost layer of the Lycian nappes and may be understood as impervious with a peridotite composition. The Gülbahar, Bodrum and Tavas nappes, although differentiated as separate units by Şenel (1997a; 1997b), are made up of carbonate rocks and are sandwiched between these two impervious units, namely the Yeşilbarak nappe at the bottom, and the Marmaris nappe at the top. This arrangement of pervious and impervious nappes creates a somehow confined aquifer in the region (Fig. 12).

The Marmaris Nappe is situated on top of the carbonate nappes, lying as a NW-SE-oriented strip. The carbonate nappes underlie this impervious patch and crop out to the north and to the south of it (Fig. 1). The carbonate units are pervious and known to be karstic in character. The northern outcrop of the karstic nappes can be interpreted as a recharge area of the confined aquifer and the southern outcrop as the discharge area (Fig. 12). The groundwater flow is from the northern highlands towards the southern lowlands, namely the Mediterranean. The southward-dipping tectonic contacts between these units also enable this groundwater movement.

The rainwater precipitated in the northern carbonate highlands travels to the southern low elevation areas below the impervious Marmaris nappe (Fig. 12). The southern boundary of the Marmaris-carbonate nappe units is cut by young normal faults, leading to the formation of a NW-SE lying depression. This depression is filled either by water or by sediments. For example, in the Köyceğiz area it is filled with water forming Köyceğiz Lake. However, around Dalaman, it is filled with alluvium, forming the Dalaman plain. The groundwater traveling from north to south is not able to discharge to the surface due to the overlying Marmaris nappe. However, the heated groundwater immediately emerges at the southern boundary of the

555 Marmaris-carbonate nappe units. This is either due to the normal faults that enable the vertical
556 permeability or to the lack of an impervious cap rock in the south.

557 The subaqueous hot spring of the Fethiye-Göcek Bay (SUB-7) most probably emerges at the
558 southern Marmaris-carbonate nappe boundary. Since the boundary is covered by seawater and
559 alluvium, its exact location is not visible. We do not know whether the spring emerges exactly
560 at the boundary. The location may be on the carbonate side, since the boundary is covered by
561 alluvium, and there may be a shift where the alluvium is thin enough to allow the groundwater
562 to percolate. Alternatively, the water may emerge on the Marmaris nappe side. The Marmaris
563 nappe may get thinner towards the boundary and become pervious to semi-pervious due to
564 fractures and joints in the rock. In both cases, we can suppose that the hot water emerges not
565 too far away from the boundary.

566 **5. Conclusion**

567 This study aimed to find subaqueous hot springs by making horizontal temperature
568 measurements. Measurements revealed 49 temperature anomalies in the study area and among
569 these anomalies seven of them were confirmed as subaqueous hot springs: three in Köyceğiz
570 Lake, three in the Dalyan Channel, and one in the Fethiye-Göcek Bay. There are no temperature
571 anomalies at the bottom of the Alagöl, Sülüngür and Kocagöl lakes. The temperature of the
572 subaqueous hot springs in the study area ranges between 26 and 29 °C.

573 According to the chemical analysis results, inland cold waters and stream waters are of the Mg
574 or Ca – HCO3 type. The other samples (subaqueous, lake, channel etc.) are Na-Cl type waters.
575 The on-land fresh waters are of meteoric origin and display highly negative δD and $\delta^{18}O$ values.
576 This is an indication of recharge from inland and high altitudes. However, there is a seawater
577 effect, obvious in the $\delta^{18}O$ and δD values of the remaining waters.

578 The geology of the region greatly affects the geothermal system in the study area. The Marmaris
579 nappe acts as an impervious cap rock. Especially in the south of the study area, this unit is
580 buried under alluvium and/or lake/seawater. Similarly, the Yeşilbarak nappe also underlies all
581 units as an impervious base rock. Pervious and even karstic carbonate units are sandwiched
582 between these two impervious rocks forming a somehow confined aquifer. The tectonic
583 boundaries between these units are dipping mainly southward. This allows groundwater
584 originating from the northern highlands to travel through the pervious carbonate rocks below
585 the impervious Marmaris nappe. The water travels towards the lowlands in the south, is heated
586 at depth, and mixes with seawater while traveling up through high angle normal faults, it
587 emerges as hot springs from the southern boundary of the carbonate-Marmaris nappe units. The
588 type of hot spring (either on-land or subaqueous) is determined by the local occurrence of
589 alluvium or water. If the boundary is covered by alluvium, like in the case of the Dalaman plain,
590 the hot springs (MUS, THER, KAP, CUR) emerge on land. If the boundary is covered by thin
591 alluvium and a water body (lake/sea/channel), the hot springs emerge either on-land (SUL,
592 DEL, KEL) or subaqueous (SUB-1-7).

593 According to the total gas analysis results, the majority of the gas samples are composed mainly
594 of nitrogen (N_2) with variable amounts of CO_2, Ar, O_2, CH_4, H_2 and He. N_2/Ar ratios of the gas
595 samples are close to the atmospheric value (up to 119). The $^4He/^{20}Ne$ ratios of the samples
596 indicate that atmospheric contribution is generally negligible, but is significant in some samples
597 such as those taken from Köyceğiz Lake, which might be due to admixing of lake water during
598 sampling. The $(^3He/^4He)_c$ of all samples are above the crustal value (~0.05 R_a) which indicate
599 a mantle contribution. According to a mixing model between mantle and crustal endmembers,
600 the lowest mantle He contributions were found in on-land springs located near Köyceğiz Lake
601 (SUL-2, KEL, DEL), whereas the highest ones were observed in springs located around
602 Dalaman plain (THER, MUS, CUR, KAP-2). The differences in mantle helium contributions

603 of subaqueous and on-land Köyceğiz Lake hot springs and Dalaman plain hot springs indicate
604 that they are the products of two different geothermal systems. The $CO_2/^3He$ ratios in free gas
605 samples (0.05×10^9 to 1.097×10^9) are lower than the average ratio reported for the upper mantle
606 ($2x10^9$) and much lower than the ones reported for western Anatolia, which may be attributed
607 to the effects of gas fractionation processes in the hydrothermal system.

608 S, Cl, Ca, and Sr elements are enriched around Fethiye-Göcek subaqueous hot spring (SUB-7),
609 whereas S, Cl, Br, elements are enriched, Mn element is depleted around Köyceğiz lake
610 subaqueous hot springs. Fluid mineral equilibria calculations reveal that Ca enrichment around
611 SUB-7 is probable from precipitation of aragonite, calcite, dolomite, and fluorite minerals from
612 the hot spring. Sr has a similar atomic structure and chemical properties with Ca. It most
613 probably replaces Ca and displays a parallel anomaly. Cl and S enrichment around both
614 Köyceğiz and Fethiye-Göcek subaqueous hot springs cannot be explained by the fluid mineral
615 equilibria study. S enrichment could be related to biochemical processes.

616 **Acknowledgements**

617 This study was carried out as part of a project supported by The Scientific and Technological
618 Research Council of Turkey (TÜBİTAK, Project Number 112Y137). We acknowledge Nesrin
619 Tüfekçi Avşar for helping with the preparation of plots and spatial distribution maps of
620 sediment elemental ratios. We thank Martin Zimmer for determining the total gas compositions
621 and Enzio Schnabel for performing the noble gas analyses.

622 **References**

623 Andrews, J.N., 1985. The isotopic composition of radiogenic helium and its use to study
624 groundwater movement in confined aquifers. Chemical Geology. 49, 339-351.

625 Arango-Galván, C., Prol-Ledesma, R.M., Flores-Márquez, E.L., Canet, C., Estrada, R.E.V.,
626 2011. Shallow submarine and subaerial, low-enthalpy hydrothermal manifestations in
627 Punta Banda, Baja California, Mexico: Geophysical and geochemical characterization.
628 Geothermics. 40, 102-111.

629 Avşar, Ö., Kurtuluş, B., Gürsu, S., Gençalioğlu Kuşcu, G., Kaçaroğlu, F., 2016. Geochemical
630 and isotopic characteristics of structurally controlled geothermal and mineral waters of
631 Muğla (SW Turkey). Geothermics. 64, 466–481.

632 Baba, A., Sözbilir, H., 2012. Source of arsenic based on geological and hydrogeochemical
633 properties of geothermal systems in Western Turkey. Chemical Geology. 334, 364–377.

634 Balderer, W., Synal, H.-A., 1997. Use of chlorine-36 as a tracer for the evolution of waters in
635 geothermal and tectonically active areas in western Turkey. Nuclear Instruments and
636 Methods in Physics Research Section B: Beam Interactions with Materials and Atoms.
637 123, 387–393.

638 Barry, P.H., Hilton, D.R., Fischer, T.P., de Moor, J.M., Mangasini, F., Ramirez, C., 2013.
639 Helium and carbon isotope systematics of cold "mazuku" CO_2 vents and hydrothermal
640 gases and fluids from Rungwe Volcanic Province, southern Tanzania. Chemical
641 Geology. 339, 141-156. http://dx.doi.org/10.1016/j.chemgeo.2012.07.003.

642 Bayarı, C.S., Kazancı, N., Koyuncu, H., Çağlar, S.S., Gökçe, D., 1995. Determination of the
643 origin of the waters of Köyceğiz Lake, Turkey. Journal of Hydrology. 166, 171-191.

644 Bertani, R., 2015. Geothermal Power Generation in the World 2010-2014 Update Report.
645 Proceedings World Geothermal Congress 2015, Melbourne-Australia.

646 Bundschuh, J., Maity, J.P., Nath, B., Baba, A., Gunduz, O., Kulp, T.R., Jean, J.-S., Kar, S.,
647 Yang, H.-J., Tseng, Y.-J., Bhattacharya, P., Chen, C.-Y., 2013. Naturally occurring
648 arsenic in terrestrial geothermal systems of western Anatolia, Turkey: potential role in
649 contamination of freshwater resources. Journal of Hazardous Materials. 262, 951–959.

650 Clesceri, L. S., Greenberg, A.E., Trussell, R.R., 1989. Standard Methods for the Examination
651 of Water and Wastewater, Methods, 17th edition, American Public Health Association.
652 Washington, DC.

653 Corliss J.B., Dymond J., Gordon L.I., Edmond J.M., von Herzen R.P., Ballard, R.D.; Green,
654 K.; Williams, D., Bainbridge, A.; Crane, K., van Andel, T.H., 1979. Submarine thermal
655 sprirngs on the Galapagos rift. Science. 203, 1073-1083.

656 Craig, H., 1961. Isotopic Variations in Meteoric Waters. Science. 133, 1702-1703.

657 Craig, H., Lupton, J.E., Horibe, Y., 1978. A mantle helium component in circum-Pacific
658 volcanic gasses: Hakone, the Marianas and Mt Lassen. In: Alexander, E.C., Ozima, M.,
659 (Eds). Terrestrial Rare Gases. Japan. Science Society Press, Tokyo, 3-16.

660 Croudace, I.W., Rindby, A., Rothwell, R.G., 2006. ITRAX: description and evaluation of a new
661 multi-function X-ray core scanner. In: Rothwell, R.G. (Ed.), New Techniques in
662 Sediment Core Analysis, Geological Society London Special Publications. 267, 51-63.

663 De Batist, M., Klerkx, J., Rensbergen, P.V., Vanneste, M., Poort, P., Golmshtok, A.Y.,
664 Kremlev, A.A., Khlystov, O.M., Krinitsky, P., 2002. Active hydrate destabilization in
665 Lake Baikal, Siberia? Terra Nova. 14, 436–442.

666 Duchkov, A.D., Kutasov, I.M., Sokolova, L.S., 2009. Estimating heat flow from an unsteady
667 temperature log of submarine borehole BDP-98 (Lake Baikal). Russian Geology and
668 Geophysics. 50, 131–135.

669 Esposito, A., Giordano, G., Anzidei, M., 2006. The 2002–2003 submarine gas eruption at
670 Panarea volcano (Aeolian Islands, Italy): Volcanology of the seafloor and implications
671 for the hazard scenario. Marine Geology. 227, 119-134.

672 Fitzsimons, M.F., Dando, P.R., Hughes, J.A., Thiermann, F., Akoumianaki, I., Pratt, S.M.,
673 1997. Submarine hydrothermal brine seeps off Milos, Greece: Observations and
674 geochemistry. Marine Chemistry. 57, 325-340.

675 Glasby, G.B., Notsu, K., 2003. Submarine hydrothermal mineralization in the Okinawa Trough,
676 SW of Japan: an overview. Ore Geology Reviews. 23, 299–339.

677 Gökgöz, A., Tarcan, G., 2006. Mineral equilibria and geothermometry of the Dalaman–
678 Köyceğiz thermal springs, southern Turkey. Applied Geochemistry. 21, 253-268.

679 Güleç, N., 1988. He-3 distribution in western Turkey. Bulletin of the Mineral Research and
680 Exploration Institute of Turkey. 108, 35–42.

681 Güleç, N., Hilton, D.R., 2006. Helium and heat distribution in western Anatolia, Turkey:
682 Relationship to active extension and volcanism. Geological Society of America Special
683 Paper. 409, 305-319.

684 Hall, J., Aksu, A.E., Elitez, I., Yaltırak, C., Çifçi, G. 2014. The Fethiye–Burdur Fault Zone: A
685 component of upper plate extension of the subduction transform edge propagator fault
686 linking Hellenic and Cyprus Arcs, Eastern Mediterranean. Tectonophysics, 635, 80-99.

687 Hannington, M., Herzig, P., Stoffers, P., Scholten, J., Botz, R., Garbe-Schönberg, D., Jonasson,
688 I.R., Roest, W., 2001. First observations of high-temperature submarine hydrothermal
689 vents and massive anhydrite deposits off the north coast of Iceland. Marine Geology. 177,
690 199-220.

691 Heineke, C., Niedermann, S., Hetzel, R., Akal, C., 2016. Surface exposure dating of Holocene
692 basalt flows and cinder cones in the Kula volcanic field (Western Turkey) using
693 cosmogenic ^{3}He and ^{10}Be. Quaternary Geochronology. 34, 81-91.

694 Hem, J.D., 1985. Study and Interpretation of the Chemical Characteristics of Natural Water.
695 Water Supply Paper 2254, 3rd edition, US Geological Survey, Washington, D.C., pp. 263.

696 IAEA, 1981. Stable isotope hydrology. Deuterium and oxygen-18 in water cycle, In: Gat, J.R.,
697 Gonfiantini, R. (Eds.), International Atomic Energy Agency. Technical Report No. 210,
698 Vienna, 339.

699 IEA, 2012. World energy outlook 2012 Paris: International Energy Agency.

700 Italiano, F., Nuccio, P.M., 1991. Geochemical investigations of submarine volcanic exhalations
701 to the east of Panarea, Aeolian Islands, Italy. Journal of Volcanology and Geothermal
702 Research. 46, 125-141.

703 İlkışık, O.M., 1995. Regional heat flow in western Anatolia using silica temperature estimates
704 from thermal springs. Tectonophysics. 244, 175-184.

705 Karakus, H., Aydin, H., 2016. HNC-Plot: an excel VBA for visualization of helium, nitrogen
706 and CO2 isotope data of crustal and mantle gases, Earth Science Informatics. DOI
707 10.1007/s12145-016-0272-4

708 Karakuş, H., Şimşek, Ş., 2013. Tracing deep thermal water circulation systems in the E–W
709 trending Büyük Menderes Graben, western Turkey. Journal of Volcanology and
710 Geothermal Research. 252, 38-52.

711 Kennedy, B.M., van Soest, M.C., 2007. Flow of mantle fluids through the ductile lower crust:
712 Helium isotope trends. Science. 318, 1433-1436.

713 Koschinsky, A., Seifert, R., Knappe, A., Schmidt, K., Halbach, P., 2007. Hydrothermal fluid
714 emanations from the submarine Kick'em Jenny volcano, Lesser Antilles island arc.
715 Marine Geology. 244, 129-141.

716 Kylander, M.E., Ampel, L., Wohlfarth, B., Veres, D., 2011. High-resolution X-ray fluorescence
717 core scanning analysis of Les Echets (France) sedimentary sequence: new insights from
718 chemical proxies. Journal of Quaternary Science. 26, 109-117.

719 Mamyrin, B.A., Tolstikhin, I.N., 1984. Helium isotopes in Nature. Elsevier, Amsterdam, pp.
720 273.

721 Marty, B., Jambon, A., 1987. C/^{3}He in volatile fluxes from the solid Earth: implications for
722 carbon geodynamics. Earth and Planetary Science Letters. 83, 16-26.

723 McCarthy, K.T., Pichler, T., Price, R.E., 2005. Geochemistry of Champagne Hot Springs
724 shallow hydrothermal vent field and associated sediments, Dominica, Lesser Antilles.
725 Chemical Geology. 224, 55-68.

726 McMurtry, G.M., Sedwick, P.N., Fryer, P., VonderHaar, D.L., Yeh, H.W., 1993. Unusual
727 geochemistry of hydrothermal vents on submarine arc volcanoes: Kasuga Seamounts,
728 Northern Mariana Arc. Earth and Planetary Science Letters. 114, 517-528.

729 Mertoğlu, O., Şimşek, S., Başarır, N., 2015. Geothermal Country Update Report of Turkey
730 (2005-2010). Proceedings World Geothermal Congress 2010, Bali-Indonesia.

731 Mertoğlu, O., Şimşek, S., Dağıstan, H., Bakır, N., Doğdu, N., 2010. Geothermal Country
732 Update Report of Turkey (2010-2015). Proceedings World Geothermal Congress 2015,
733 Melbourne-Australia.

734 Michard, A., Michard, G., Stüben, D., Stoffers, P., Cheminée, J., Binard, N. 1993. Submarine
735 thermal springs associated with young volcanoes: The Teahitia vents, Society Islands,
736 Pacific Ocean. Geochimica et Cosmochimica Acta. 57, 4977-4986.

737 Michel, F.A., Allen, D.M., Grant, M.B., 2001. Hydrogeochemistry and geothermal
738 characteristics of the White Lake basin, South-central British Columbia, Canada.
739 Geothermics. 31, 169-194.

740 MTA, 2005. Inventory of Geothermal Resources of Turkey (in Turkish), MTA, Ankara.

741 Mutlu, H., Güleç, N., 1998. Hydrogeochemical outline of thermal waters and geothermometry
742 applications in Anatolia (Turkey). Journal of Volcanology and Geothermal Research. 85,
743 495–515.

744 Mutlu, H., Güleç, N., Hilton, D.R., 2008. Helium-carbon relationships in geothermal fluids of
745 western Anatolia, Turkey. Chemical Geology. 247, 305-321.

746 Niedermann, S., Bach, W., Erzinger, J., 1997. Noble gas evidence for a lower mantle
747 component in MORBs from the southern East Pacific Rise: Decoupling of helium and
748 neon isotope systematics. Geochimica et Cosmochimica Acta. 61, 2697-2715.

749 O'Nions, R.K., Oxburgh, E.R., 1988. Helium, volatile fluxes and the development of
750 continental crust. Earth and Planetary Science Letters. 90, 331-347.

751 Ocakoğlu, N., 2011. Investigation of Fethiye-Marmaris Bay (SW Anatolia): seismic and
752 morphologic evidences from the missing link between the Pliny Trench and the Fethiye-
753 Burdur Fault Zone. Geo-Marine Letters. 32, 17-28. doi 10.1007/s00367-011-0234-2.

754 Ozima, M., Podosek, F.A., 2002. Noble Gas Geochemistry, 2nd edition. Cambridge University
755 Press, Cambridge, pp. 286.

756 Özgür, N., Çalışkan, T.A., 2013. Active geothermal systems in the Menderes Massif, western
757 Anatolia, Turkey. Procedia Earth and Planetary Science. 7, 652–655.

758 Parkhurst, D.L., Appelo, C.A.J., 1999. User's Guide to PHREEQC (Version 2-A) Computer
759 Program for Speciation, Batch-Reaction, One-Dimensional Transport, and Inverse
760 Geochemical Calculations.

761 Pekçetinöz, B., Kayseri, M.S., Eftelioğlu, M., Özel, E., 2009. High-resolution shallow seismic
762 and palynological studies in determining hydrothermal activity in Gülbahçe Bay.
763 Geological Bulletin of Turkey. 52, 325-366. (in Turkish)

764 Pichler, T., 2005. Stable and radiogenic isotopes as tracers for the origin, mixing and subsurface
765 history of fluids in submarine shallow-water hydrothermal systems. Journal of
766 Volcanology and Geothermal Research. 139, 211-226.

767 Prol-Ledesma, R.M., 2003. Similarities in the chemistry of shallow submarine hydrothermal
768 vents. Geothermics. 32, 639-644.

769 Prol-Ledesma, R.M., Canet, C., Torres-Vera, M.A., Forrest, M.J., Armienta, M.A., 2004. Vent
770 fluid chemistry in Bahia Concepcion coastal submarine hydrothermal system, Baja
771 California Sur, Mexico. Journal of Volcanology and Geothermal Research. 137, 311-328.

772 Prol-Ledesma, R.M., Dando, P.R., de Ronde, C.E.J., 2005. Special issue on “shallow-water
773 hydrothermal venting. Chemical Geology. 224, 1–4.

774 Remsen, C. C., Maki, J. S., Klump, J. V., Aguilar, C., Anderson, P. D., Buchholz, L., Cuhel,
775 R. L., Lovalvo, D., Paddock, R. W., Waples, J., Bruckner, J. C., Schroeder, C. M., 2002.
776 Sublacustrine geothermal activity in Yellowstone Lake: studies past and present. In:
777 Yellowstone Lake: Hotbed of Chaos or Reservoir of Resilience?: Proceedings of the 6th
778 Biennial Scientific Conference on the Greater Yellowstone Ecosystem. Anderson, R. J.,
779 Harmon, D. (Eds.), pp. 192–212.

780 Ronde, C.E.J., Stoffers, P., Garbe-Schönberg, D., Christenson, B.W., Jones, B., Manconi, R.,
781 Browne, P.R.L., Hissmann, K., Botz, R., Davy, B.W., Schmitt, M., Battershill, C.N.,
782 2002. Discovery of active hydrothermal venting in Lake Taupo. Journal of Volcanology
783 and Geothermal Research. 115, 257-275.

784 Sano, Y., Wakita, H., 1985. Geographical distribution of 3He/4He ratios in Japan: Implications
785 for arc tectonics and incipient magmatism. Journal of Geophysical Research. 90, 8729-8741:

786 Suarez-Arriaga, M.C., Bundschuh, J., Samaniego, F., 2014. Assessment of submarine
787 geothermal resources and development of tools to quantify their energy potentials for
788 environmentally sustainable development. Journal of Cleaner Production. 83, 21-32.

789 Süer, S., Güleç, N., Mutlu, H., Hilton, D.R., Çifter, C., Sayın, M., 2008. Geochemical
790 monitoring of geothermal waters (2002–2004) along the North Anatolian Fault Zone,
791 Turkey: spatial and temporal variation and relationship to seismic activity. Pure and
792 Applied Geophysics. 165, 17–43.

793 Şenel, M., 1997a. Geological Map Series of Turkey 1:100 000 scale. No. 1, Geologic Map of
794 Fethiye L7 Quadrangle. General Directorate of Mineral Research and Exploration,
795 Geological Research Department, Ankara (in Turkish).

796 Şenel, M., 1997b. Geological Map Series of Turkey 1:100 000 scale. No. 2, Geologic Map of
797 Fethiye L8 Quadrangle. General Directorate of Mineral Research and Exploration,
798 Geological Research Department, Ankara (in Turkish).

799 Tarcan, G., 2005. Mineral saturation and scaling tendencies of waters discharged from wells
800 (>150°C) in geothermal areas of Turkey. Journal of Volcanology and Geothermal
801 Research. 142, 263–283.

802 Tüfekçi, N., Süzen, M.L., Güleç, N., 2010. GIS based geothermal potential assessment: A case
803 study from Western Anatolia, Turkey. Energy. 35, 246-261.

804 Valsami-Jones, E., Baltatzis, E., Bailey, E.H., Boyce, A.J., Alexander, J.L., Magganas, A.,
805 Anderson, L., Waldron, S., Ragnarsdottir, K.V., 2005. The geochemistry of fluids from
806 an active shallow submarine hydrothermal system: Milos island, Hellenic Volcanic Arc.
807 Journal of Volcanology and Geothermal Research. 148, 130-151.

808 Vengosh, A., Helvaci, C., Karamanderesi, İ.H., 2002. Geochemical constraints for the origin of
809 thermal waters from western Turkey. Applied Geochemistry. 17, 163–183.

810 Wiersberg, T., Süer, S., Güleç, N., Erzinger, J., Parlaktuna, M., 2011. Noble gas isotopes and
811 the chemical composition of geothermal gases from the eastern part of the Büyük
812 Menderes Graben (Turkey). Journal of Volcanology and Geothermal Research. 208, 112-
813 121.

814 Williams, D.L., 1976. Submarine Geothermal Resources. Journal of Volcanology and
815 Geothermal Research. 1, 85-100.

816 Williams, D.L., Von Herzen, R.P., Sclater, J.G., Anderson, R.N., 1974. The Galapagos
817 spreading centre: lithospheric cooling and hydrothermal circulation. Geophysical Journal
818 International. 38(3), 587-608.

819 Yağmurlu, F., Bozcu, M., Şentürk, M., 2005. Investigation of seismotectonic characteristics of
820 Burdur Faults in between Burdur and Fethiye region. TÜBİTAK report, Project No.
821 101Y027. (in Turkish).

822 Yamanaka, T., Maeto, K., Akashi, H., Ishibashi, J., Miyoshi, Y., Okamura, K., Noguchi, T.,
823 Kuwahara, Y., Toki, T., Tsunogai, U., Ura, T., Nakatani, T., Maki, T., Kubokawa, K.,
824 Chiba H., 2013. Shallow submarine hydrothermal activity with significant contribution
825 of magmatic water producing talc chimneys in the Wakamiko Crater of Kagoshima Bay,
826 southern Kyushu, Japan. Journal of Volcanology and Geothermal Research. 258, 74–84.

827 **Figure Captions**

828 **Fig. 1.** Geological map of the study region (modified from Şenel, 1997a; Şenel, 1997b) with
829 water sampling locations indicated. Sample labels are given in Table 1 along with sample
830 information. Fethiye-Burdur and Pliny-Strabo fault zones are shown on the upper right inset
831 map as FBFZ and PSFZ, respectively (Hall et al., 2014).

832 **Fig. 2.** Physicochemical measurement routes in (a) Dalyan Channel, Köyceğiz, Alagöl, and
833 Sülüngür Lakes; (b) Fethiye-Göcek Bay and Kocagöl Lake (in the west). Bathymetry maps of
834 (c) Köyceğiz Lake and (d) Fethiye-Göcek Bay.

Fig. 3. Locations of 233 gravity cores collected from a) Köyceğiz Lake, b) Dalyan Channel, and c) Fethiye-Göcek Bay. The white dots are "Cold Location Cores" (CLC), while the red dots are "Hot Location Cores" (HLC). The insets are close-up views around the HLCs.

Fig. 4. a) An example illustration ofthe comparison of the mean Sr/Ti ratios in the HLCs and CLCs from the Fethiye-Göcek Bay. The mean of the Sr/Ti ratio in HLCs (i.e., around the subaqueous hot spring) is significantly higher than the mean of the CLCs (by approximately 4σ), which implies that sediments around the subaqueous hot spring are enriched in Sr. b) Spatial distribution of the Sr/Ti ratio over the Fethiye-Göcek Bay. The maximum around the F-71 core also implies the presence of another subaqueous hot spring around that location.

Fig. 5. Matrices illustrating the magnitude of deviations between absolute means of HLCs and CLCs for all possible elemental ratios; a) Köyceğiz Lake, b) Dalyan Channel, c) Fethiye-Göcek Bay. For example, in the Köyceğiz matrix, the cell at the intersection of the 4^{th} column and the 5^{th} row shows that the mean Cl/K ratio of the HLCs is 2.5σ higher than the mean Cl/K ratio of the CLCs.

Fig. 6. Plots and spatial distributions of the mean ratios of enriched elements in Köyceğiz Lake (left) and Fethiye-Göcek Bay (right). The gray lines in the plots stand for individual elemental ratios, while the black and red lines indicate the mean of these ratios for the CLCs and HLCs, respectively. The horizontal lines on the graphs indicate ±1σ boundaries for CLCs. Note the significant difference in elemental enrichments in the southern basin of Köyceğiz Lake. The basinwide difference is attributed to the lack of tributaries in the southern basin, which enhances the effect of subaqueous hot springs on the overall sediment chemistry.

Fig. 7. Piper diagram of waters.

Fig. 8. Cl vs. Total Dissolved Solids (TDS) graph.

858 **Fig. 9.** Temperature vs. Saturation Index (SI) diagrams for samples SUB-1 and SUB-7.

859 **Fig. 10.** $\delta^{18}O$ vs. δD diagram of waters [GMWL: **G**lobal **M**eteoric **W**ater **L**ine (Craig, 1961);
860 MMWL: **M**editerranean **M**eteoric **W**ater **L**ine (IAEA, 1981)] (a) wet, (b) dry season
861 measurements.

862 **Fig. 11.** $^{3}He/^{4}He$ (R_a) versus $^{4}He/^{20}Ne$ graph for hydrothermal fluids and gases. Binary mixing
863 lines between air saturated water (ASW) ($^{3}He/^{4}He$ =1 R_a), mantle ($^{3}He/^{4}He_{mantle}$=8 R_a) and
864 crustal ($^{3}He/^{4}He_{crust}$ =0.02 R_a) endmember compositions, 1% and 20% air-mantle mixing lines
865 (mantle %) and 1%, 10%, 20% and 50% air proportions (air %) are also presented herein. The
866 graph was prepared using the HNC-Plot application (Karakuş and Aydın, 2016).

867 **Fig. 12.** Sketch of a conceptual hydrogeochemical model for the study area. Not to scale.
868 Modified from Gökgöz and Tarcan (2006) and Avşar et al. (2016).

869 **Supplementary Fig. 1.** (a) Temperature and probe depth measurements taken around the
870 submarine hot springs. The anomalies of SUB-1, SUB-4, SUB-5 and SUB-7 hot springs are
871 marked by circles. Temperature anomaly at 18:02:14 on 26.08.2013 indicates SUB-7 hot spring.
872 A second measurement on 31.08.2014 verified the existence of SUB-7 hot spring. See the
873 anomaly at 15:21:00 marked by a circle. (b) Sonar profiles used to detect SUB-2 and SUB-3.

874 **Supplementary Fig. 2.** Optical and radiographic images of the artificial cores composed of the
875 top 3-5 cm sediments from 233 gravity cores. Labels and coordinates of each gravity core are
876 presented as well. “K”: Köyceğiz, “D”: Dalyan, “F”: Fethiye-Göcek, and “I”: İnlice Bay in
877 Fethiye-Göcek Bay.

878 **Supplementary Fig. 3.** Plots of elemental ratios based on the standardized “kcps” values for
879 (a) Köyceğiz Lake, (b) Dalyan Channel, (c) Fethiye-Göcek Bay.

880 **Supplementary Fig. 4.** Spatial distribution maps of elemental ratios over the study area. (a)

881 Köyceğiz Lake, (b) Dalyan Channel, (c) Fethiye-Göcek Bay.

882

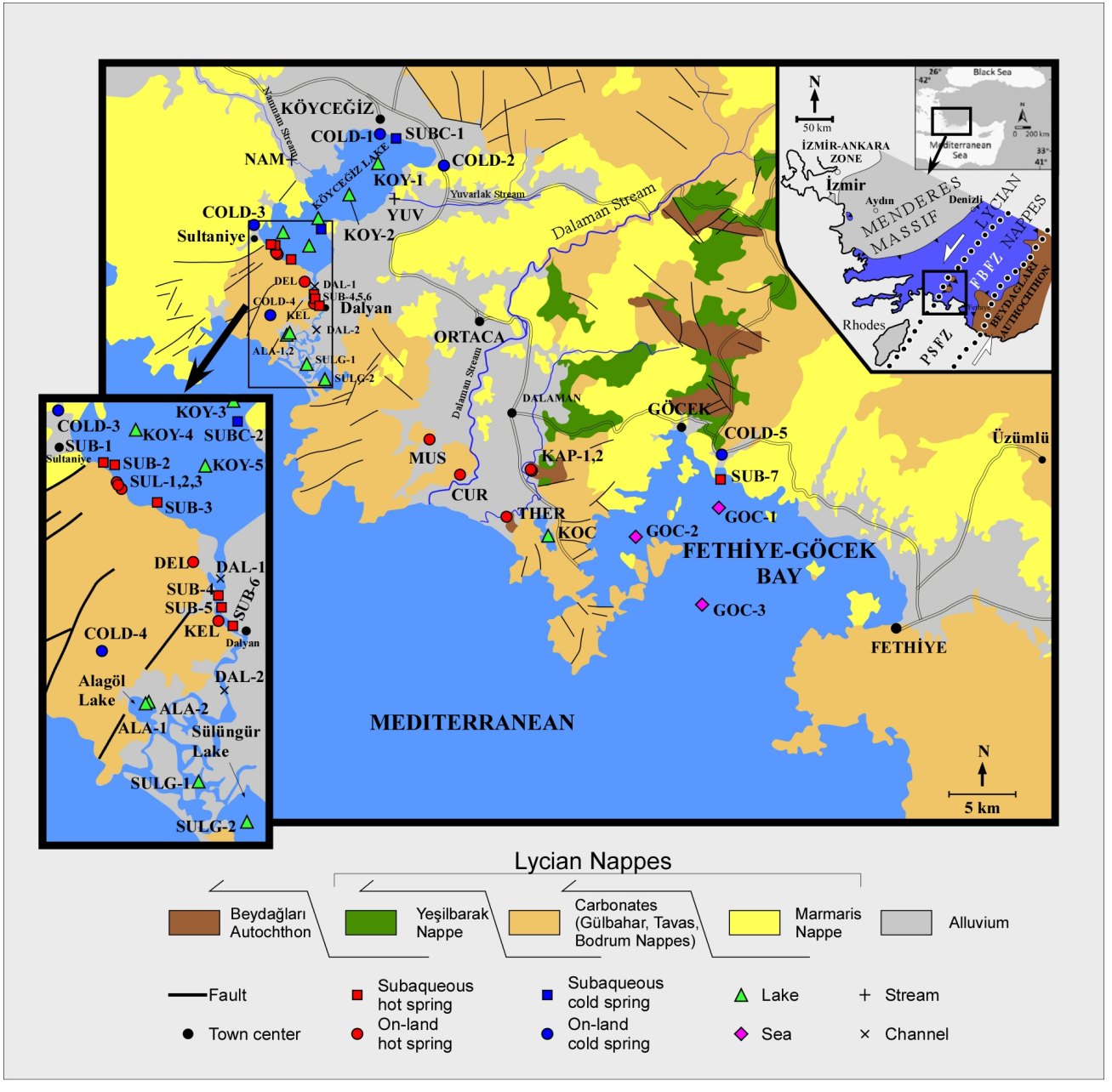
KÖYCEĞİZ
COLD-1
SUBC-1
NAM
COLD-2
KOY-1
YUV
KOY-2
COLD-3
Sultaniye
Yuvarlak Stream
Dalaman Stream
DEL
DAL-1
SUB-4,5,6
COLD-4
KEL
Dalyan
DAL-2
ALA-1,2
SULG-1
SULG-2
ORTACA
DALAMAN
GÖCEK
COLD-5
Üzümlü
MUS
KAP-1,2
SUB-7
CUR
THER
KOC
GOC-1
GOC-2
FETHİYE-GÖCEK BAY
GOC-3
FETHİYE
MEDITERRANEAN
KOY-3
COLD-3
KOY-4
SUBC-2
SUB-1
SUB-2
KOY-5
SUL-1,2,3
SUB-3
DEL
DAL-1
SUB-4
SUB-5
SUB-6
COLD-4
KEL
Dalyan
DAL-2
Alagöl Lake
ALA-2
ALA-1
Sülüngür Lake
SULG-1
SULG-2
N
50 km
İZMİR-ANKARA ZONE
İzmir
Aydın
Denizli
MENDERES MASSIF
LYCIAN NAPPES
FBFZ
BEYDAĞLARI AUTHOCHTHON
PSFZ
Rhodes
Black Sea
Mediterranean Sea
5 km
Lycian Nappes
Beydağları Autochthon
Yeşilbarak Nappe
Carbonates (Gülbahar, Tavas, Bodrum Nappes)
Marmaris Nappe
Alluvium
Fault
Subaqueous hot spring
Subaqueous cold spring
Lake
Stream
Town center
On-land hot spring
On-land cold spring
Sea
Channel

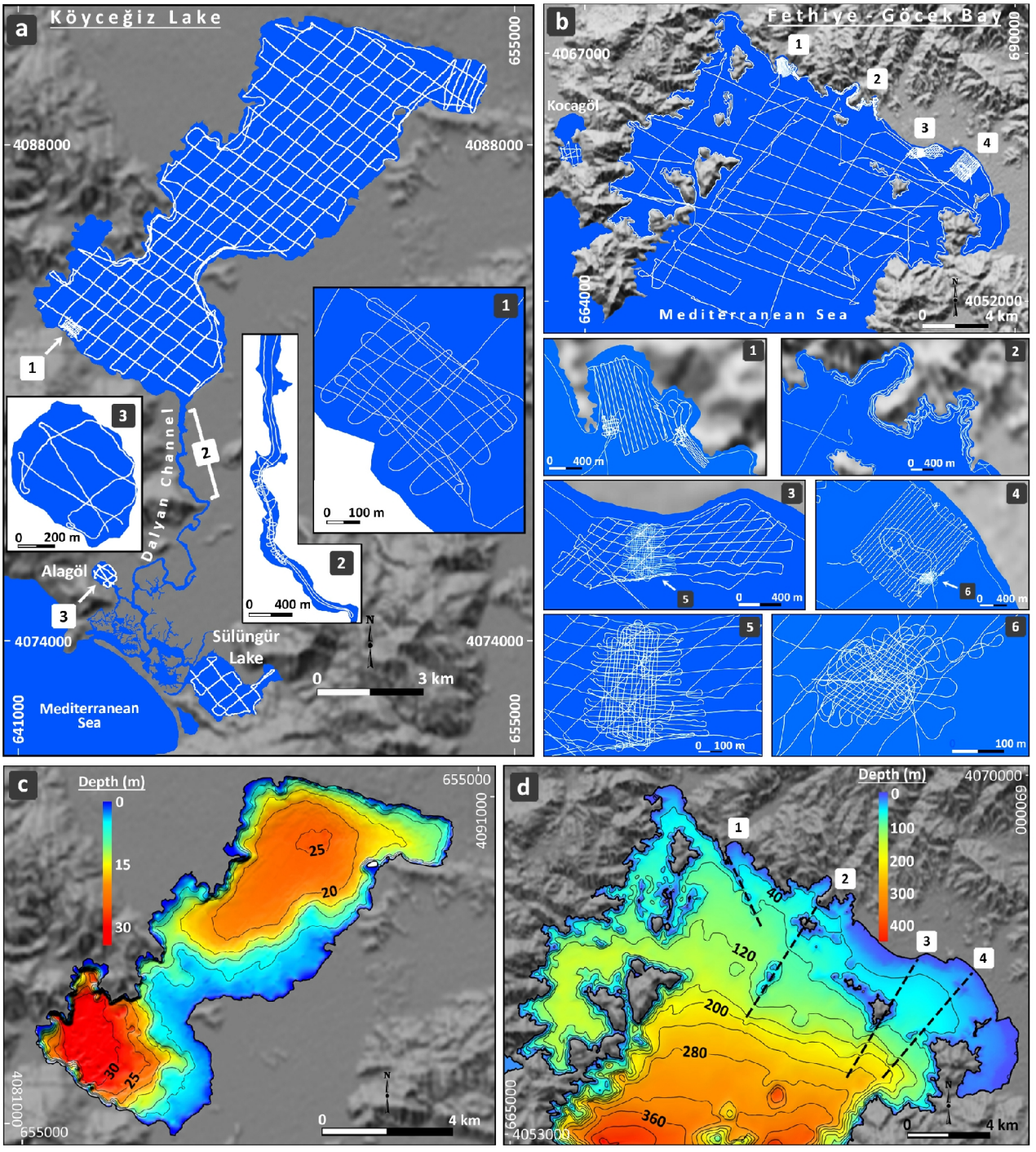
a
Köyceğiz Lake
655000
4088000
4088000
1
2
3
Dalyan Channel
0 200 m
0 100 m
0 400 m
Alagöl
3
4074000
Sülüngür
Lake
4074000
0 3 km
641000
Mediterranean
Sea
655000
b
Fethiye - Göcek Bay
690000
4067000
Kocagöl
1
2
3
4
664000
Mediterranean Sea
4052000
0 4 km
1
0 400 m
2
0 400 m
3
5
0 400 m
4
6
0 400 m
5
0 100 m
6
100 m
c
Depth (m)
0
15
30
655000
4091000
25
20
30
25
4081000
655000
0 4 km
d
Depth (m)
4070000
690000
0
100
200
300
400
1
2
3
4
40
120
200
280
360
665000
4053000
0 4 km

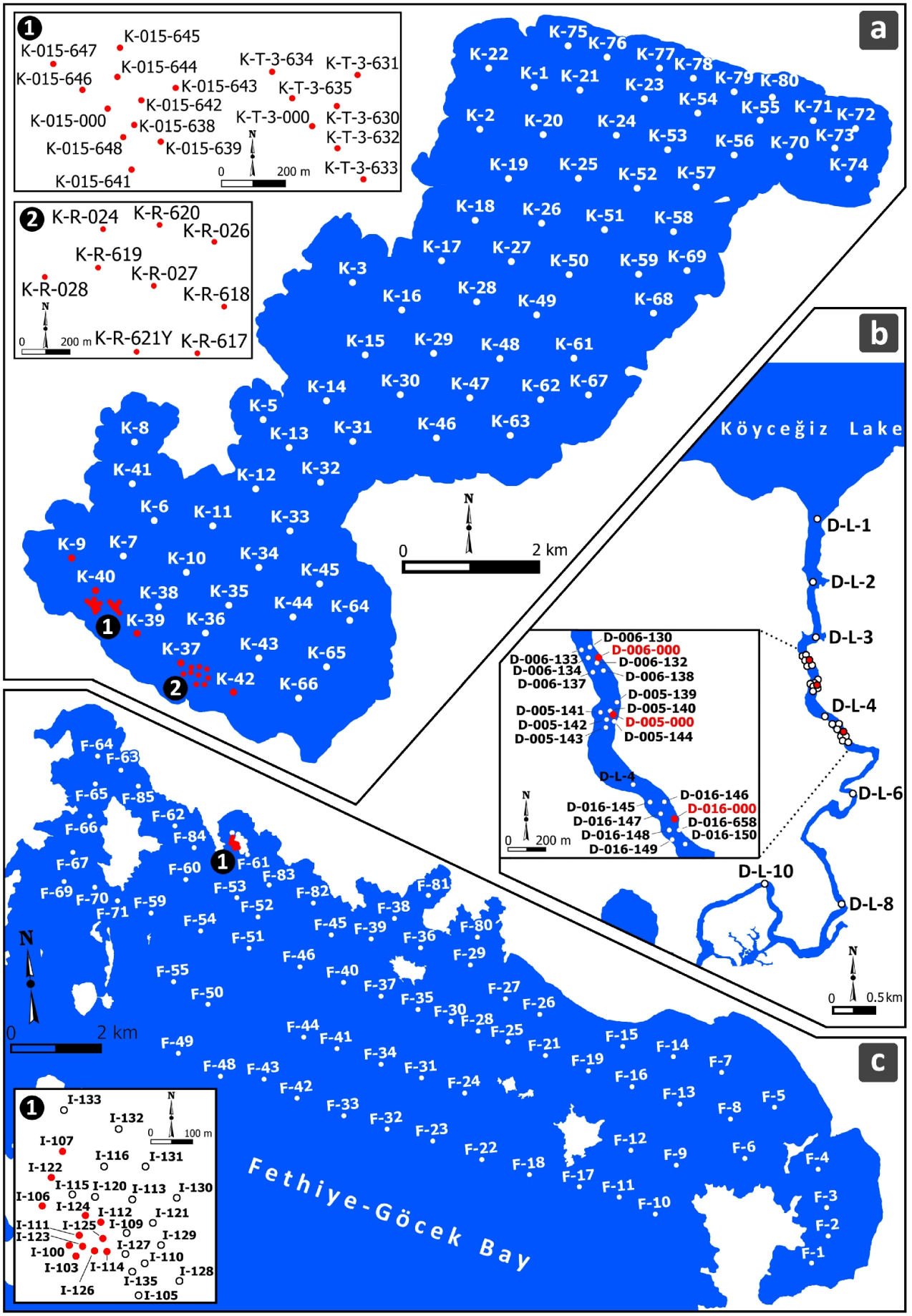
a
b
c
1
K-015-645
K-015-647
K-015-644
K-T-3-634
K-T-3-631
K-015-646
K-015-643
K-T-3-635
K-015-642
K-015-000
K-015-638
K-T-3-000
K-T-3-630
K-T-3-632
K-015-648
K-015-639
K-T-3-633
K-015-641
0
200 m
2
K-R-024
K-R-620
K-R-026
K-R-619
K-R-027
K-R-028
K-R-618
K-R-621Y
K-R-617
K-1
K-2
K-3
K-5
K-6
K-7
K-8
K-9
K-10
K-11
K-12
K-13
K-14
K-15
K-16
K-17
K-18
K-19
K-20
K-21
K-22
K-23
K-24
K-25
K-26
K-27
K-28
K-29
K-30
K-31
K-32
K-33
K-34
K-35
K-36
K-37
K-38
K-39
K-40
K-41
K-42
K-43
K-44
K-45
K-46
K-47
K-48
K-49
K-50
K-51
K-52
K-53
K-54
K-55
K-56
K-57
K-58
K-59
K-61
K-62
K-63
K-64
K-65
K-66
K-67
K-68
K-69
K-70
K-71
K-72
K-73
K-74
K-75
K-76
K-77
K-78
K-79
K-80
0
2 km
Köyceğiz Lake
D-L-1
D-L-2
D-L-3
D-L-4
D-L-6
D-L-8
D-L-10
D-006-130
D-006-000
D-006-133
D-006-132
D-006-134
D-006-138
D-006-137
D-005-139
D-005-141
D-005-140
D-005-142
D-005-000
D-005-143
D-005-144
D-L-4
D-016-146
D-016-145
D-016-000
D-016-147
D-016-658
D-016-148
D-016-150
D-016-149
0
200 m
0
0.5 km
F-64
F-63
F-65
F-85
F-62
F-66
F-84
F-67
F-60
F-61
F-83
F-69
F-70
F-53
F-82
F-81
F-59
F-71
F-52
F-38
F-54
F-45
F-39
F-80
F-51
F-36
F-46
F-29
F-40
F-55
F-37
F-27
F-50
F-35
F-26
F-30
F-28
F-44
F-25
F-41
F-21
F-15
F-14
F-49
F-34
F-19
F-7
F-48
F-43
F-31
F-16
F-42
F-24
F-13
F-5
F-33
F-8
F-32
F-23
F-12
F-22
F-9
F-6
F-18
F-4
F-17
F-11
F-3
F-10
F-2
F-1
0
2 km
Fethiye-Göcek Bay
1
I-133
I-132
0
100 m
I-107
I-116
I-131
I-122
I-115
I-120
I-113
I-130
I-106
I-124
I-112
I-121
I-111
I-125
I-109
I-123
I-129
I-127
I-100
I-110
I-103
I-114
I-128
I-135
I-126
I-105

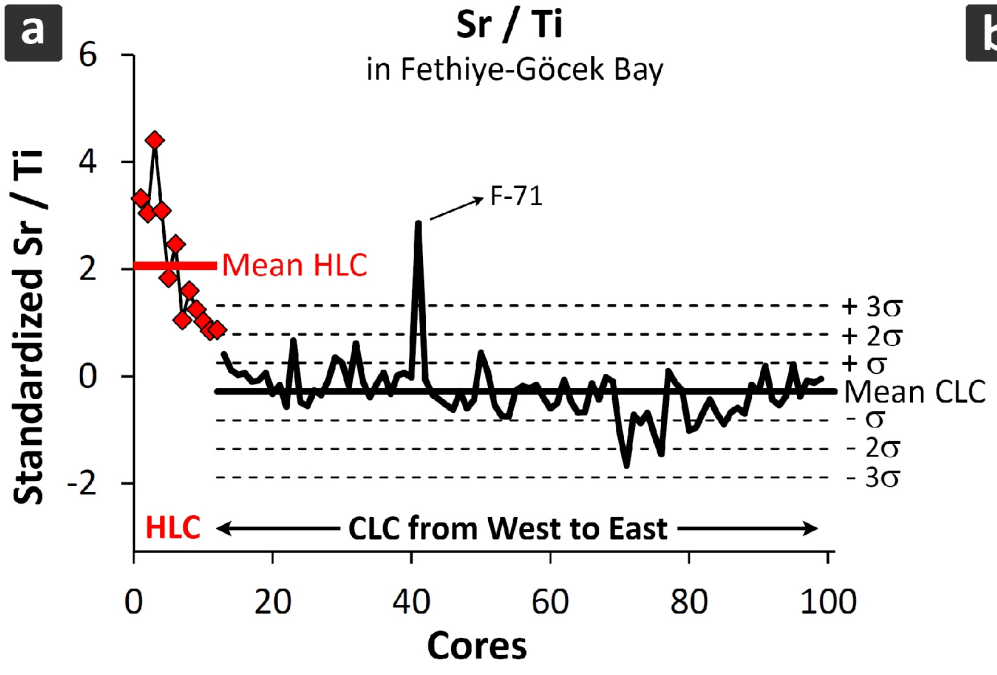
a
Sr / Ti
in Fethiye-Göcek Bay
Standardized Sr / Ti
6
4
2
0
-2
F-71
Mean HLC
+ 3σ
+ 2σ
+ σ
Mean CLC
- σ
- 2σ
- 3σ
HLC
CLC from West to East
0
20
40
60
80
100
Cores

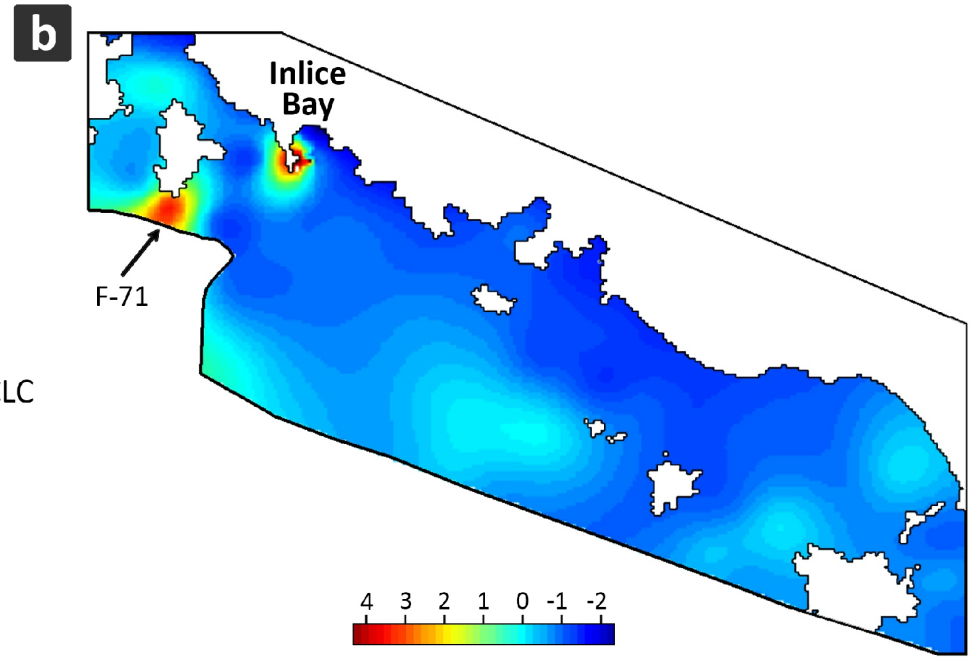
b
Inlice
Bay
F-71
4
3
2
1
0
-1
-2

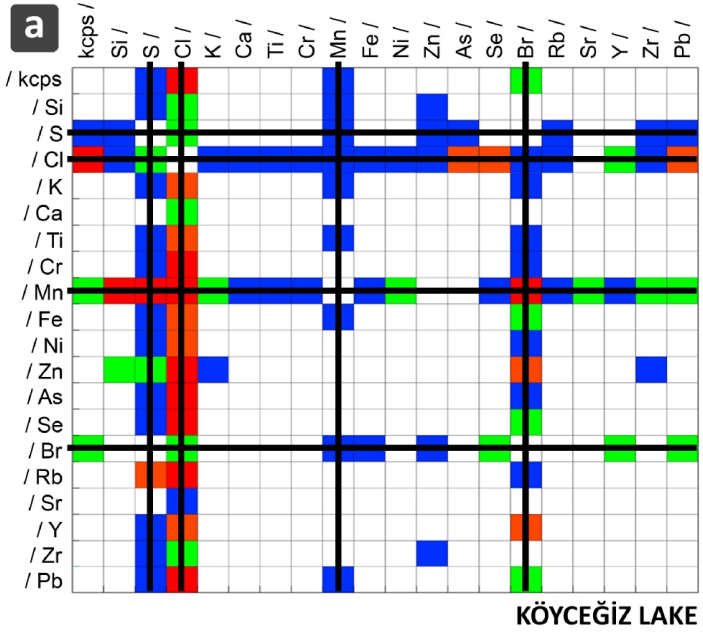

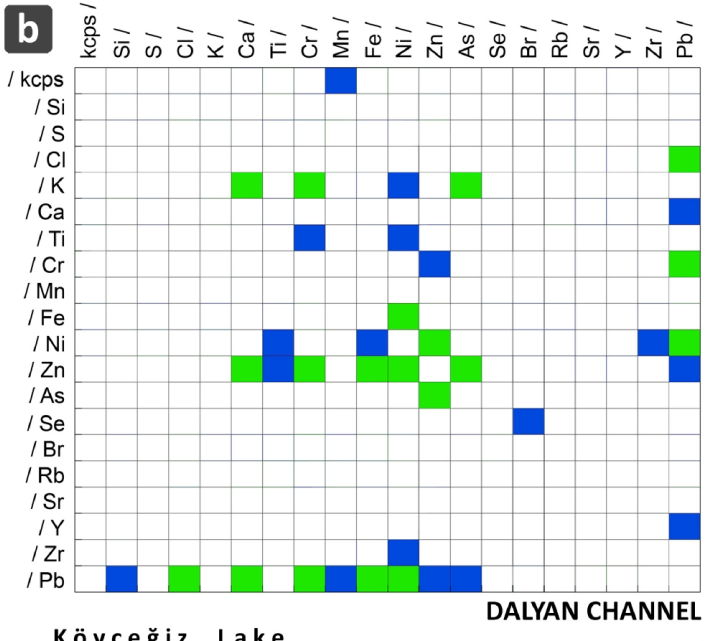

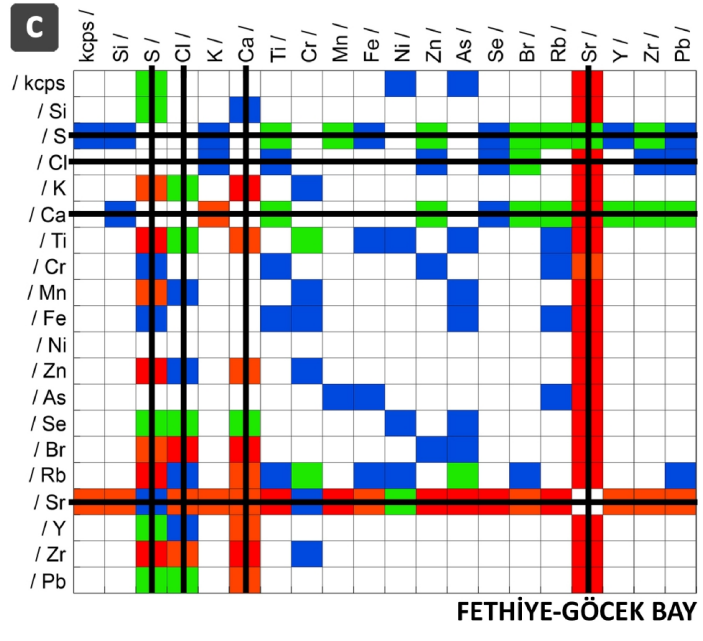

Köyceğiz Lake

- $|Ave_{CLC} \pm 2.5\sigma_{CLC}| \leq |Ave_{HLC}|$
- $|Ave_{CLC} \pm 2.0\sigma_{CLC}| \leq |Ave_{HLC}| < |Ave_{CLC} \pm 2.5\sigma_{CLC}|$
- $|Ave_{CLC} \pm 1.5\sigma_{CLC}| \leq |Ave_{HLC}| < |Ave_{CLC} \pm 2.0\sigma_{CLC}|$
- $|Ave_{CLC} \pm 1.0\sigma_{CLC}| \leq |Ave_{HLC}| < |Ave_{CLC} \pm 1.5\sigma_{CLC}|$
- $|Ave_{HLC}| < |Ave_{CLC} \pm 1.0\sigma_{CLC}|$

Dalyan Channel

- $|Ave_{CLC} \pm 2.5\sigma_{CLC}| \leq |Ave_{HLC}|$
- $|Ave_{CLC} \pm 2.0\sigma_{CLC}| \leq |Ave_{HLC}| < |Ave_{CLC} \pm 2.5\sigma_{CLC}|$
- $|Ave_{CLC} \pm 1.5\sigma_{CLC}| \leq |Ave_{HLC}| < |Ave_{CLC} \pm 2.0\sigma_{CLC}|$
- $|Ave_{CLC} \pm 1.0\sigma_{CLC}| \leq |Ave_{HLC}| < |Ave_{CLC} \pm 1.5\sigma_{CLC}|$
- $|Ave_{HLC}| < |Ave_{CLC} \pm 1.0\sigma_{CLC}|$

Fethiye-Göcek Bay

- $|Ave_{CLC} \pm 5.0\sigma_{CLC}| \leq |Ave_{HLC}|$
- $|Ave_{CLC} \pm 4.0\sigma_{CLC}| \leq |Ave_{HLC}| < |Ave_{CLC} \pm 5.0\sigma_{CLC}|$
- $|Ave_{CLC} \pm 3.0\sigma_{CLC}| \leq |Ave_{HLC}| < |Ave_{CLC} \pm 4.0\sigma_{CLC}|$
- $|Ave_{CLC} \pm 2.0\sigma_{CLC}| \leq |Ave_{HLC}| < |Ave_{CLC} \pm 3.0\sigma_{CLC}|$
- $|Ave_{HLC}| < |Ave_{CLC} \pm 2.0\sigma_{CLC}|$

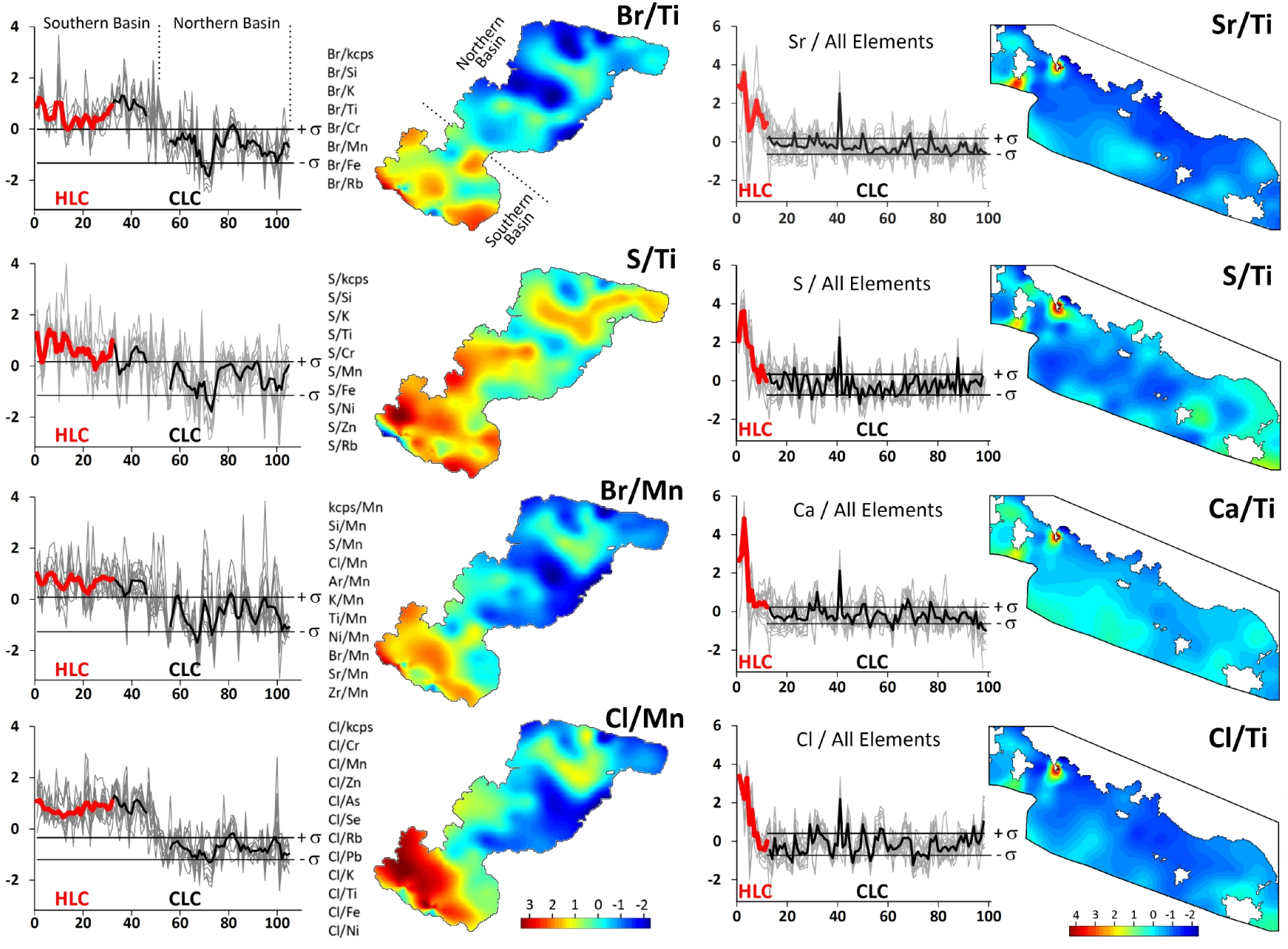
Southern Basin
Northern Basin
HLC
CLC
+ σ
- σ
Br/kcps
Br/Si
Br/K
Br/Ti
Br/Cr
Br/Mn
Br/Fe
Br/Rb
Br/Ti
Northern Basin
Southern Basin
Sr / All Elements
Sr/Ti
S/kcps
S/Si
S/K
S/Ti
S/Cr
S/Mn
S/Fe
S/Ni
S/Zn
S/Rb
S / All Elements
S/Ti
kcps/Mn
Si/Mn
S/Mn
Cl/Mn
Ar/Mn
K/Mn
Ti/Mn
Ni/Mn
Br/Mn
Sr/Mn
Zr/Mn
Br/Mn
Ca / All Elements
Ca/Ti
Cl/kcps
Cl/Cr
Cl/Mn
Cl/Zn
Cl/As
Cl/Se
Cl/Rb
Cl/Pb
Cl/K
Cl/Ti
Cl/Fe
Cl/Ni
Cl/Mn
3 2 1 0 -1 -2
Cl / All Elements
Cl/Ti
4 3 2 1 0 -1 -2

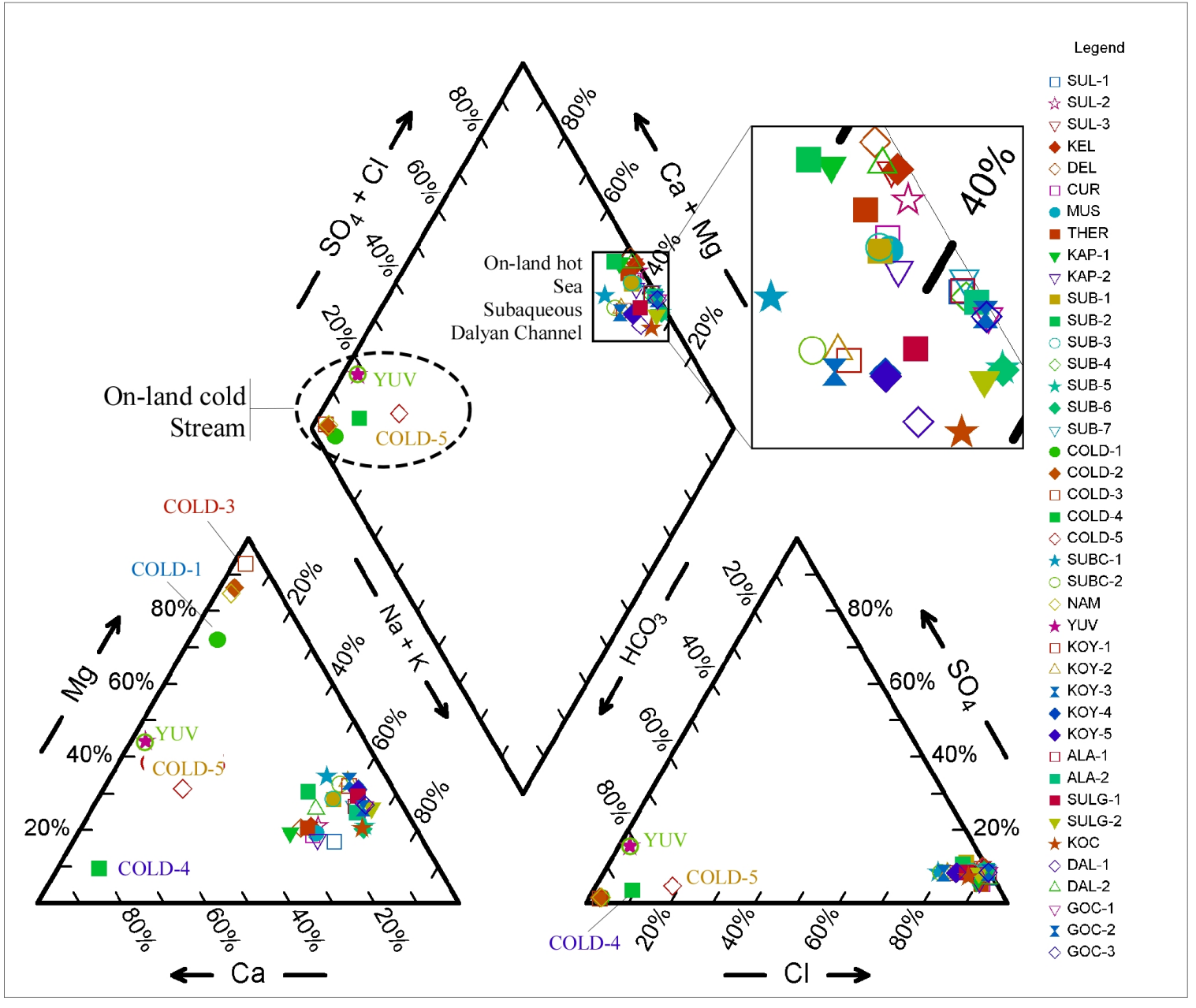
Legend
SUL-1
SUL-2
SUL-3
KEL
DEL
CUR
MUS
THER
KAP-1
KAP-2
SUB-1
SUB-2
SUB-3
SUB-4
SUB-5
SUB-6
SUB-7
COLD-1
COLD-2
COLD-3
COLD-4
COLD-5
SUBC-1
SUBC-2
NAM
YUV
KOY-1
KOY-2
KOY-3
KOY-4
KOY-5
ALA-1
ALA-2
SULG-1
SULG-2
KOC
DAL-1
DAL-2
GOC-1
GOC-2
GOC-3
On-land hot Sea Subaqueous Dalyan Channel
On-land cold Stream
SO4 + Cl
Ca + Mg
Na + K
HCO3
Mg
Ca
SO4
Cl
40%
YUV
COLD-5
COLD-3
COLD-1
COLD-4

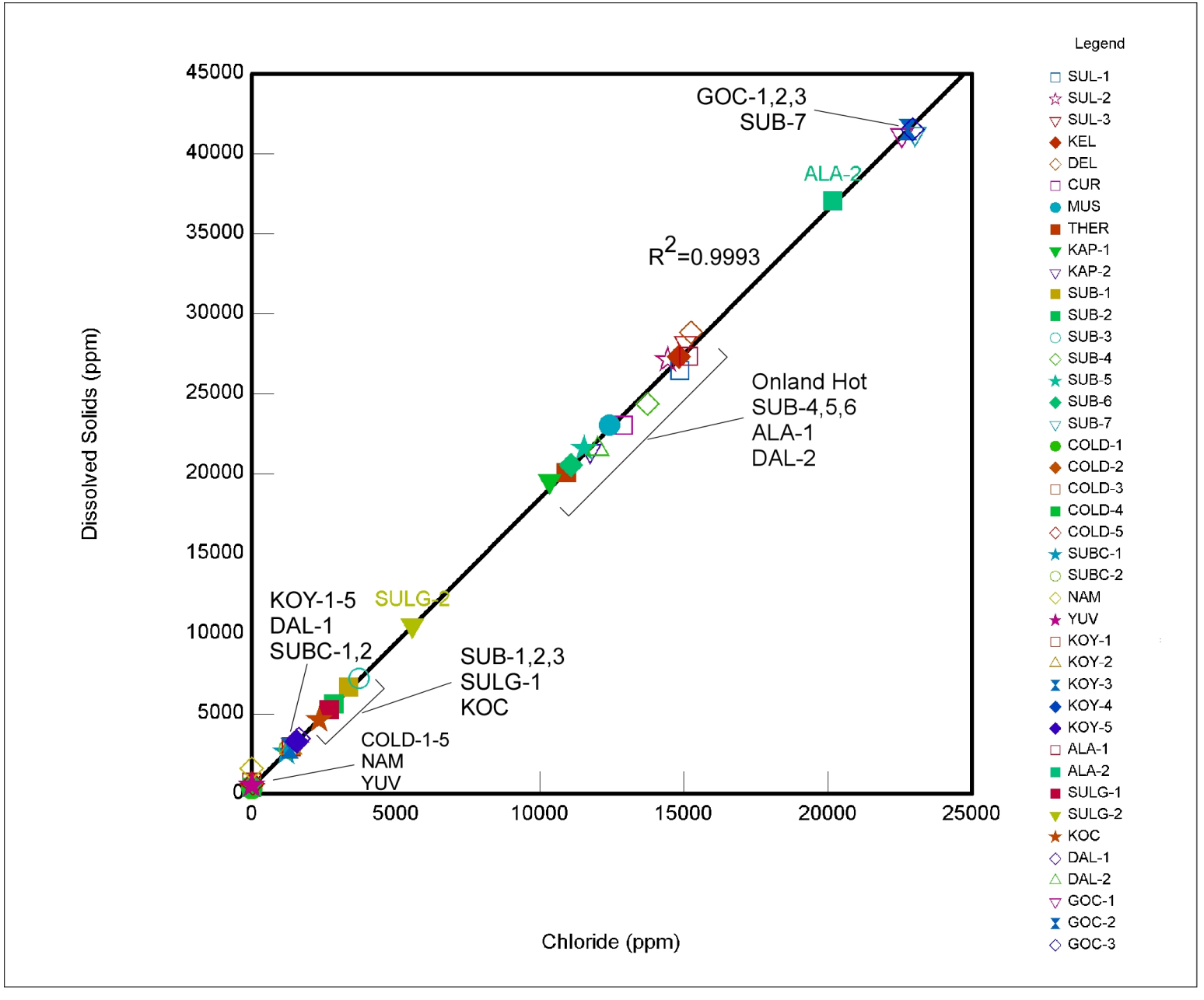
Dissolved Solids (ppm)
Chloride (ppm)
45000
40000
35000
30000
25000
20000
15000
10000
5000
0
0
5000
10000
15000
20000
25000
GOC-1,2,3
SUB-7
ALA-2
R2=0.9993
Onland Hot
SUB-4,5,6
ALA-1
DAL-2
KOY-1-5
DAL-1
SUBC-1,2
SULG-2
SUB-1,2,3
SULG-1
KOC
COLD-1-5
NAM
YUV
Legend
SUL-1
SUL-2
SUL-3
KEL
DEL
CUR
MUS
THER
KAP-1
KAP-2
SUB-1
SUB-2
SUB-3
SUB-4
SUB-5
SUB-6
SUB-7
COLD-1
COLD-2
COLD-3
COLD-4
COLD-5
SUBC-1
SUBC-2
NAM
YUV
KOY-1
KOY-2
KOY-3
KOY-4
KOY-5
ALA-1
ALA-2
SULG-1
SULG-2
KOC
DAL-1
DAL-2
GOC-1
GOC-2
GOC-3

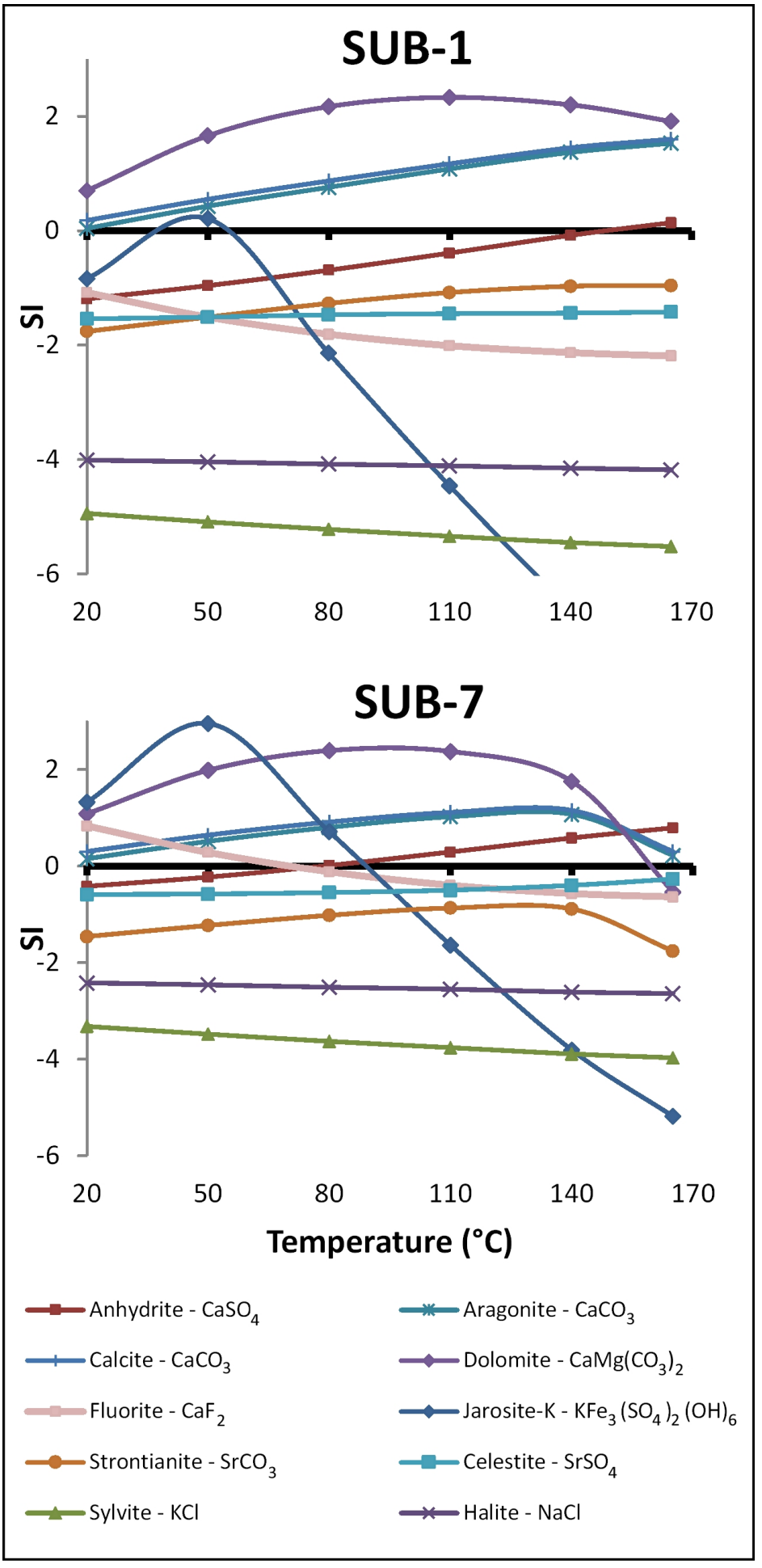
SUB-1
2
0
-2
-4
-6
SI
20
50
80
110
140
170
SUB-7
2
0
-2
-4
-6
SI
20
50
80
110
140
170
Temperature (°C)
Anhydrite - CaSO4
Aragonite - CaCO3
Calcite - CaCO3
Dolomite - CaMg(CO3)2
Fluorite - CaF2
Jarosite-K - KFe3(SO4)2(OH)6
Strontianite - SrCO3
Celestite - SrSO4
Sylvite - KCl
Halite - NaCl

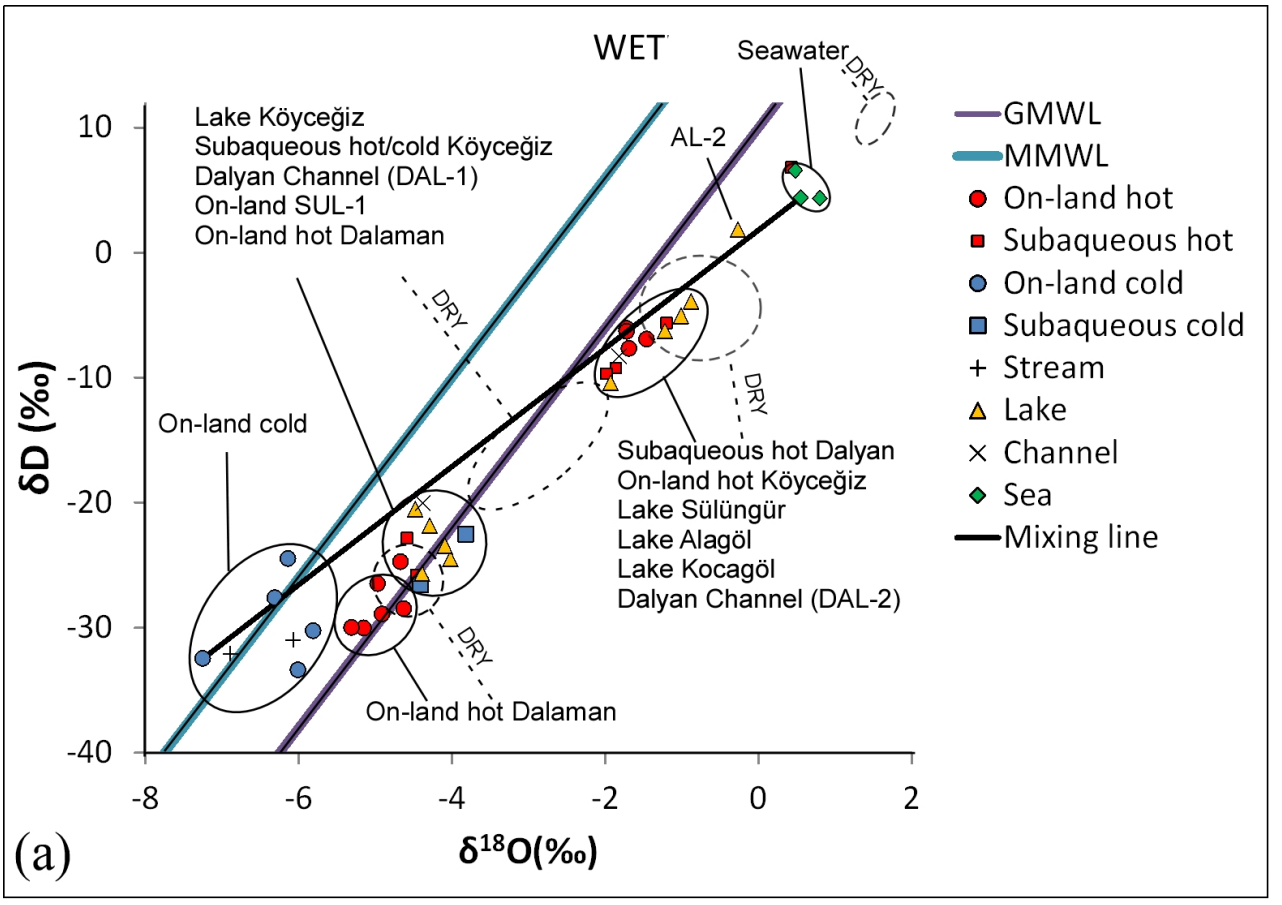
WET
Seawater
DRY
Lake Köyceğiz
Subaqueous hot/cold Köyceğiz
Dalyan Channel (DAL-1)
On-land SUL-1
On-land hot Dalaman
AL-2
DRY
On-land cold
DRY
Subaqueous hot Dalyan
On-land hot Köyceğiz
Lake Sülüngür
Lake Alagöl
Lake Kocagöl
Dalyan Channel (DAL-2)
DRY
On-land hot Dalaman
GMWL
MMWL
On-land hot
Subaqueous hot
On-land cold
Subaqueous cold
Stream
Lake
Channel
Sea
Mixing line
10
0
-10
-20
-30
-40
-8
-6
-4
-2
0
2
δD (‰)
δ18O(‰)
(a)

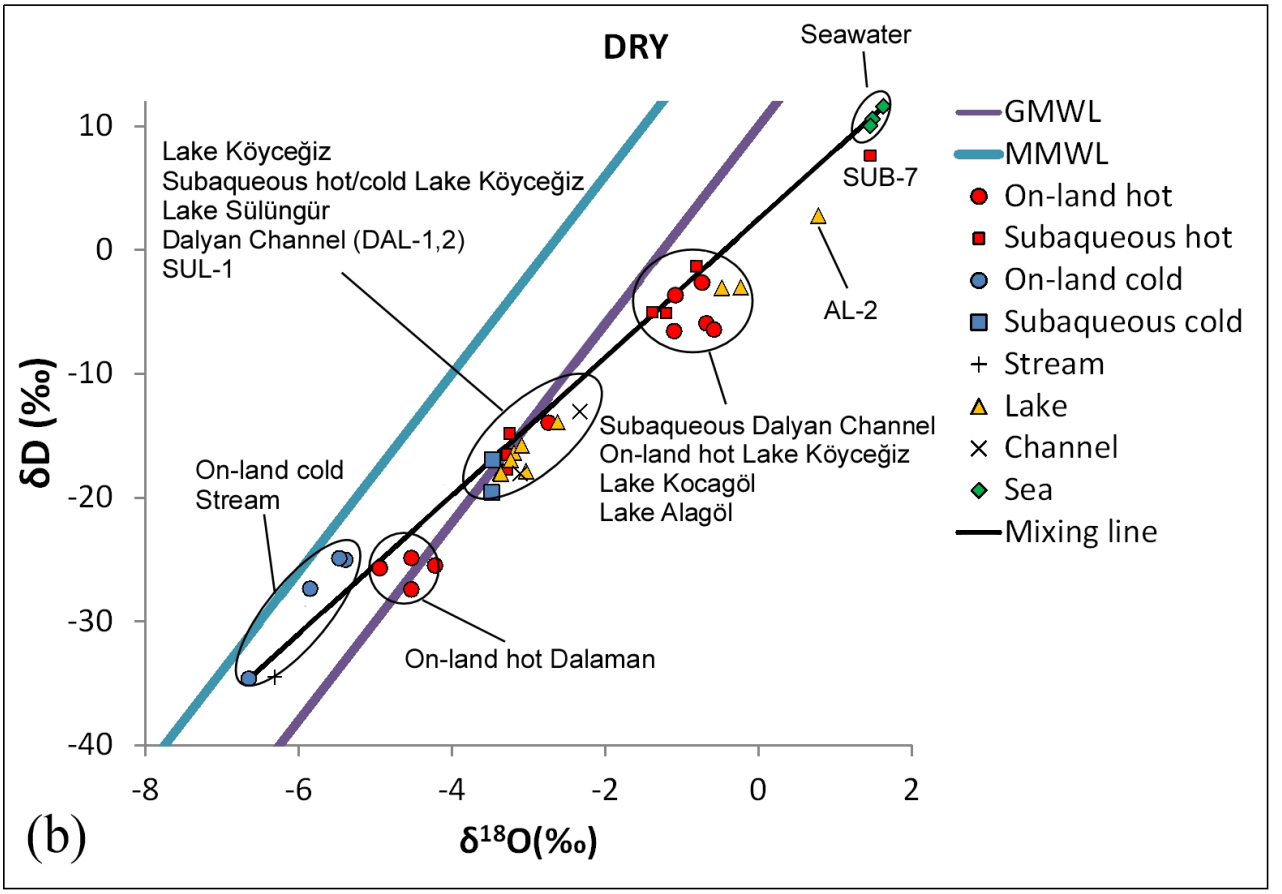
DRY
Seawater
Lake Köyceğiz
Subaqueous hot/cold Lake Köyceğiz
Lake Sülüngür
Dalyan Channel (DAL-1,2)
SUL-1
SUB-7
AL-2
Subaqueous Dalyan Channel
On-land hot Lake Köyceğiz
Lake Kocagöl
Lake Alagöl
On-land cold
Stream
On-land hot Dalaman
GMWL
MMWL
On-land hot
Subaqueous hot
On-land cold
Subaqueous cold
Stream
Lake
Channel
Sea
Mixing line
10
0
-10
-20
-30
-40
-8
-6
-4
-2
0
2
δD (‰)
δ18O(‰)
(b)

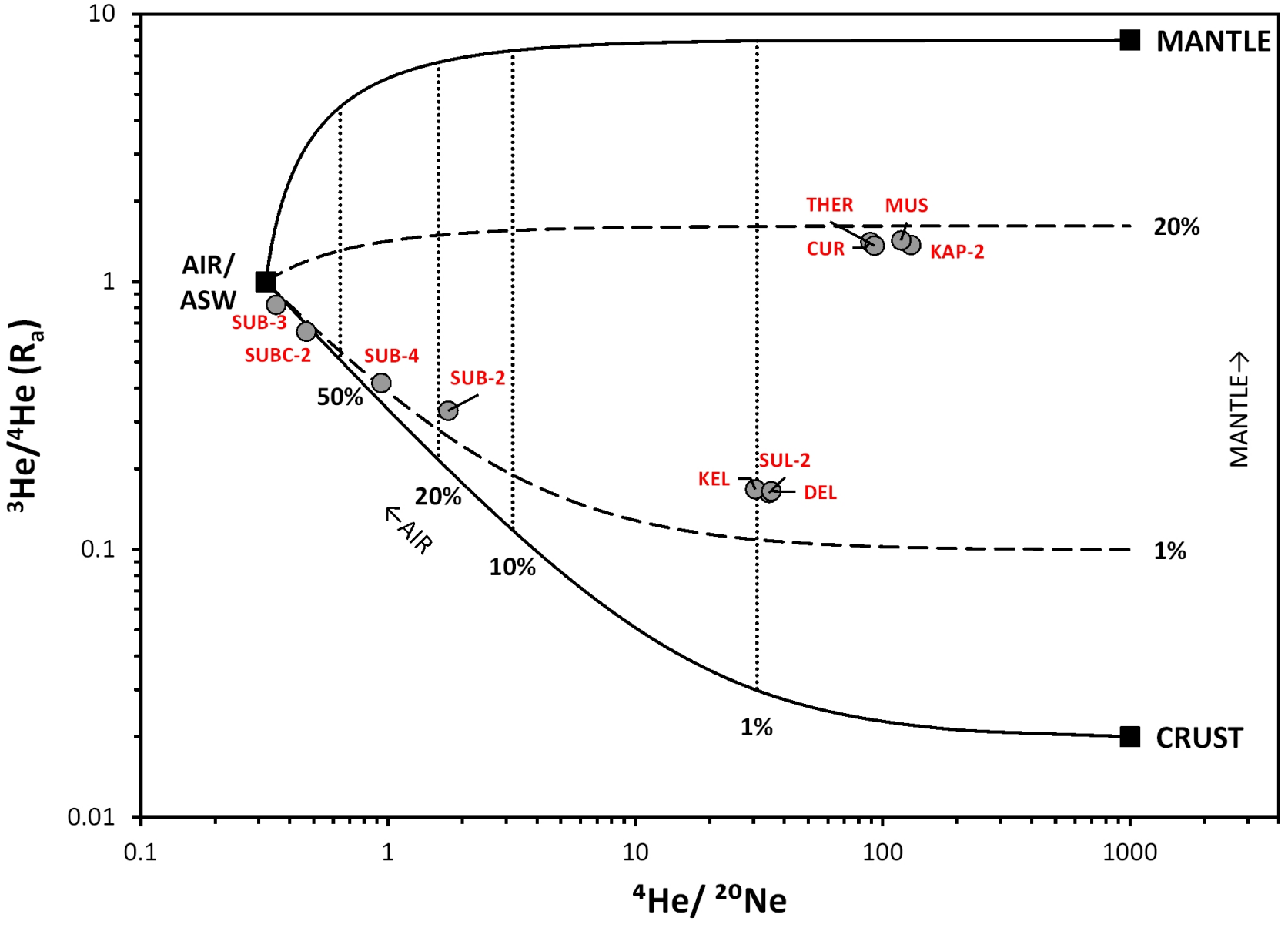
MANTLE
20%
THER
MUS
CUR
KAP-2
AIR/
ASW
SUB-3
SUBC-2
SUB-4
SUB-2
50%
20%
←AIR
10%
1%
SUL-2
KEL
DEL
1%
CRUST
MANTLE→
10
1
0.1
0.01
0.1
1
10
100
1000
$^3He/^4He$ (R_a)
$^4He/^{20}Ne$

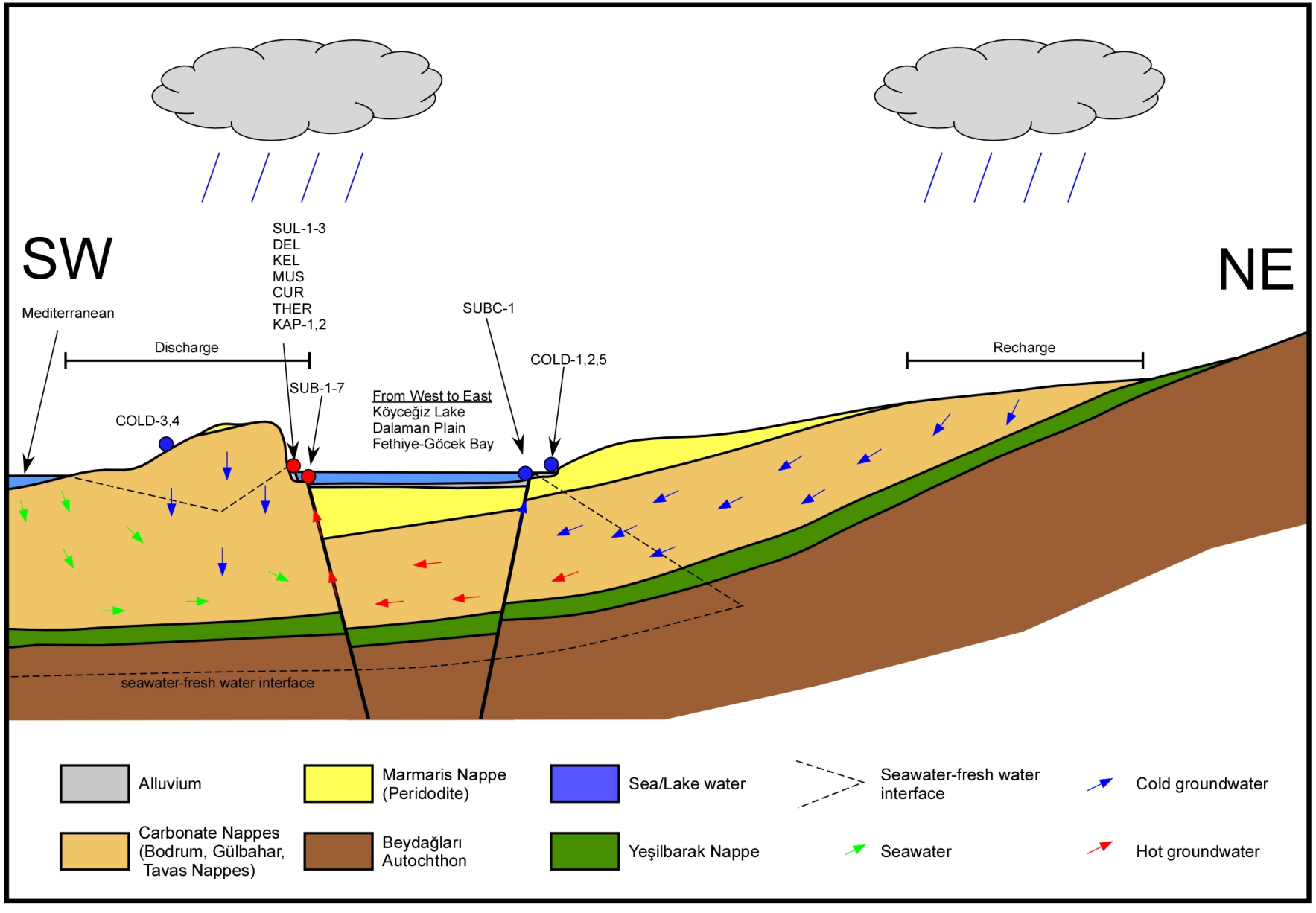
SW
NE
SUL-1-3
DEL
KEL
MUS
CUR
THER
KAP-1,2
SUBC-1
Mediterranean
Discharge
Recharge
COLD-1,2,5
SUB-1-7
From West to East
Köyceğiz Lake
Dalaman Plain
Fethiye-Göcek Bay
COLD-3,4
seawater-fresh water interface
Alluvium
Marmaris Nappe
(Peridodite)
Sea/Lake water
Seawater-fresh water
interface
Cold groundwater
Carbonate Nappes
(Bodrum, Gülbahar,
Tavas Nappes)
Beydağları
Autochthon
Yeşilbarak Nappe
Seawater
Hot groundwater

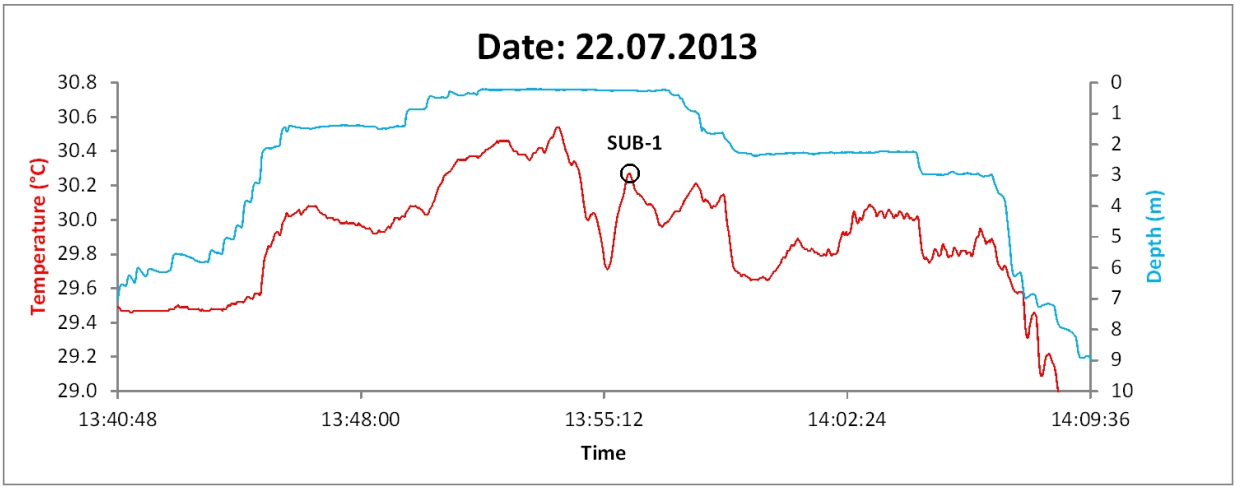
Date: 22.07.2013
Temperature (°C)
Depth (m)
SUB-1
30.8
30.6
30.4
30.2
30.0
29.8
29.6
29.4
29.2
29.0
0
1
2
3
4
5
6
7
8
9
10
13:40:48
13:48:00
13:55:12
14:02:24
14:09:36
Time

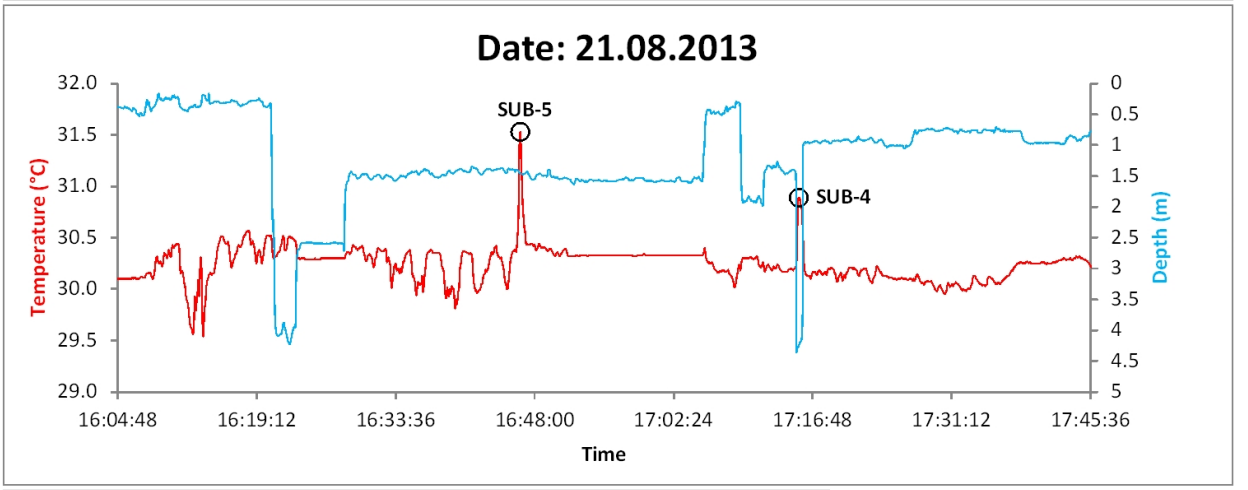
Date: 21.08.2013
Temperature (°C)
Depth (m)
SUB-5
SUB-4
32.0
31.5
31.0
30.5
30.0
29.5
29.0
0
0.5
1
1.5
2
2.5
3
3.5
4
4.5
5
16:04:48
16:19:12
16:33:36
16:48:00
17:02:24
17:16:48
17:31:12
17:45:36
Time

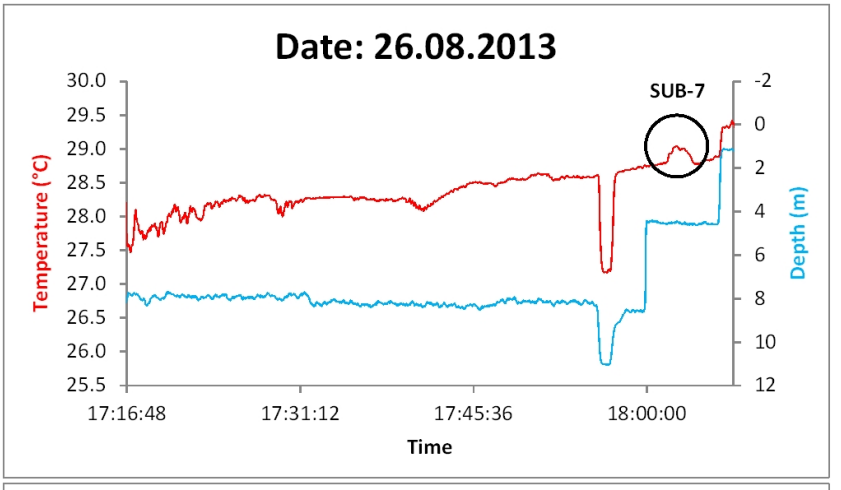
Date: 26.08.2013
Temperature (°C)
Depth (m)
SUB-7
30.0
29.5
29.0
28.5
28.0
27.5
27.0
26.5
26.0
25.5
-2
0
2
4
6
8
10
12
17:16:48
17:31:12
17:45:36
18:00:00
Time

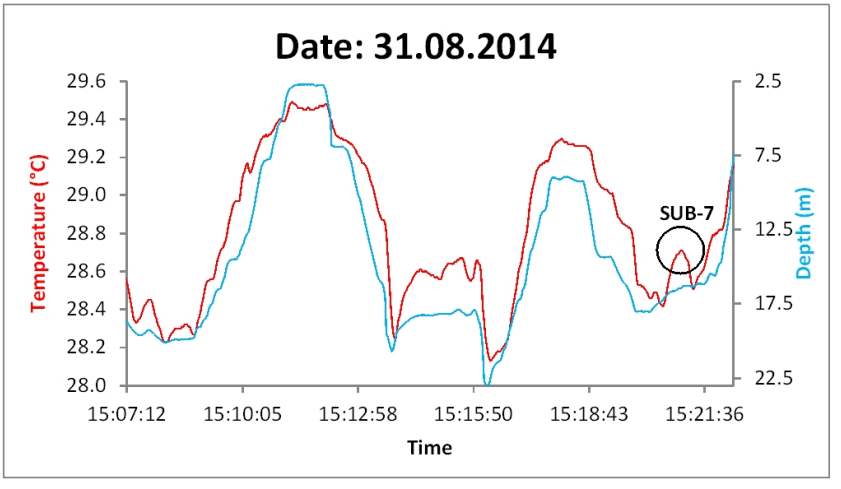
Date: 31.08.2014
Temperature (°C)
Depth (m)
SUB-7
29.6
29.4
29.2
29.0
28.8
28.6
28.4
28.2
28.0
2.5
7.5
12.5
17.5
22.5
15:07:12
15:10:05
15:12:58
15:15:50
15:18:43
15:21:36
Time


GPS Speed
4.0
Arrive
16:07
Wtr Tmp
30.67
Dist (Dest)
970
Off Course
L409
Bearing
153
30m
6.9
0
50kHz
10
Time
15:54:32
Position
35 S 0642722
UTM 4082886

SUB-2

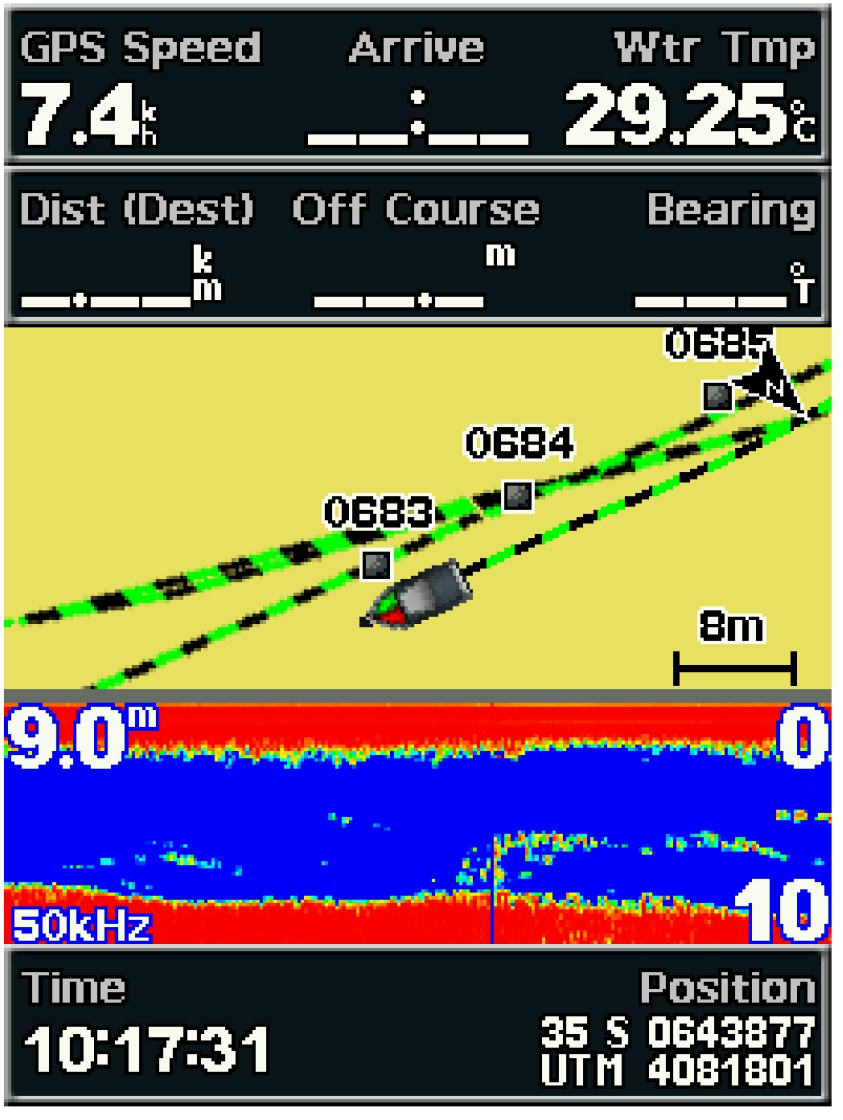
GPS Speed
7.4
Arrive
__:__
Wtr Tmp
29.25
Dist (Dest)
Off Course
Bearing
0685
0684
0683
8m
9.0
0
50kHz
10
Time
10:17:31
Position
35 S 0643877
UTM 4081801

SUB-3

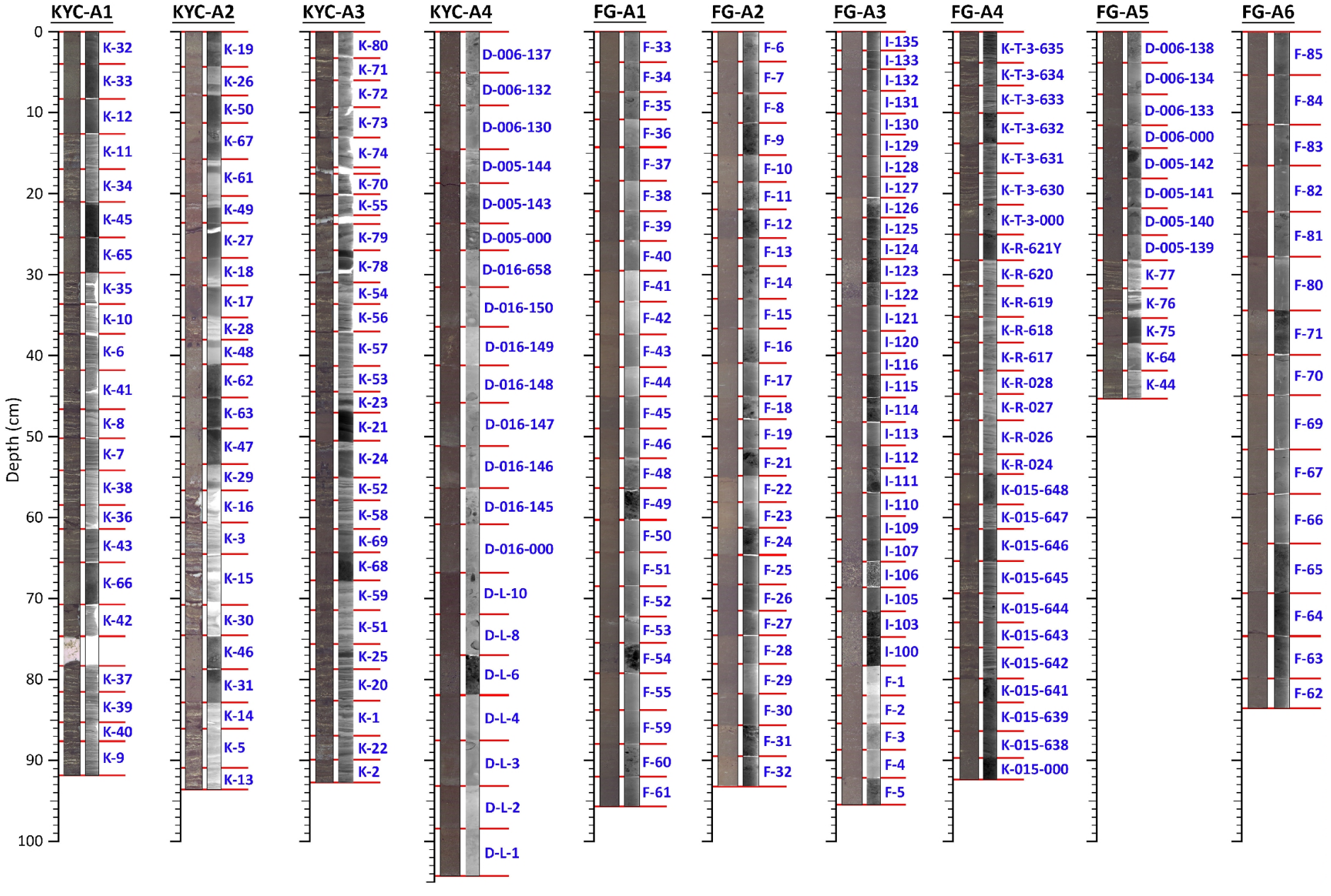
KYC-A1
KYC-A2
KYC-A3
KYC-A4
FG-A1
FG-A2
FG-A3
FG-A4
FG-A5
FG-A6
Depth (cm)
0
10
20
30
40
50
60
70
80
90
100
K-32
K-33
K-12
K-11
K-34
K-45
K-65
K-35
K-10
K-6
K-41
K-8
K-7
K-38
K-36
K-43
K-66
K-42
K-37
K-39
K-40
K-9
K-19
K-26
K-50
K-67
K-61
K-49
K-27
K-18
K-17
K-28
K-48
K-62
K-63
K-47
K-29
K-16
K-3
K-15
K-30
K-46
K-31
K-14
K-5
K-13
K-80
K-71
K-72
K-73
K-74
K-70
K-55
K-79
K-78
K-54
K-56
K-57
K-53
K-23
K-21
K-24
K-52
K-58
K-69
K-68
K-59
K-51
K-25
K-20
K-1
K-22
K-2
D-006-137
D-006-132
D-006-130
D-005-144
D-005-143
D-005-000
D-016-658
D-016-150
D-016-149
D-016-148
D-016-147
D-016-146
D-016-145
D-016-000
D-L-10
D-L-8
D-L-6
D-L-4
D-L-3
D-L-2
D-L-1
F-33
F-34
F-35
F-36
F-37
F-38
F-39
F-40
F-41
F-42
F-43
F-44
F-45
F-46
F-48
F-49
F-50
F-51
F-52
F-53
F-54
F-55
F-59
F-60
F-61
F-6
F-7
F-8
F-9
F-10
F-11
F-12
F-13
F-14
F-15
F-16
F-17
F-18
F-19
F-21
F-22
F-23
F-24
F-25
F-26
F-27
F-28
F-29
F-30
F-31
F-32
I-135
I-133
I-132
I-131
I-130
I-129
I-128
I-127
I-126
I-125
I-124
I-123
I-122
I-121
I-120
I-116
I-115
I-114
I-113
I-112
I-111
I-110
I-109
I-107
I-106
I-105
I-103
I-100
F-1
F-2
F-3
F-4
F-5
K-T-3-635
K-T-3-634
K-T-3-633
K-T-3-632
K-T-3-631
K-T-3-630
K-T-3-000
K-R-621Y
K-R-620
K-R-619
K-R-618
K-R-617
K-R-028
K-R-027
K-R-026
K-R-024
K-015-648
K-015-647
K-015-646
K-015-645
K-015-644
K-015-643
K-015-642
K-015-641
K-015-639
K-015-638
K-015-000
D-006-138
D-006-134
D-006-133
D-006-000
D-005-142
D-005-141
D-005-140
D-005-139
K-77
K-76
K-75
K-64
K-44
F-85
F-84
F-83
F-82
F-81
F-80
F-71
F-70
F-69
F-67
F-66
F-65
F-64
F-63
F-62

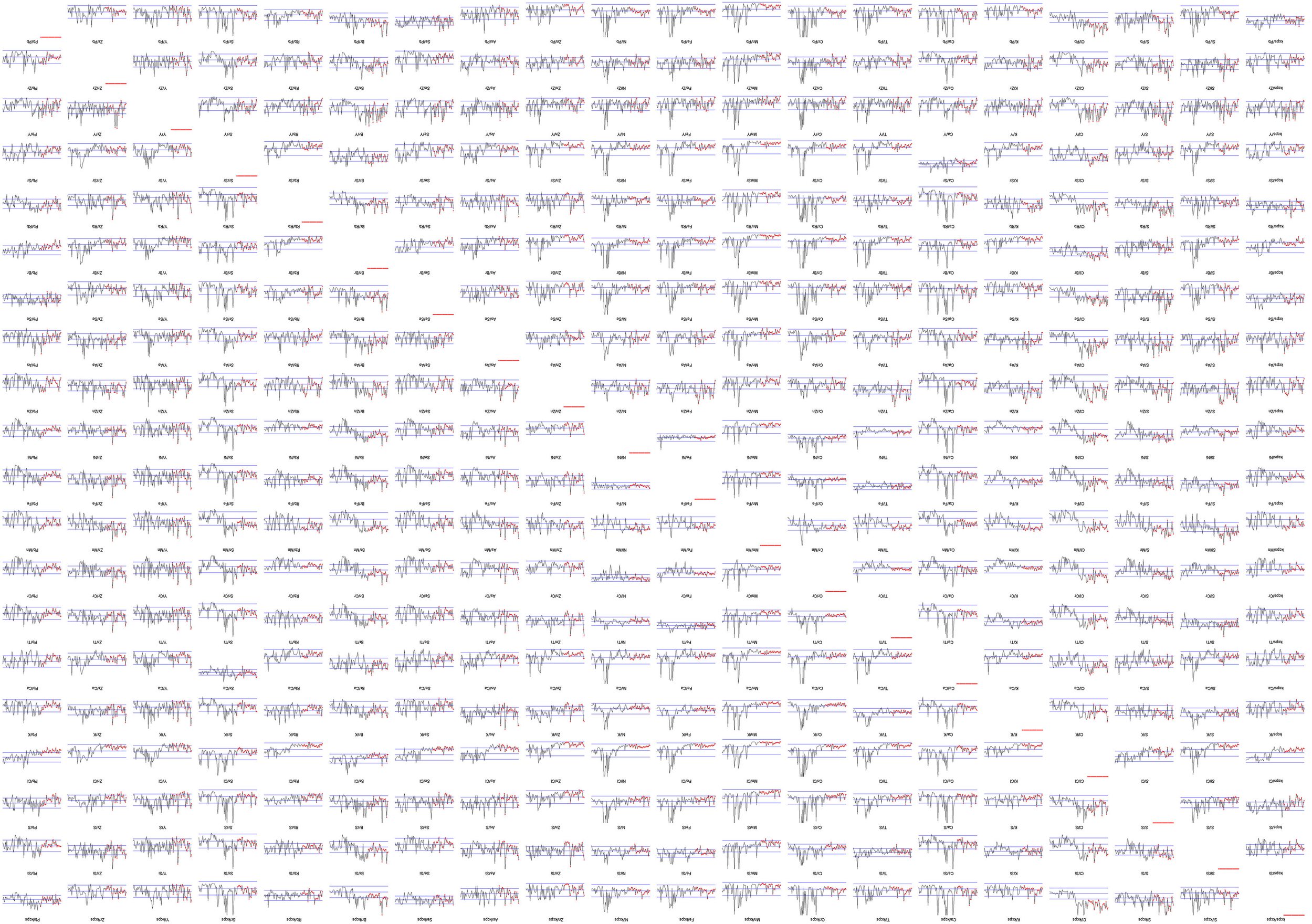
Kcps/Pb
Si/Pb
S/Pb
Cl/Pb
K/Pb
Ca/Pb
Ti/Pb
Cr/Pb
Mn/Pb
Fe/Pb
Ni/Pb
Zn/Pb
As/Pb
Se/Pb
Br/Pb
Rb/Pb
Sr/Pb
Y/Pb
Zr/Pb
Pb/Pb
Kcps/Z
Si/Z
S/Z
Cl/Z
K/Z
Ca/Z
Ti/Z
Cr/Z
Mn/Z
Fe/Z
Ni/Z
Zn/Z
As/Z
Se/Z
Br/Z
Rb/Z
Sr/Z
Y/Z
Zr/Z
Pb/Z
Kcps/Y
Si/Y
S/Y
Cl/Y
K/Y
Ca/Y
Ti/Y
Cr/Y
Mn/Y
Fe/Y
Ni/Y
Zn/Y
As/Y
Se/Y
Br/Y
Rb/Y
Sr/Y
Y/Y
Zr/Y
Pb/Y
Kcps/Sr
Si/Sr
S/Sr
Cl/Sr
K/Sr
Ca/Sr
Ti/Sr
Cr/Sr
Mn/Sr
Fe/Sr
Ni/Sr
Zn/Sr
As/Sr
Se/Sr
Br/Sr
Rb/Sr
Sr/Sr
Y/Sr
Zr/Sr
Pb/Sr
Kcps/Rb
Si/Rb
S/Rb
Cl/Rb
K/Rb
Ca/Rb
Ti/Rb
Cr/Rb
Mn/Rb
Fe/Rb
Ni/Rb
Zn/Rb
As/Rb
Se/Rb
Br/Rb
Rb/Rb
Sr/Rb
Y/Rb
Zr/Rb
Pb/Rb
Kcps/Br
Si/Br
S/Br
Cl/Br
K/Br
Ca/Br
Ti/Br
Cr/Br
Mn/Br
Fe/Br
Ni/Br
Zn/Br
As/Br
Se/Br
Br/Br
Rb/Br
Sr/Br
Y/Br
Zr/Br
Pb/Br
Kcps/Se
Si/Se
S/Se
Cl/Se
K/Se
Ca/Se
Ti/Se
Cr/Se
Mn/Se
Fe/Se
Ni/Se
Zn/Se
As/Se
Se/Se
Br/Se
Rb/Se
Sr/Se
Y/Se
Zr/Se
Pb/Se
Kcps/As
Si/As
S/As
Cl/As
K/As
Ca/As
Ti/As
Cr/As
Mn/As
Fe/As
Ni/As
Zn/As
As/As
Se/As
Br/As
Rb/As
Sr/As
Y/As
Zr/As
Pb/As
Kcps/Zn
Si/Zn
S/Zn
Cl/Zn
K/Zn
Ca/Zn
Ti/Zn
Cr/Zn
Mn/Zn
Fe/Zn
Ni/Zn
Zn/Zn
As/Zn
Se/Zn
Br/Zn
Rb/Zn
Sr/Zn
Y/Zn
Zr/Zn
Pb/Zn
Kcps/Ni
Si/Ni
S/Ni
Cl/Ni
K/Ni
Ca/Ni
Ti/Ni
Cr/Ni
Mn/Ni
Fe/Ni
Ni/Ni
Zn/Ni
As/Ni
Se/Ni
Br/Ni
Rb/Ni
Sr/Ni
Y/Ni
Zr/Ni
Pb/Ni
Kcps/Fe
Si/Fe
S/Fe
Cl/Fe
K/Fe
Ca/Fe
Ti/Fe
Cr/Fe
Mn/Fe
Fe/Fe
Ni/Fe
Zn/Fe
As/Fe
Se/Fe
Br/Fe
Rb/Fe
Sr/Fe
Y/Fe
Zr/Fe
Pb/Fe
Kcps/Mn
Si/Mn
S/Mn
Cl/Mn
K/Mn
Ca/Mn
Ti/Mn
Cr/Mn
Mn/Mn
Fe/Mn
Ni/Mn
Zn/Mn
As/Mn
Se/Mn
Br/Mn
Rb/Mn
Sr/Mn
Y/Mn
Zr/Mn
Pb/Mn
Kcps/Cr
Si/Cr
S/Cr
Cl/Cr
K/Cr
Ca/Cr
Ti/Cr
Cr/Cr
Mn/Cr
Fe/Cr
Ni/Cr
Zn/Cr
As/Cr
Se/Cr
Br/Cr
Rb/Cr
Sr/Cr
Y/Cr
Zr/Cr
Pb/Cr
Kcps/Ti
Si/Ti
S/Ti
Cl/Ti
K/Ti
Ca/Ti
Ti/Ti
Cr/Ti
Mn/Ti
Fe/Ti
Ni/Ti
Zn/Ti
As/Ti
Se/Ti
Br/Ti
Rb/Ti
Sr/Ti
Y/Ti
Zr/Ti
Pb/Ti
Kcps/Ca
Si/Ca
S/Ca
Cl/Ca
K/Ca
Ca/Ca
Ti/Ca
Cr/Ca
Mn/Ca
Fe/Ca
Ni/Ca
Zn/Ca
As/Ca
Se/Ca
Br/Ca
Rb/Ca
Sr/Ca
Y/Ca
Zr/Ca
Pb/Ca
Kcps/K
Si/K
S/K
Cl/K
K/K
Ca/K
Ti/K
Cr/K
Mn/K
Fe/K
Ni/K
Zn/K
As/K
Se/K
Br/K
Rb/K
Sr/K
Y/K
Zr/K
Pb/K
Kcps/Cl
Si/Cl
S/Cl
Cl/Cl
K/Cl
Ca/Cl
Ti/Cl
Cr/Cl
Mn/Cl
Fe/Cl
Ni/Cl
Zn/Cl
As/Cl
Se/Cl
Br/Cl
Rb/Cl
Sr/Cl
Y/Cl
Zr/Cl
Pb/Cl
Kcps/S
Si/S
S/S
Cl/S
K/S
Ca/S
Ti/S
Cr/S
Mn/S
Fe/S
Ni/S
Zn/S
As/S
Se/S
Br/S
Rb/S
Sr/S
Y/S
Zr/S
Pb/S
Kcps/Si
Si/Si
S/Si
Cl/Si
K/Si
Ca/Si
Ti/Si
Cr/Si
Mn/Si
Fe/Si
Ni/Si
Zn/Si
As/Si
Se/Si
Br/Si
Rb/Si
Sr/Si
Y/Si
Zr/Si
Pb/Si
Kcps/Kcps
Si/Kcps
S/Kcps
Cl/Kcps
K/Kcps
Ca/Kcps
Ti/Kcps
Cr/Kcps
Mn/Kcps
Fe/Kcps
Ni/Kcps
Zn/Kcps
As/Kcps
Se/Kcps
Br/Kcps
Rb/Kcps
Sr/Kcps
Y/Kcps
Zr/Kcps
Pb/Kcps


kcps/Pb
Si/Pb
S/Pb
Ca/Pb
K/Pb
Cl/Pb
C/Pb
T1/Pb
Mn/Pb
Fe/Pb
Ni/Pb
Zn/Pb
As/Pb
Se/Pb
Ba/Pb
Rb/Pb
Si/Pb
Si/Pb
Pb/Pb
kcps/Zn
Si/Zn
S/Zn
Ca/Zn
K/Zn
Cl/Zn
C/Zn
T1/Zn
Mn/Zn
Fe/Zn
Ni/Zn
Zn/Zn
As/Zn
Se/Zn
Ba/Zn
Rb/Zn
Si/Zn
Si/Zn
Pb/Zn
kcps/As
Si/As
S/As
Ca/As
K/As
Cl/As
C/As
T1/As
Mn/As
Fe/As
Ni/As
Zn/As
As/As
Se/As
Ba/As
Rb/As
Si/As
Si/As
Pb/As
kcps/Se
Si/Se
S/Se
Ca/Se
K/Se
Cl/Se
C/Se
T1/Se
Mn/Se
Fe/Se
Ni/Se
Zn/Se
As/Se
Se/Se
Ba/Se
Rb/Se
Si/Se
Si/Se
Pb/Se
kcps/Ba
Si/Ba
S/Ba
Ca/Ba
K/Ba
Cl/Ba
C/Ba
T1/Ba
Mn/Ba
Fe/Ba
Ni/Ba
Zn/Ba
As/Ba
Se/Ba
Ba/Ba
Rb/Ba
Si/Ba
Si/Ba
Pb/Ba
kcps/Rb
Si/Rb
S/Rb
Ca/Rb
K/Rb
Cl/Rb
C/Rb
T1/Rb
Mn/Rb
Fe/Rb
Ni/Rb
Zn/Rb
As/Rb
Se/Rb
Ba/Rb
Rb/Rb
Si/Rb
Si/Rb
Pb/Rb
kcps/Y
Si/Y
S/Y
Ca/Y
K/Y
Cl/Y
C/Y
T1/Y
Mn/Y
Fe/Y
Ni/Y
Zn/Y
As/Y
Se/Y
Ba/Y
Rb/Y
Si/Y
Si/Y
Pb/Y
kcps/Z
Si/Z
S/Z
Ca/Z
K/Z
Cl/Z
C/Z
T1/Z
Mn/Z
Fe/Z
Ni/Z
Zn/Z
As/Z
Se/Z
Ba/Z
Rb/Z
Si/Z
Si/Z
Pb/Z
kcps/Si
Si/Si
S/Si
Ca/Si
K/Si
Cl/Si
C/Si
T1/Si
Mn/Si
Fe/Si
Ni/Si
Zn/Si
As/Si
Se/Si
Ba/Si
Rb/Si
Si/Si
Si/Si
Pb/Si
kcps/Ca
Si/Ca
S/Ca
Ca/Ca
K/Ca
Cl/Ca
C/Ca
T1/Ca
Mn/Ca
Fe/Ca
Ni/Ca
Zn/Ca
As/Ca
Se/Ca
Ba/Ca
Rb/Ca
Si/Ca
Si/Ca
Pb/Ca
kcps/K
Si/K
S/K
Ca/K
K/K
Cl/K
C/K
T1/K
Mn/K
Fe/K
Ni/K
Zn/K
As/K
Se/K
Ba/K
Rb/K
Si/K
Si/K
Pb/K
kcps/Cl
Si/Cl
S/Cl
Ca/Cl
K/Cl
Cl/Cl
C/Cl
T1/Cl
Mn/Cl
Fe/Cl
Ni/Cl
Zn/Cl
As/Cl
Se/Cl
Ba/Cl
Rb/Cl
Si/Cl
Si/Cl
Pb/Cl
kcps/S
Si/S
S/S
Ca/S
K/S
Cl/S
C/S
T1/S
Mn/S
Fe/S
Ni/S
Zn/S
As/S
Se/S
Ba/S
Rb/S
Si/S
Si/S
Pb/S
kcps/Si
Si/Si
S/Si
Ca/Si
K/Si
Cl/Si
C/Si
T1/Si
Mn/Si
Fe/Si
Ni/Si
Zn/Si
As/Si
Se/Si
Ba/Si
Rb/Si
Si/Si
Si/Si
Pb/Si
kcps/kcps
Si/kcps
S/kcps
Ca/kcps
K/kcps
Cl/kcps
C/kcps
T1/kcps
Mn/kcps
Fe/kcps
Ni/kcps
Zn/kcps
As/kcps
Se/kcps
Ba/kcps
Rb/kcps
Si/kcps
Si/kcps
Pb/kcps
kcps/N
Si/N
S/N
Ca/N
K/N
Cl/N
C/N
T1/N
Mn/N
Fe/N
Ni/N
Zn/N
As/N
Se/N
Ba/N
Rb/N
Si/N
Si/N
Pb/N
kcps/Fe
Si/Fe
S/Fe
Ca/Fe
K/Fe
Cl/Fe
C/Fe
T1/Fe
Mn/Fe
Fe/Fe
Ni/Fe
Zn/Fe
As/Fe
Se/Fe
Ba/Fe
Rb/Fe
Si/Fe
Si/Fe
Pb/Fe
kcps/Mn
Si/Mn
S/Mn
Ca/Mn
K/Mn
Cl/Mn
C/Mn
T1/Mn
Mn/Mn
Fe/Mn
Ni/Mn
Zn/Mn
As/Mn
Se/Mn
Ba/Mn
Rb/Mn
Si/Mn
Si/Mn
Pb/Mn
kcps/Cr
Si/Cr
S/Cr
Ca/Cr
K/Cr
Cl/Cr
C/Cr
T1/Cr
Mn/Cr
Fe/Cr
Ni/Cr
Zn/Cr
As/Cr
Se/Cr
Ba/Cr
Rb/Cr
Si/Cr
Si/Cr
Pb/Cr
kcps/Fl
Si/Fl
S/Fl
Ca/Fl
K/Fl
Cl/Fl
C/Fl
T1/Fl
Mn/Fl
Fe/Fl
Ni/Fl
Zn/Fl
As/Fl
Se/Fl
Ba/Fl
Rb/Fl
Si/Fl
Si/Fl
Pb/Fl
kcps/Ca
Si/Ca
S/Ca
Ca/Ca
K/Ca
Cl/Ca
C/Ca
T1/Ca
Mn/Ca
Fe/Ca
Ni/Ca
Zn/Ca
As/Ca
Se/Ca
Ba/Ca
Rb/Ca
Si/Ca
Si/Ca
Pb/Ca
kcps/K
Si/K
S/K
Ca/K
K/K
Cl/K
C/K
T1/K
Mn/K
Fe/K
Ni/K
Zn/K
As/K
Se/K
Ba/K
Rb/K
Si/K
Si/K
Pb/K
kcps/Cl
Si/Cl
S/Cl
Ca/Cl
K/Cl
Cl/Cl
C/Cl
T1/Cl
Mn/Cl
Fe/Cl
Ni/Cl
Zn/Cl
As/Cl
Se/Cl
Ba/Cl
Rb/Cl
Si/Cl
Si/Cl
Pb/Cl
kcps/S
Si/S
S/S
Ca/S
K/S
Cl/S
C/S
T1/S
Mn/S
Fe/S
Ni/S
Zn/S
As/S
Se/S
Ba/S
Rb/S
Si/S
Si/S
Pb/S
kcps/Si
Si/Si
S/Si
Ca/Si
K/Si
Cl/Si
C/Si
T1/Si
Mn/Si
Fe/Si
Ni/Si
Zn/Si
As/Si
Se/Si
Ba/Si
Rb/Si
Si/Si
Si/Si
Pb/Si
kcps/kcps
Si/kcps
S/kcps
Ca/kcps
K/kcps
Cl/kcps
C/kcps
T1/kcps
Mn/kcps
Fe/kcps
Ni/kcps
Zn/kcps
As/kcps
Se/kcps
Ba/kcps
Rb/kcps
Si/kcps
Si/kcps
Pb/kcps

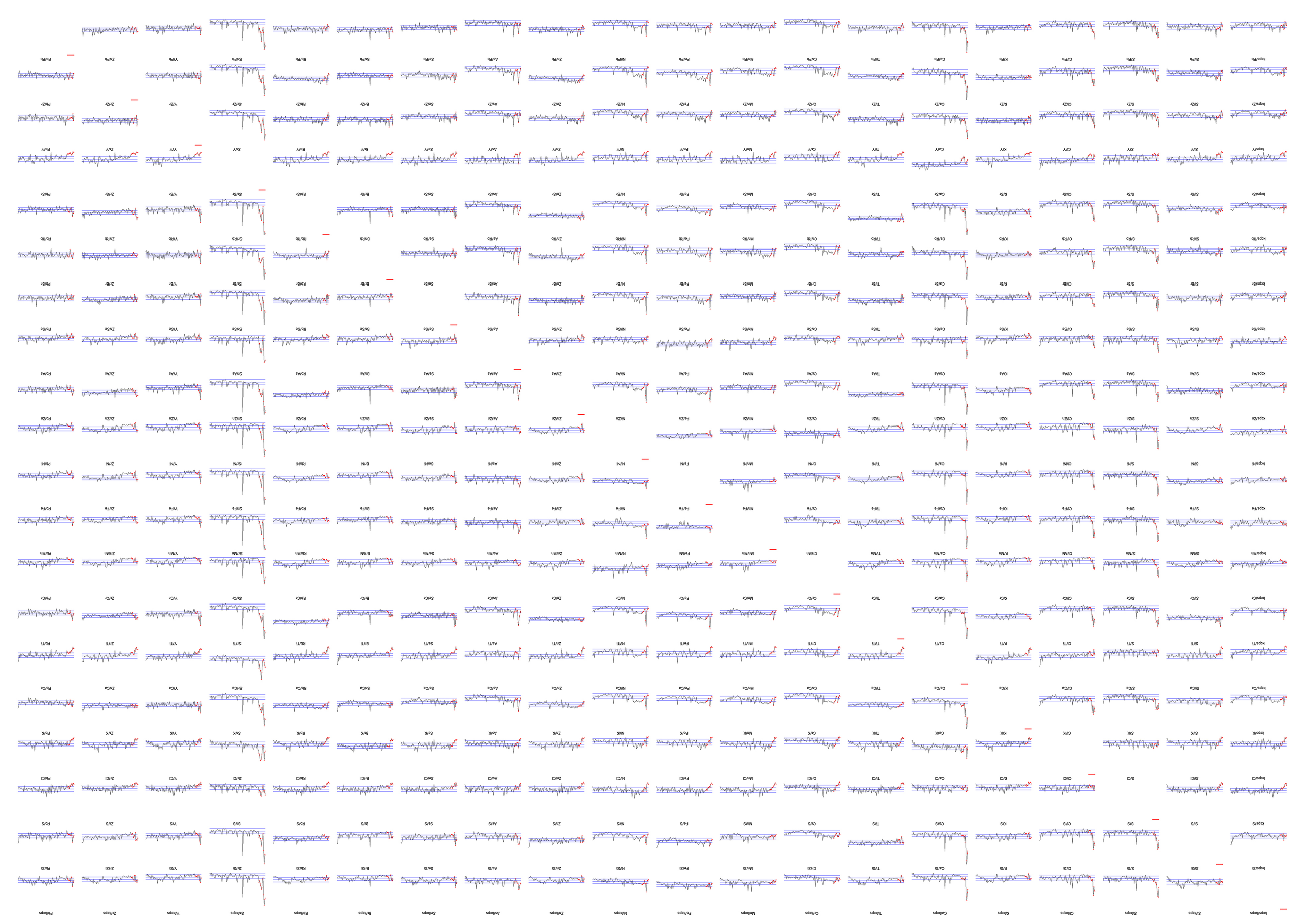
kcps/Pb
Si/Pb
S/Pb
O/Pb
K/Pb
Ca/Pb
Ti/Pb
Cr/Pb
Mn/Pb
Fe/Pb
Ni/Pb
Zn/Pb
As/Pb
Se/Pb
Br/Pb
Rb/Pb
Sr/Pb
Y/Pb
Zr/Pb
Pb/Pb
kcps/Zr
Si/Zr
S/Zr
O/Zr
K/Zr
Ca/Zr
Ti/Zr
Cr/Zr
Mn/Zr
Fe/Zr
Ni/Zr
Zn/Zr
As/Zr
Se/Zr
Br/Zr
Rb/Zr
Sr/Zr
Y/Zr
Zr/Zr
Pb/Zr
kcps/Y
Si/Y
S/Y
O/Y
K/Y
Ca/Y
Ti/Y
Cr/Y
Mn/Y
Fe/Y
Ni/Y
Zn/Y
As/Y
Se/Y
Br/Y
Rb/Y
Sr/Y
Y/Y
Zr/Y
Pb/Y
kcps/Sr
Si/Sr
S/Sr
O/Sr
K/Sr
Ca/Sr
Ti/Sr
Cr/Sr
Mn/Sr
Fe/Sr
Ni/Sr
Zn/Sr
As/Sr
Se/Sr
Br/Sr
Rb/Sr
Sr/Sr
Y/Sr
Zr/Sr
Pb/Sr
kcps/Rb
Si/Rb
S/Rb
O/Rb
K/Rb
Ca/Rb
Ti/Rb
Cr/Rb
Mn/Rb
Fe/Rb
Ni/Rb
Zn/Rb
As/Rb
Se/Rb
Br/Rb
Rb/Rb
Sr/Rb
Y/Rb
Zr/Rb
Pb/Rb
kcps/Br
Si/Br
S/Br
O/Br
K/Br
Ca/Br
Ti/Br
Cr/Br
Mn/Br
Fe/Br
Ni/Br
Zn/Br
As/Br
Se/Br
Br/Br
Rb/Br
Sr/Br
Y/Br
Zr/Br
Pb/Br
kcps/Se
Si/Se
S/Se
O/Se
K/Se
Ca/Se
Ti/Se
Cr/Se
Mn/Se
Fe/Se
Ni/Se
Zn/Se
As/Se
Se/Se
Br/Se
Rb/Se
Sr/Se
Y/Se
Zr/Se
Pb/Se
kcps/As
Si/As
S/As
O/As
K/As
Ca/As
Ti/As
Cr/As
Mn/As
Fe/As
Ni/As
Zn/As
As/As
Se/As
Br/As
Rb/As
Sr/As
Y/As
Zr/As
Pb/As
kcps/Zn
Si/Zn
S/Zn
O/Zn
K/Zn
Ca/Zn
Ti/Zn
Cr/Zn
Mn/Zn
Fe/Zn
Ni/Zn
Zn/Zn
As/Zn
Se/Zn
Br/Zn
Rb/Zn
Sr/Zn
Y/Zn
Zr/Zn
Pb/Zn
kcps/Ni
Si/Ni
S/Ni
O/Ni
K/Ni
Ca/Ni
Ti/Ni
Cr/Ni
Mn/Ni
Fe/Ni
Ni/Ni
Zn/Ni
As/Ni
Se/Ni
Br/Ni
Rb/Ni
Sr/Ni
Y/Ni
Zr/Ni
Pb/Ni
kcps/Fe
Si/Fe
S/Fe
O/Fe
K/Fe
Ca/Fe
Ti/Fe
Cr/Fe
Mn/Fe
Fe/Fe
Ni/Fe
Zn/Fe
As/Fe
Se/Fe
Br/Fe
Rb/Fe
Sr/Fe
Y/Fe
Zr/Fe
Pb/Fe
kcps/Mn
Si/Mn
S/Mn
O/Mn
K/Mn
Ca/Mn
Ti/Mn
Cr/Mn
Mn/Mn
Fe/Mn
Ni/Mn
Zn/Mn
As/Mn
Se/Mn
Br/Mn
Rb/Mn
Sr/Mn
Y/Mn
Zr/Mn
Pb/Mn
kcps/Cr
Si/Cr
S/Cr
O/Cr
K/Cr
Ca/Cr
Ti/Cr
Cr/Cr
Mn/Cr
Fe/Cr
Ni/Cr
Zn/Cr
As/Cr
Se/Cr
Br/Cr
Rb/Cr
Sr/Cr
Y/Cr
Zr/Cr
Pb/Cr
kcps/Ti
Si/Ti
S/Ti
O/Ti
K/Ti
Ca/Ti
Ti/Ti
Cr/Ti
Mn/Ti
Fe/Ti
Ni/Ti
Zn/Ti
As/Ti
Se/Ti
Br/Ti
Rb/Ti
Sr/Ti
Y/Ti
Zr/Ti
Pb/Ti
kcps/Ca
Si/Ca
S/Ca
O/Ca
K/Ca
Ca/Ca
Ti/Ca
Cr/Ca
Mn/Ca
Fe/Ca
Ni/Ca
Zn/Ca
As/Ca
Se/Ca
Br/Ca
Rb/Ca
Sr/Ca
Y/Ca
Zr/Ca
Pb/Ca
kcps/K
Si/K
S/K
O/K
K/K
Ca/K
Ti/K
Cr/K
Mn/K
Fe/K
Ni/K
Zn/K
As/K
Se/K
Br/K
Rb/K
Sr/K
Y/K
Zr/K
Pb/K
kcps/Cl
Si/Cl
S/Cl
O/Cl
K/Cl
Ca/Cl
Ti/Cl
Cr/Cl
Mn/Cl
Fe/Cl
Ni/Cl
Zn/Cl
As/Cl
Se/Cl
Br/Cl
Rb/Cl
Sr/Cl
Y/Cl
Zr/Cl
Pb/Cl
kcps/S
Si/S
S/S
O/S
K/S
Ca/S
Ti/S
Cr/S
Mn/S
Fe/S
Ni/S
Zn/S
As/S
Se/S
Br/S
Rb/S
Sr/S
Y/S
Zr/S
Pb/S
kcps/Si
Si/Si
S/Si
O/Si
K/Si
Ca/Si
Ti/Si
Cr/Si
Mn/Si
Fe/Si
Ni/Si
Zn/Si
As/Si
Se/Si
Br/Si
Rb/Si
Sr/Si
Y/Si
Zr/Si
Pb/Si
kcps/kcps
Si/kcps
S/kcps
O/kcps
K/kcps
Ca/kcps
Ti/kcps
Cr/kcps
Mn/kcps
Fe/kcps
Ni/kcps
Zn/kcps
As/kcps
Se/kcps
Br/kcps
Rb/kcps
Sr/kcps
Y/kcps
Zr/kcps
Pb/kcps

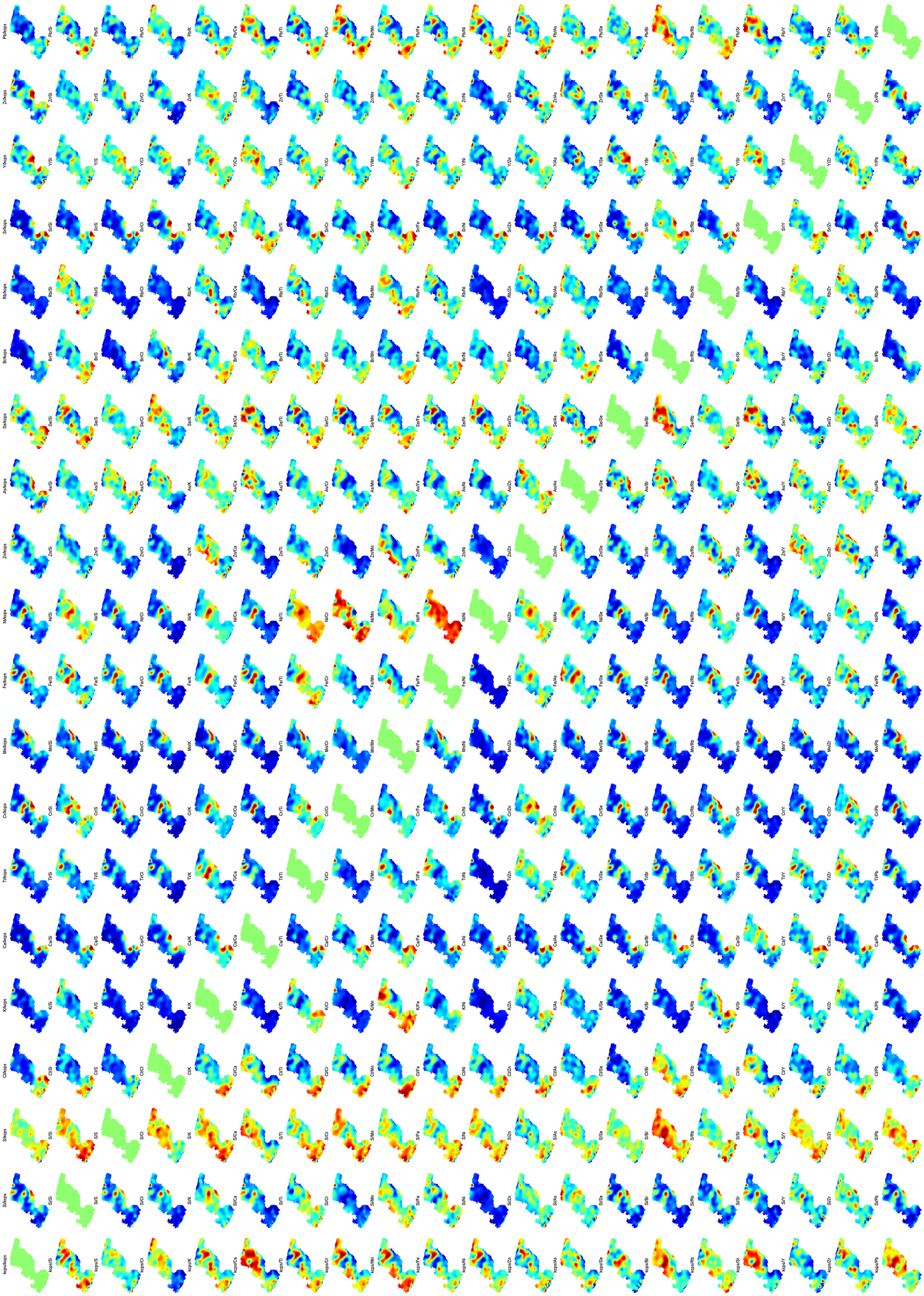
Pb/kcps
Pb/Si
Pb/S
Pb/Cl
Pb/K
Pb/Ca
Pb/Ti
Pb/Cr
Pb/Mn
Pb/Fe
Pb/Ni
Pb/Zn
Pb/As
Pb/Se
Pb/Br
Pb/Rb
Pb/Sr
Pb/Y
Pb/Zr
Pb/Pb
Zn/kcps
Zn/Si
Zn/S
Zn/Cl
Zn/K
Zn/Ca
Zn/Ti
Zn/Cr
Zn/Mn
Zn/Fe
Zn/Ni
Zn/Zn
Zn/As
Zn/Se
Zn/Br
Zn/Rb
Zn/Sr
Zn/Y
Zn/Zr
Zn/Pb
Y/kcps
Y/Si
Y/S
Y/Cl
Y/K
Y/Ca
Y/Ti
Y/Cr
Y/Mn
Y/Fe
Y/Ni
Y/Zn
Y/As
Y/Se
Y/Br
Y/Rb
Y/Sr
Y/Y
Y/Zr
Y/Pb
Sr/kcps
Sr/Si
Sr/S
Sr/Cl
Sr/K
Sr/Ca
Sr/Ti
Sr/Cr
Sr/Mn
Sr/Fe
Sr/Ni
Sr/Zn
Sr/As
Sr/Se
Sr/Br
Sr/Rb
Sr/Sr
Sr/Y
Sr/Zr
Sr/Pb
Rb/kcps
Rb/Si
Rb/S
Rb/Cl
Rb/K
Rb/Ca
Rb/Ti
Rb/Cr
Rb/Mn
Rb/Fe
Rb/Ni
Rb/Zn
Rb/As
Rb/Se
Rb/Br
Rb/Rb
Rb/Sr
Rb/Y
Rb/Zr
Rb/Pb
Br/kcps
Br/Si
Br/S
Br/Cl
Br/K
Br/Ca
Br/Ti
Br/Cr
Br/Mn
Br/Fe
Br/Ni
Br/Zn
Br/As
Br/Se
Br/Br
Br/Rb
Br/Sr
Br/Y
Br/Zr
Br/Pb
Se/kcps
Se/Si
Se/S
Se/Cl
Se/K
Se/Ca
Se/Ti
Se/Cr
Se/Mn
Se/Fe
Se/Ni
Se/Zn
Se/As
Se/Se
Se/Br
Se/Rb
Se/Sr
Se/Y
Se/Zr
Se/Pb
As/kcps
As/Si
As/S
As/Cl
As/K
As/Ca
As/Ti
As/Cr
As/Mn
As/Fe
As/Ni
As/Zn
As/As
As/Se
As/Br
As/Rb
As/Sr
As/Y
As/Zr
As/Pb
Ni/kcps
Ni/Si
Ni/S
Ni/Cl
Ni/K
Ni/Ca
Ni/Ti
Ni/Cr
Ni/Mn
Ni/Fe
Ni/Ni
Ni/Zn
Ni/As
Ni/Se
Ni/Br
Ni/Rb
Ni/Sr
Ni/Y
Ni/Zr
Ni/Pb
Fe/kcps
Fe/Si
Fe/S
Fe/Cl
Fe/K
Fe/Ca
Fe/Ti
Fe/Cr
Fe/Mn
Fe/Fe
Fe/Ni
Fe/Zn
Fe/As
Fe/Se
Fe/Br
Fe/Rb
Fe/Sr
Fe/Y
Fe/Zr
Fe/Pb
Mn/kcps
Mn/Si
Mn/S
Mn/Cl
Mn/K
Mn/Ca
Mn/Ti
Mn/Cr
Mn/Mn
Mn/Fe
Mn/Ni
Mn/Zn
Mn/As
Mn/Se
Mn/Br
Mn/Rb
Mn/Sr
Mn/Y
Mn/Zr
Mn/Pb
Cr/kcps
Cr/Si
Cr/S
Cr/Cl
Cr/K
Cr/Ca
Cr/Ti
Cr/Cr
Cr/Mn
Cr/Fe
Cr/Ni
Cr/Zn
Cr/As
Cr/Se
Cr/Br
Cr/Rb
Cr/Sr
Cr/Y
Cr/Zr
Cr/Pb
Ti/kcps
Ti/Si
Ti/S
Ti/Cl
Ti/K
Ti/Ca
Ti/Ti
Ti/Cr
Ti/Mn
Ti/Fe
Ti/Ni
Ti/Zn
Ti/As
Ti/Se
Ti/Br
Ti/Rb
Ti/Sr
Ti/Y
Ti/Zr
Ti/Pb
Ca/kcps
Ca/Si
Ca/S
Ca/Cl
Ca/K
Ca/Ca
Ca/Ti
Ca/Cr
Ca/Mn
Ca/Fe
Ca/Ni
Ca/Zn
Ca/As
Ca/Se
Ca/Br
Ca/Rb
Ca/Sr
Ca/Y
Ca/Zr
Ca/Pb
K/kcps
K/Si
K/S
K/Cl
K/K
K/Ca
K/Ti
K/Cr
K/Mn
K/Fe
K/Ni
K/Zn
K/As
K/Se
K/Br
K/Rb
K/Sr
K/Y
K/Zr
K/Pb
Cl/kcps
Cl/Si
Cl/S
Cl/Cl
Cl/K
Cl/Ca
Cl/Ti
Cl/Cr
Cl/Mn
Cl/Fe
Cl/Ni
Cl/Zn
Cl/As
Cl/Se
Cl/Br
Cl/Rb
Cl/Sr
Cl/Y
Cl/Zr
Cl/Pb
Si/kcps
Si/Si
Si/S
Si/Cl
Si/K
Si/Ca
Si/Ti
Si/Cr
Si/Mn
Si/Fe
Si/Ni
Si/Zn
Si/As
Si/Se
Si/Br
Si/Rb
Si/Sr
Si/Y
Si/Zr
Si/Pb
Si/kcps
Si/Si
Si/S
Si/Cl
Si/K
Si/Ca
Si/Ti
Si/Cr
Si/Mn
Si/Fe
Si/Ni
Si/Zn
Si/As
Si/Se
Si/Br
Si/Rb
Si/Sr
Si/Y
Si/Zr
Si/Pb
kcps/kcps
kcps/Si
kcps/S
kcps/Cl
kcps/K
kcps/Ca
kcps/Ti
kcps/Cr
kcps/Mn
kcps/Fe
kcps/Ni
kcps/Zn
kcps/As
kcps/Se
kcps/Br
kcps/Rb
kcps/Sr
kcps/Y
kcps/Zr
kcps/Pb

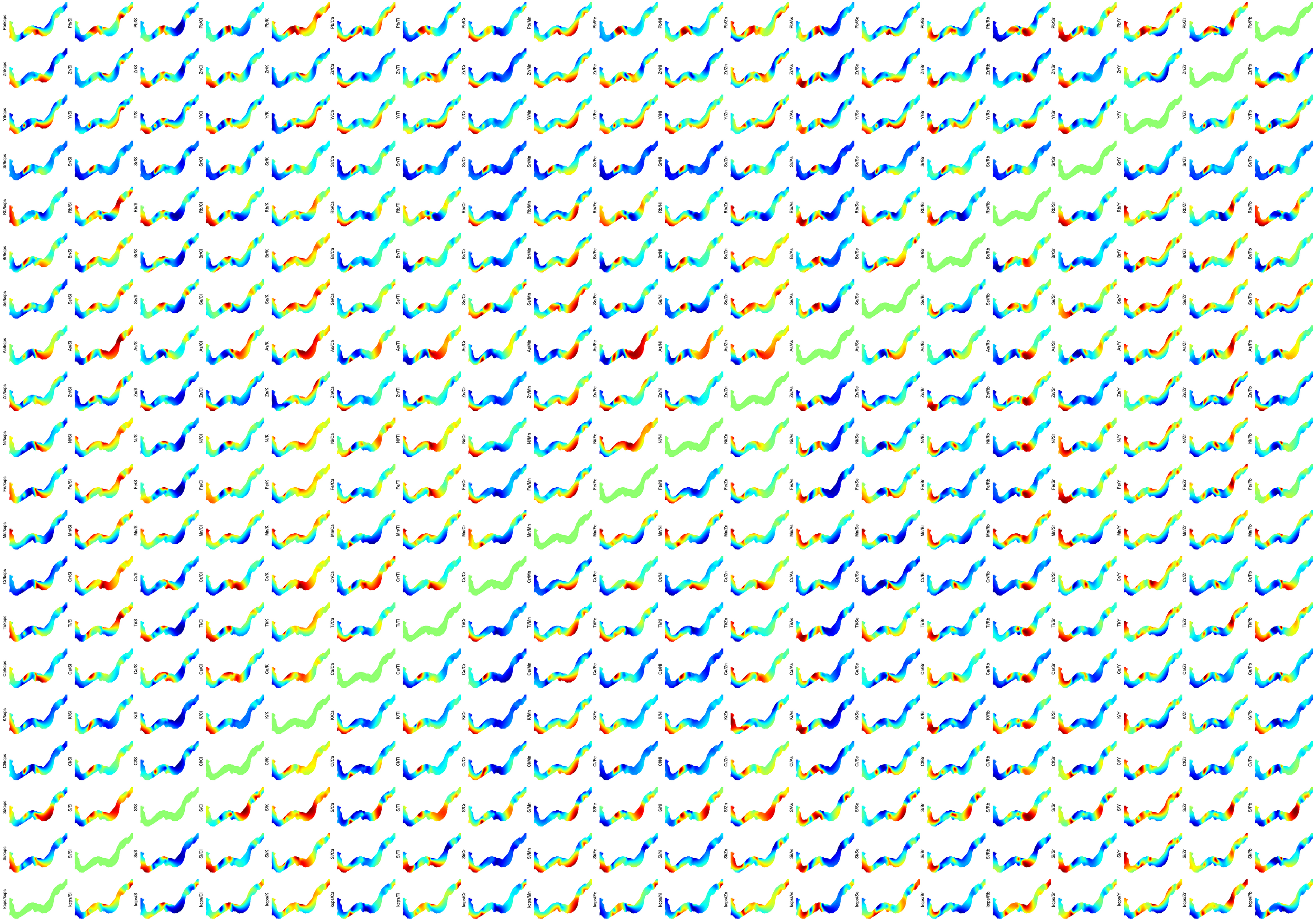
Pb/kcps
Pb/Si
Pb/S
Pb/Cl
Pb/K
Pb/Ca
Pb/Ti
Pb/Cr
Pb/Mn
Pb/Fe
Pb/Ni
Pb/Zn
Pb/As
Pb/Se
Pb/Br
Pb/Rb
Pb/Sr
Pb/Y
Pb/Zr
Pb/Pb
Zr/kcps
Zr/Si
Zr/S
Zr/Cl
Zr/K
Zr/Ca
Zr/Ti
Zr/Cr
Zr/Mn
Zr/Fe
Zr/Ni
Zr/Zn
Zr/As
Zr/Se
Zr/Br
Zr/Rb
Zr/Sr
Zr/Y
Zr/Zr
Zr/Pb
Y/kcps
Y/Si
Y/S
Y/Cl
Y/K
Y/Ca
Y/Ti
Y/Cr
Y/Mn
Y/Fe
Y/Ni
Y/Zn
Y/As
Y/Se
Y/Br
Y/Rb
Y/Sr
Y/Y
Y/Zr
Y/Pb
Sr/kcps
Sr/Si
Sr/S
Sr/Cl
Sr/K
Sr/Ca
Sr/Ti
Sr/Cr
Sr/Mn
Sr/Fe
Sr/Ni
Sr/Zn
Sr/As
Sr/Se
Sr/Br
Sr/Rb
Sr/Sr
Sr/Y
Sr/Zr
Sr/Pb
Rb/kcps
Rb/Si
Rb/S
Rb/Cl
Rb/K
Rb/Ca
Rb/Ti
Rb/Cr
Rb/Mn
Rb/Fe
Rb/Ni
Rb/Zn
Rb/As
Rb/Se
Rb/Br
Rb/Rb
Rb/Sr
Rb/Y
Rb/Zr
Rb/Pb
Br/kcps
Br/Si
Br/S
Br/Cl
Br/K
Br/Ca
Br/Ti
Br/Cr
Br/Mn
Br/Fe
Br/Ni
Br/Zn
Br/As
Br/Se
Br/Br
Br/Rb
Br/Sr
Br/Y
Br/Zr
Br/Pb
Se/kcps
Se/Si
Se/S
Se/Cl
Se/K
Se/Ca
Se/Ti
Se/Cr
Se/Mn
Se/Fe
Se/Ni
Se/Zn
Se/As
Se/Se
Se/Br
Se/Rb
Se/Sr
Se/Y
Se/Zr
Se/Pb
As/kcps
As/Si
As/S
As/Cl
As/K
As/Ca
As/Ti
As/Cr
As/Mn
As/Fe
As/Ni
As/Zn
As/As
As/Se
As/Br
As/Rb
As/Sr
As/Y
As/Zr
As/Pb
Zn/kcps
Zn/Si
Zn/S
Zn/Cl
Zn/K
Zn/Ca
Zn/Ti
Zn/Cr
Zn/Mn
Zn/Fe
Zn/Ni
Zn/Zn
Zn/As
Zn/Se
Zn/Br
Zn/Rb
Zn/Sr
Zn/Y
Zn/Zr
Zn/Pb
Ni/kcps
Ni/Si
Ni/S
Ni/Cl
Ni/K
Ni/Ca
Ni/Ti
Ni/Cr
Ni/Mn
Ni/Fe
Ni/Ni
Ni/Zn
Ni/As
Ni/Se
Ni/Br
Ni/Rb
Ni/Sr
Ni/Y
Ni/Zr
Ni/Pb
Fe/kcps
Fe/Si
Fe/S
Fe/Cl
Fe/K
Fe/Ca
Fe/Ti
Fe/Cr
Fe/Mn
Fe/Fe
Fe/Ni
Fe/Zn
Fe/As
Fe/Se
Fe/Br
Fe/Rb
Fe/Sr
Fe/Y
Fe/Zr
Fe/Pb
Mn/kcps
Mn/Si
Mn/S
Mn/Cl
Mn/K
Mn/Ca
Mn/Ti
Mn/Cr
Mn/Mn
Mn/Fe
Mn/Ni
Mn/Zn
Mn/As
Mn/Se
Mn/Br
Mn/Rb
Mn/Sr
Mn/Y
Mn/Zr
Mn/Pb
Cr/kcps
Cr/Si
Cr/S
Cr/Cl
Cr/K
Cr/Ca
Cr/Ti
Cr/Cr
Cr/Mn
Cr/Fe
Cr/Ni
Cr/Zn
Cr/As
Cr/Se
Cr/Br
Cr/Rb
Cr/Sr
Cr/Y
Cr/Zr
Cr/Pb
Ti/kcps
Ti/Si
Ti/S
Ti/Cl
Ti/K
Ti/Ca
Ti/Ti
Ti/Cr
Ti/Mn
Ti/Fe
Ti/Ni
Ti/Zn
Ti/As
Ti/Se
Ti/Br
Ti/Rb
Ti/Sr
Ti/Y
Ti/Zr
Ti/Pb
Ca/kcps
Ca/Si
Ca/S
Ca/Cl
Ca/K
Ca/Ca
Ca/Ti
Ca/Cr
Ca/Mn
Ca/Fe
Ca/Ni
Ca/Zn
Ca/As
Ca/Se
Ca/Br
Ca/Rb
Ca/Sr
Ca/Y
Ca/Zr
Ca/Pb
K/kcps
K/Si
K/S
K/Cl
K/K
K/Ca
K/Ti
K/Cr
K/Mn
K/Fe
K/Ni
K/Zn
K/As
K/Se
K/Br
K/Rb
K/Sr
K/Y
K/Zr
K/Pb
Cl/kcps
Cl/Si
Cl/S
Cl/Cl
Cl/K
Cl/Ca
Cl/Ti
Cl/Cr
Cl/Mn
Cl/Fe
Cl/Ni
Cl/Zn
Cl/As
Cl/Se
Cl/Br
Cl/Rb
Cl/Sr
Cl/Y
Cl/Zr
Cl/Pb
Si/kcps
Si/Si
Si/S
Si/Cl
Si/K
Si/Ca
Si/Ti
Si/Cr
Si/Mn
Si/Fe
Si/Ni
Si/Zn
Si/As
Si/Se
Si/Br
Si/Rb
Si/Sr
Si/Y
Si/Zr
Si/Pb
Si/kcps
Si/Si
Si/S
Si/Cl
Si/K
Si/Ca
Si/Ti
Si/Cr
Si/Mn
Si/Fe
Si/Ni
Si/Zn
Si/As
Si/Se
Si/Br
Si/Rb
Si/Sr
Si/Y
Si/Zr
Si/Pb
kcps/kcps
kcps/Si
kcps/S
kcps/Cl
kcps/K
kcps/Ca
kcps/Ti
kcps/Cr
kcps/Mn
kcps/Fe
kcps/Ni
kcps/Zn
kcps/As
kcps/Se
kcps/Br
kcps/Rb
kcps/Sr
kcps/Y
kcps/Zr
kcps/Pb

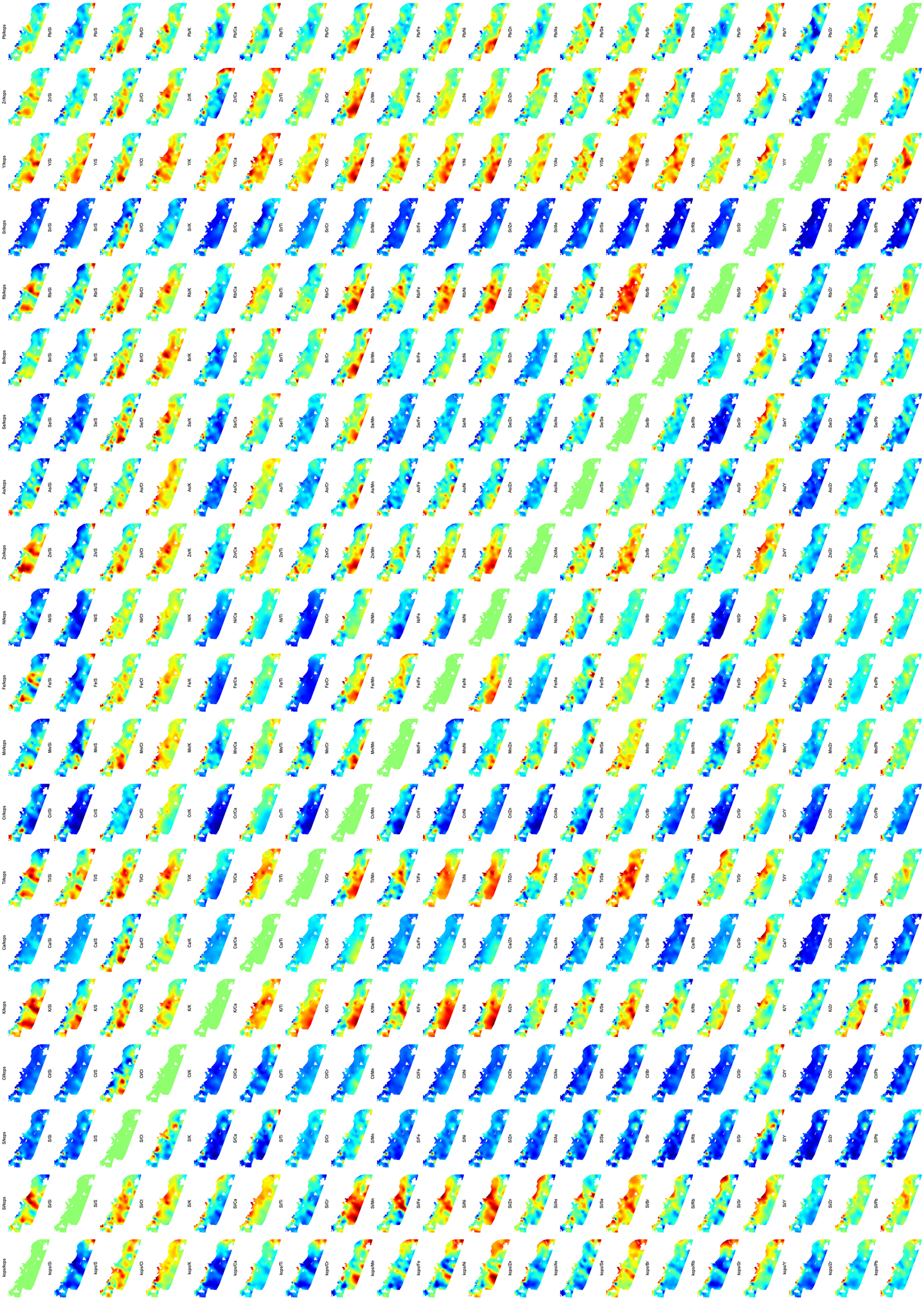
Pb/kcps
Pb/Si
Pb/S
Pb/Cl
Pb/K
Pb/Ca
Pb/Ti
Pb/Cr
Pb/Mn
Pb/Fe
Pb/Ni
Pb/Zn
Pb/As
Pb/Se
Pb/Br
Pb/Rb
Pb/Sr
Pb/Y
Pb/Zr
Pb/Pb
Zr/kcps
Zr/Si
Zr/S
Zr/Cl
Zr/K
Zr/Ca
Zr/Ti
Zr/Cr
Zr/Mn
Zr/Fe
Zr/Ni
Zr/Zn
Zr/As
Zr/Se
Zr/Br
Zr/Rb
Zr/Sr
Zr/Y
Zr/Zr
Zr/Pb
Y/kcps
Y/Si
Y/S
Y/Cl
Y/K
Y/Ca
Y/Ti
Y/Cr
Y/Mn
Y/Fe
Y/Ni
Y/Zn
Y/As
Y/Se
Y/Br
Y/Rb
Y/Sr
Y/Y
Y/Zr
Y/Pb
Sr/kcps
Sr/Si
Sr/S
Sr/Cl
Sr/K
Sr/Ca
Sr/Ti
Sr/Cr
Sr/Mn
Sr/Fe
Sr/Ni
Sr/Zn
Sr/As
Sr/Se
Sr/Br
Sr/Rb
Sr/Sr
Sr/Y
Sr/Zr
Sr/Pb
Rb/kcps
Rb/Si
Rb/S
Rb/Cl
Rb/K
Rb/Ca
Rb/Ti
Rb/Cr
Rb/Mn
Rb/Fe
Rb/Ni
Rb/Zn
Rb/As
Rb/Se
Rb/Br
Rb/Rb
Rb/Sr
Rb/Y
Rb/Zr
Rb/Pb
Br/kcps
Br/Si
Br/S
Br/Cl
Br/K
Br/Ca
Br/Ti
Br/Cr
Br/Mn
Br/Fe
Br/Ni
Br/Zn
Br/As
Br/Se
Br/Br
Br/Rb
Br/Sr
Br/Y
Br/Zr
Br/Pb
Se/kcps
Se/Si
Se/S
Se/Cl
Se/K
Se/Ca
Se/Ti
Se/Cr
Se/Mn
Se/Fe
Se/Ni
Se/Zn
Se/As
Se/Se
Se/Br
Se/Rb
Se/Sr
Se/Y
Se/Zr
Se/Pb
As/kcps
As/Si
As/S
As/Cl
As/K
As/Ca
As/Ti
As/Cr
As/Mn
As/Fe
As/Ni
As/Zn
As/As
As/Se
As/Br
As/Rb
As/Sr
As/Y
As/Zr
As/Pb
Zn/kcps
Zn/Si
Zn/S
Zn/Cl
Zn/K
Zn/Ca
Zn/Ti
Zn/Cr
Zn/Mn
Zn/Fe
Zn/Ni
Zn/Zn
Zn/As
Zn/Se
Zn/Br
Zn/Rb
Zn/Sr
Zn/Y
Zn/Zr
Zn/Pb
Ni/kcps
Ni/Si
Ni/S
Ni/Cl
Ni/K
Ni/Ca
Ni/Ti
Ni/Cr
Ni/Mn
Ni/Fe
Ni/Ni
Ni/Zn
Ni/As
Ni/Se
Ni/Br
Ni/Rb
Ni/Sr
Ni/Y
Ni/Zr
Ni/Pb
Fe/kcps
Fe/Si
Fe/S
Fe/Cl
Fe/K
Fe/Ca
Fe/Ti
Fe/Cr
Fe/Mn
Fe/Fe
Fe/Ni
Fe/Zn
Fe/As
Fe/Se
Fe/Br
Fe/Rb
Fe/Sr
Fe/Y
Fe/Zr
Fe/Pb
Mn/kcps
Mn/Si
Mn/S
Mn/Cl
Mn/K
Mn/Ca
Mn/Ti
Mn/Cr
Mn/Mn
Mn/Fe
Mn/Ni
Mn/Zn
Mn/As
Mn/Se
Mn/Br
Mn/Rb
Mn/Sr
Mn/Y
Mn/Zr
Mn/Pb
Cr/kcps
Cr/Si
Cr/S
Cr/Cl
Cr/K
Cr/Ca
Cr/Ti
Cr/Cr
Cr/Mn
Cr/Fe
Cr/Ni
Cr/Zn
Cr/As
Cr/Se
Cr/Br
Cr/Rb
Cr/Sr
Cr/Y
Cr/Zr
Cr/Pb
Ti/kcps
Ti/Si
Ti/S
Ti/Cl
Ti/K
Ti/Ca
Ti/Ti
Ti/Cr
Ti/Mn
Ti/Fe
Ti/Ni
Ti/Zn
Ti/As
Ti/Se
Ti/Br
Ti/Rb
Ti/Sr
Ti/Y
Ti/Zr
Ti/Pb
Ca/kcps
Ca/Si
Ca/S
Ca/Cl
Ca/K
Ca/Ca
Ca/Ti
Ca/Cr
Ca/Mn
Ca/Fe
Ca/Ni
Ca/Zn
Ca/As
Ca/Se
Ca/Br
Ca/Rb
Ca/Sr
Ca/Y
Ca/Zr
Ca/Pb
K/kcps
K/Si
K/S
K/Cl
K/K
K/Ca
K/Ti
K/Cr
K/Mn
K/Fe
K/Ni
K/Zn
K/As
K/Se
K/Br
K/Rb
K/Sr
K/Y
K/Zr
K/Pb
Cl/kcps
Cl/Si
Cl/S
Cl/Cl
Cl/K
Cl/Ca
Cl/Ti
Cl/Cr
Cl/Mn
Cl/Fe
Cl/Ni
Cl/Zn
Cl/As
Cl/Se
Cl/Br
Cl/Rb
Cl/Sr
Cl/Y
Cl/Zr
Cl/Pb
S/kcps
S/Si
S/S
S/Cl
S/K
S/Ca
S/Ti
S/Cr
S/Mn
S/Fe
S/Ni
S/Zn
S/As
S/Se
S/Br
S/Rb
S/Sr
S/Y
S/Zr
S/Pb
Si/kcps
Si/Si
Si/S
Si/Cl
Si/K
Si/Ca
Si/Ti
Si/Cr
Si/Mn
Si/Fe
Si/Ni
Si/Zn
Si/As
Si/Se
Si/Br
Si/Rb
Si/Sr
Si/Y
Si/Zr
Si/Pb
kcps/kcps
kcps/Si
kcps/S
kcps/Cl
kcps/K
kcps/Ca
kcps/Ti
kcps/Cr
kcps/Mn
kcps/Fe
kcps/Ni
kcps/Zn
kcps/As
kcps/Se
kcps/Br
kcps/Rb
kcps/Sr
kcps/Y
kcps/Zr
kcps/Pb

Table 1. Sampling locations and water parameters.

	Type	Location	Sample label	Sampling date	Coordinates (UTM / ED50) E	N	Temp. (°C)	TDS[a] (ppm)	EC[b] (mS/cm)	pH
1	On-land hot	Sultaniye-1	SUL-1	01.06.2014	642788	4082305	24.30	26438	18.700	6.92
2	On-land hot	Sultaniye-2	SUL-2	21.06.2014	642853	4082265	39.93	27127	44.250	6.74
3	On-land hot	Sultaniye-3	SUL-3	21.06.2014	642805	4082293	41.04	28163	44.100	6.70
4	On-land hot	Kelgirme	KEL	02.07.2014	645593	4078489	37.71	27302	27.410	6.76
5	On-land hot	Delibey	DEL	21.06.2014	644921	4080156	38.98	28841	44.390	6.75
6	On-land hot	Çürükardı	CUR	22.06.2014	656671	4065767	29.27	23029	24.400	6.43
7	On-land hot	Musalar	MUS	22.06.2014	654393	4068427	26.58	23031	25.630	6.5
8	On-land hot	Thermemaris	THER	26.06.2014	660168	4062670	26.60	20042	22.740	6.55
9	On-land hot	Kapukargın-1	KAP-1	22.06.2014	661828	4066361	30.02	19505	22.590	6.44
10	On-land hot	Kapukargın-2	KAP-2	22.06.2014	661869	4066291	30.16	21434	22.410	6.43
11	Subaqueous hot	Köyceğiz Lake	SUB-1	05.09.2013	642409	4082916	29.47	6671	11648	-
12	Subaqueous hot	Köyceğiz Lake	SUB-2	28.06.2014	642725	4082889	26.29	5629	5.102	8.67
13	Subaqueous hot	Köyceğiz Lake	SUB-3	28.06.2014	643870	4081804	26.17	7200	4.951	8.69
14	Subaqueous hot	Dalyan Channel	SUB-4	28.06.2014	645593	4079204	27.37	24354	34.406	8.23
15	Subaqueous hot	Dalyan Channel	SUB-5	28.06.2014	645679	4078895	27.47	21572	33.951	8.26
16	Subaqueous hot	Dalyan Channel	SUB-6	28.06.2014	646005	4078338	27.61	20547	30.134	8.25
17	Subaqueous hot	Fethiye-Göcek Bay	SUB-7	28.06.2014	675787	4066071	27.19	6671	57.734	8.35
18	On-land cold	Köyceğiz	COLD-1	21.06.2014	650135	4091604	15.03	302	0.305	8.65
19	On-land cold	Köyceğiz	COLD-2	21.06.2014	654921	4089336	18.72	611	0.627	7.92
20	On-land cold	Sultaniye Village	COLD-3	26.06.2014	641110	4084397	23.77	718	0.709	8.57
21	On-land cold	Çandır Village	COLD-4	21.06.2014	642438	4077514	17.94	409	0.470	7.02
22	On-land cold	İnlice Village	COLD-5	26.06.2014	675818	4067938	18.47	613	0.800	7.32
23	Subaqueous cold	Köyceğiz Lake	SUBC-1	28.06.2014	651338	4091283	25.07	2581	2.780	8.84
24	Subaqueous cold	Köyceğiz Lake	SUBC-2	28.06.2014	646048	4084218	27.70	2802	3.698	8.71
25	Stream	Namnam Stream	NAM	22.06.2014	644396	4087801	22.72	473	0.539	8.12
26	Stream	Yuvarlakçay Stream	YUV	22.06.2014	650966	4086369	20.07	540	0.594	7.83
27	Lake	Köyceğiz Lake	KOY-1	28.06.2014	650033	4089319	27.60	2917	3.635	8.88
28	Lake	Köyceğiz Lake	KOY-2	28.06.2014	648020	4086829	27.52	2865	3.702	8.91
29	Lake	Köyceğiz Lake	KOY-3	28.06.2014	645751	4084993	27.84	2849	3.848	8.89
30	Lake	Köyceğiz Lake	KOY-4	28.06.2014	643216	4083815	28.60	3247	3.940	8.82
31	Lake	Köyceğiz Lake	KOY-5	28.06.2014	645147	4082863	27.73	3258	4.056	8.82
32	Lake	Alagöl Lake	ALA-1	28.06.2014	643431	643431	32.15	27337	50.565	8.18
33	Lake	Alagöl Lake	ALA-2	10.09.2013	643727	4076043	32.90	37065	53.285	8.22
34	Lake	Sülüngür Lake	SULG-1	01.07.2014	645231	4073821	28.92	5254	35.698	8.26
35	Lake	Sülüngür Lake	SULG-2	01.07.2014	646606	4072741	29.75	10498	35.138	8.44
36	Lake	Kocagöl Lake	KOC	22.06.2014	663646	4061694	28.51	4621	7.261	8.31
37	Channel	Dalyan Channel	DAL-1	28.06.2014	645606	4079815	28.09	3433	5.316	8.75
38	Channel	Dalyan Channel	DAL-2	28.06.2014	645861	4076524	27.83	21549	37.126	8.21
39	Sea	Fethiye-Göcek Bay	GOC-1	02.06.2014	675724	4063884	21.13	41133	57.562	8.38
40	Sea	Fethiye-Göcek Bay	GOC-2	05.06.2014	669676	4061469	22.10	41528	56.654	8.38
41	Sea	Fethiye-Göcek Bay	GOC-3	03.06.2014	674596	4056408	22.71	41526	57.482	8.38

[a] Total dissolved solids
[b] Electrical conductivity

Table 2. Major ion concentrations of the waters. CBE: Charge Balance Error.

Sample No	Ca (ppm)	Mg (ppm)	Na (ppm)	K (ppm)	HCO_3 (ppm)	SO_4 (ppm)	Cl (ppm)	CBE (%)	Type
SUL-1	1994	946	6510	284	302	1453	14874	1.30	Na - Cl
SUL-2	2294	1280	6216	355	302	2136	14453	4.27	Na - Cl
SUL-3	2588	1289	6123	389	302	2233	15067	3.26	Na - Cl
KEL	2478	1262	6028	348	178	2068	14843	3.38	Na - Cl
DEL	2928	1321	6161	377	308	2285	15262	4.55	Na - Cl
CUR	2055	895	5009	269	847	934	12894	0.24	Na - Cl
MUS	2059	975	5353	212	900	991	12431	4.16	Na - Cl
THER	1881	907	4403	196	794	804	10932	3.53	Na - Cl
KAP-1	2183	833	4012	232	865	895	10348	4.50	Na - Cl
KAP-2	1857	785	4815	218	882	948	11749	0.50	Na - Cl
SUB-1	378	414	1514	64	302	596	3369	3.36	Na - Cl
SUB-2	414	369	1076	79	320	477	2863	1.93	Na - Cl
SUB-3	414	451	1636	82	317	498	3740	4.60	Na - Cl
SUB-4	916	1378	5929	318	255	1743	13752	-0.47	Na - Cl
SUB-5	944	1020	5962	283	267	1481	11551	4.72	Na - Cl
SUB-6	946	904	5534	304	267	1440	11081	3.12	Na - Cl
SUB-7	1739	2400	10293	532	184	2948	23037	2.05	Na - Cl
COLD-1	17.14	35.09	5.79	0.62	219	2.57	4.04	2.67	Mg - HCO3
COLD-2	16.59	84.70	6.25	0.70	444	5.01	6.91	3.18	Mg - HCO3
COLD-3	8.74	114.64	6.58	0.38	503	4.15	8.60	4.11	Mg - HCO3
COLD-4	86.03	6.03	11.58	0.99	267	8.17	16.39	2.76	Ca - HCO3
COLD-5	84.13	31.94	35.51	1.60	361	16.35	49.76	4.21	Ca - HCO3
SUBC-1	127	190	513	29	320	172	1204	2.34	Na - Cl
SUBC-2	121	196	617	31	326	184	1305	3.92	Na - Cl
NAM	16.04	70.49	5.18	0.77	354	4.22	6.31	2.09	Mg - HCO_3
YUV	77.87	40.11	5.57	0.81	302	45.43	5.79	3.38	Ca - HCO_3
KOY-1	108	204	681	34	284	185	1375	4.55	Na - Cl
KOY-2	100	207	653	30	290	182	1358	3.66	Na - Cl
KOY-3	96	207	661	30	314	180	1335	4.80	Na - Cl
KOY-4	100	224	804	34	264	207	1566	4.98	Na - Cl
KOY-5	104	221	806	36	267	207	1568	4.92	Na - Cl
ALA-1	1164	1626	7038	347	267	1604	15173	4.01	Na - Cl
ALA-2	1669	2056	9747	494	207	2616	20174	4.61	Na - Cl
SULG-1	179	332	1286	67	302	352	2702	2.81	Na - Cl
SULG-2	298	603	2847	141	290	690	5585	4.01	Na - Cl
KOC	210	204	1232	49	267	261	2355	3.21	Na - Cl
DAL-1	113	204	893	36	267	218	1647	4.84	Na - Cl
DAL-2	1715	1262	4843	215	302	1112	12023	4.84	Na - Cl
GOC-1	1426	2454	11037	629	130	2752	22574	4.83	Na - Cl
GOC-2	1529	2450	11166	555	178	2768	22782	4.94	Na - Cl
GOC-3	1378	2486	11056	554	184	2812	22940	3.94	Na - Cl

Table 3. Trace element concentrations of the waters. Pikcogram/gram

Sample No	Al (ppb)	As (ppb)	Ba (ppb)	Br (ppm)	Cr (ppb)	Cu (ppb)	F (ppm)	Fe (ppb)	Mn (ppb)	Ni (ppb)	Se (ppb)
Detection Limit	0.3	0.025	0.002	0.01	0.003	0.02	0.01	0.05	0.03	0.03	0.01
SUL-1	775	258	165	31	96	<0.02	6	3279	<0.03	125	202
SUL-2	<0.3	365	109	42	99	<0.02	11	2963	<0.03	165	334
SUL-3	<0.3	234	116	44	110	<0.02	15	3052	<0.03	49	473
KEL	<0.3	405	98	36	118	440	8	3323	<0.03	23	357
DEL	<0.3	290	104	47	130	13070	7	3574	<0.03	87	309
CUR	<0.3	319	95	22	119	<0.02	10	3439	<0.03	45	235
MUS	<0.3	121	80	25	136	<0.02	8	4602	102	35	311
THER	<0.3	216	119	18	141	<0.02	10	3897	<0.03	24	320
KAP-1	<0.3	373	97	20	154	<0.02	19	4924	115	54	210
KAP-2	<0.3	375	103	29	165	<0.02	15	5895	<0.03	47	324
SUB-1	<0.3	103	34	9	60	<0.02	1	1451	<0.03	<0.1	79
SUB-2	<0.3	98	20	5	70	<0.02	<0.01	1851	<0.03	<0.1	68
SUB-3	<0.3	113	33	8	72	<0.02	1	2025	<0.03	<0.1	72
SUB-4	<0.3	386	47	41	236	<0.02	2	11100	<0.03	50	249
SUB-5	<0.3	186	36	34	131	<0.02	4	3558	<0.03	<0.1	223
SUB-6	<0.3	253	36	36	183	<0.02	1	4925	<0.03	<0.1	267
SUB-7	<0.3	229	17	67	175	<0.02	10	4350	<0.03	<0.1	350
COLD-1	<0.3	9	24	<0.01	11	<0.02	<0.01	134	<0.03	<0.1	2
COLD-2	<0.3	6	1	<0.01	9	<0.02	<0.01	125	<0.03	<0.1	2
COLD-3	<0.3	33	2	<0.01	26	<0.02	<0.01	614	<0.03	20	11
COLD-4	<0.3	8	97	<0.01	3	<0.02	<0.01	45	<0.03	<0.1	3
COLD-5	<0.3	6	84	<0.01	4	<0.02	<0.01	43	<0.03	<0.1	<0.1
SUBC-1	<0.3	28	38	4	33	<0.02	1	1015	<0.03	<0.1	28
SUBC-2	<0.3	44	33	4	31	<0.02	<0.01	768	<0.03	2	31
NAM	26	1	11	<0.01	4	<0.02	<0.01	<0.05	<0.03	2	<0.1
YUV	<0.3	4	105	<0.01	6	<0.02	<0.01	66	<0.03	1	3
KOY-1	<0.3	50	39	4	26	<0.02	2	655	<0.03	3	61
KOY-2	<0.3	48	95	4	27	31	<0.01	735	<0.03	2	49
KOY-3	<0.3	47	34	4	30	<0.02	<0.01	726	<0.03	5	47
KOY-4	<0.3	41	36	4	39	<0.02	<0.01	1271	<0.03	9	50
KOY-5	<0.3	55	37	5	30	<0.02	1	776	<0.03	7	42
ALA-1	<0.3	215	54	41	291	<0.02	11	10280	<0.03	101	326
ALA-2	<0.3	290	26	62	173	<0.02	3	4713	<0.03	<0.1	392
SULG-1	<0.3	47	37	8	25	<0.02	3	638	<0.03	7	64
SULG-2	<0.3	140	44	16	56	<0.02	4	1394	<0.03	12	122
KOC	<0.3	63	76	6	37	<0.02	1	1470	<0.03	7	45
DAL-1	<0.3	66	37	5	28	<0.02	<0.01	771	<0.03	1	45
DAL-2	<0.3	282	69	38	210	<0.02	3	8355	<0.03	32	164
GOC-1	<0.3	266	30	68	173	549	3	5710	<0.03	17	424
GOC-2	<0.3	251	12	70	175	<0.02	5	5171	<0.03	98	344
GOC-3	<0.3	432	25	67	162	<0.02	2	4111	<0.03	18	430

Table 4. Results from the stable isotope analysis of the waters.

	DRY		WET		DIFFERENCE	
Sample no	$\delta^{18}O$ (‰)	δD (‰)	$\delta^{18}O$ (‰)	δD (‰)	$\delta^{18}O$ (‰)	δD (‰)
SUL-1	-2.74	-14.0	-4.67	-24.7	1.93	10.8
SUL-2	-0.68	-5.9	-1.72	-6.1	1.04	0.1
SUL-3	-0.58	-6.4	-1.46	-6.9	0.88	0.5
KEL	-1.10	-6.6	-1.69	-7.7	0.59	1.1
DEL	-0.73	-2.7	-1.72	-6.3	0.99	3.7
CUR	-4.53	-24.9	-4.91	-28.9	0.38	4.0
MUS	-4.22	-25.5	-4.63	-28.5	0.41	3.0
THER	-4.53	-27.4	-4.97	-26.5	0.44	-1.0
KAP-1	-4.94	-25.7	-5.15	-30.1	0.21	4.4
KAP-2	-1.08	-3.7	-5.31	-30.0	4.23	26.3
SUB-1	-3.25	-14.8				
SUB-2	-3.28	-17.7	-4.59	-22.9	1.31	5.1
SUB-3	-3.28	-16.5	-4.46	-25.8	1.18	9.3
SUB-4	-0.80	-1.3	-1.86	-9.2	1.06	7.9
SUB-5	-1.38	-5.1	-1.98	-9.7	0.60	4.6
SUB-6	-1.20	-5.1	-1.20	-5.7	0.00	0.5
SUB-7	1.46	7.6	0.43	6.8	1.03	0.8
COLD-1	-6.65	-34.6	-7.25	-32.5	0.60	-2.2
COLD-2	5.86	-28.4	-6.01	-33.4	11.87	5.0
COLD-3	-5.39	-25.0	-6.14	-24.5	0.75	-0.6
COLD-4	-5.47	-24.9	-5.81	-30.3	0.34	5.4
COLD-5	-5.85	-27.4	-6.31	-27.6	0.46	0.3
SUBC-1	-3.47	-16.9	-4.41	-26.6	0.94	9.6
SUBC-2	-3.48	-19.6	-3.82	-22.5	0.34	2.9
NAM	-	-	-6.07	-31.0	-	-
YUV	-6.31	-34.5	-6.89	-32.1	0.58	-2.4
KOY-1	-3.37	-18.0	-4.02	-24.5	0.65	6.5
KOY-2	-3.36	-18.1	-4.39	-25.7	1.03	7.6
KOY-3	-3.03	-17.9	-4.09	-23.5	1.06	5.6
KOY-4	-3.19	-16.4	-4.29	-21.9	1.10	5.5
KOY-5	-3.09	-15.8	-4.48	-20.5	1.39	4.7
ALA-1	-0.48	-3.07	-1.93	-10.4	1.45	7.3
ALA-2	0.78	2.76	-0.27	1.8	1.05	0.9
SULG-1	-3.23	-17.0	-0.88	-3.9	-2.35	-13.1
SULG-2	-2.62	-13.9	-1.22	-6.3	-1.40	-7.7
KOC	-0.23	-3.0	-1.01	-5.1	0.78	2.1
DAL-1	-3.11	-18.0	-4.38	-20.1	1.27	2.0
DAL-2	-2.33	-13.1	-1.82	-8.3	-0.51	-4.8
GOC-1	1.63	11.6	0.80	4.3	0.83	7.2
GOC-2	1.49	10.5	0.55	4.4	0.94	6.2
GOC-3	1.46	10.0	0.48	6.6	0.98	3.5

Table 5. Total gas composition, $^{3}He/^{4}He$, $^{4}He/^{20}Ne$ and $CO_2/^{3}He$ ratios for free gas samples and $^{3}He/^{4}He$ and $^{4}He/^{20}Ne$ ratios for dissolved gases from hot springs. Error limits are 2σ.

Sample ID	Sample type	Sampling date	Ar (%)	CH_4 (%)	CO_2 (%)	N_2 (%)	O_2 (%)	He ppm	H_2 (ppm)	N_2/CH_4	N_2/Ar	$CO_2/^{3}He$ (*10^9)	$^{4}He/^{20}Ne$	$^{4}He/^{20}Ne$ error	$^{3}He/^{4}He$ (R_a)	$^{3}He/^{4}He$ (Ra) error	$(^{3}He/^{4}He)_c$[a] (R_a)	$(^{3}He/^{4}He)_c$ (R_a) error	Mantle Helium[b] (%)
SUL-2	Free Gas	7/8/2014	1.17	0.1	5.1	93	0.2	220	165	650	79	1.026	34.6	±1.7	0.163	±0.012	0.156	±0.012	2
KEL	Free Gas	7/17/2014	1.17	0	4.6	92	2.5	180	165		78	1.097	30.5	±1.6	0.168	±0.012	0.160	±0.012	2
DEL	Free Gas	7/8/2014	1	0.1	4.5	94	0	210	300	870	94	0.932	35.4	±1.8	0.165	±0.011	0.158	±0.011	2
MUS	Free Gas	7/9/2014	0.76	0	4.2	91	4.3	420	50	9100	119	0.050	118.7	±6.0	1.426	±0.027	1.427	±0.027	18
THER	Free Gas	7/9/2014	0.94	0	10.3	88	0.3	460	170	8800	94	0.118	92.6	±4.7	1.365	±0.029	1.366	±0.029	17
KAP-2	Free Gas	7/9/2014	0.72	0.1	21.4	78	0.3	440	135	1270	108	0.255	130.1	±6.5	1.372	±0.027	1.373	±0.027	17
SUB-2	Free Gas	7/17/2014	0.36	62	0.19	34	3.1	28	1460	0.55	96	0.150	1.75	±0.09	0.330	±0.027	0.194	±0.036	2
SUB-3	Dissolved Gas	7/17/2014											0.352	±0.023	0.822	±0.058	<0.61		<7.4
CUR	Dissolved Gas	7/9/2014											89.0	±4.5	1.408	±0.041	1.409	±0.041	17
SUB-4	Dissolved Gas	7/17/2014											0.937	±0.051	0.419	±0.033	0.152	±0.062	2
SUBC-2	Dissolved Gas	7/17/2014											0.466	±0.028	0.651	±0.032	0.05	±0.19	1
Atmosphere/ ASW (25 °C)											83/38		0.319/0.274						

[a] assuming $(^{4}He/^{20}Ne)_{air} = 0.295 \pm 0.025$, i.e. a range including air (0.319; Sano and Wakita, 1985) and ASW (25°C) (0.274; Ozima and Podosek, 2002)

[b] assuming $(^{3}He/^{4}He)_{crust} = 0.02\ R_a$ and $(^{3}He/^{4}He)_{mantle} = 8\ R_a$

Supplementary Table 1. Standardized ITRAX analysis results for Köyceğiz cores.

	ID	Type	X	Y	kcps	Si	S	Cl	K	Ca	Ti	Cr	Mn	Fe	Ni	Zn	As	Se	Br	Rb	Sr	Y	Zr	Pb
1	**K-9**	HLC	642097	4083621	-0.74	-0.63	0.43	0.96	-0.65	-0.12	-0.74	-0.62	-0.80	-0.77	-0.55	0.41	1.52	0.34	0.17	-1.05	0.35	1.09	-0.26	-0.53
2	**K-40**	HLC	642452	4083142	-0.75	-0.60	-0.24	1.16	-0.94	-0.58	-0.72	-0.71	-0.73	-0.67	-0.53	-0.06	0.64	-0.83	0.38	-0.36	-0.16	1.52	0.42	-0.62
3	**K-015-648**	HLC	642433	4082872	-0.21	-0.63	-0.84	1.24	0.10	0.59	-0.12	-0.36	-0.31	-0.22	-0.03	-0.35	0.59	-0.98	2.77	-0.44	0.93	0.42	-0.38	-0.64
4	**K-015-647**	HLC	642325	4082985	0.32	-0.06	-0.17	0.79	-0.40	-0.32	-0.35	-0.36	-0.62	-0.35	-0.30	-1.06	-0.39	0.47	0.82	-0.65	-0.35	-0.41	-0.12	0.54
5	**K-015-646**	HLC	642370	4082945	-0.43	-0.06	2.17	1.29	0.31	0.30	0.14	-0.18	-0.48	0.00	0.11	-0.64	0.53	-0.18	0.73	-0.40	0.43	-0.43	-0.09	0.68
6	**K-015-645**	HLC	642428	4083010	-0.46	-0.52	1.10	0.85	-0.32	0.09	-0.40	-0.52	-0.71	-0.52	-0.33	-1.06	0.44	0.08	0.21	0.22	0.36	-0.03	-0.34	-0.71
7	**K-015-644**	HLC	642424	4082965	-0.29	-0.34	1.30	0.69	-0.22	-0.19	-0.37	-0.55	-0.67	-0.39	-0.22	-0.37	-0.94	-1.08	0.35	-0.37	0.04	-1.13	0.17	0.32
8	**K-015-643**	HLC	642514	4082948	-0.71	-0.22	0.50	0.38	-0.47	-0.05	-0.38	-0.51	-0.72	-0.51	-0.35	-0.55	-0.81	0.02	0.32	-0.04	0.10	1.11	-0.56	-0.26
9	**K-015-642**	HLC	642461	4082929	-0.36	-0.20	1.97	0.80	-0.24	-0.24	-0.16	-0.33	-0.59	-0.15	-0.06	-0.98	1.31	-0.29	0.57	0.25	-0.41	0.90	-1.27	-1.72
10	**K-015-641**	HLC	642446	4082822	-1.20	-0.36	-1.37	0.87	0.15	0.69	-0.20	-0.42	-0.29	-0.35	-0.24	-0.18	0.11	-0.87	3.40	-0.34	0.94	0.13	-0.39	-0.46
11	**K-015-639**	HLC	642450	4082891	-1.20	0.05	1.97	0.60	-0.07	0.68	-0.27	-0.32	-0.50	-0.35	-0.24	-0.29	-0.48	-1.16	0.60	-0.25	0.79	0.21	-0.56	-0.59
12	**K-015-638**	HLC	642491	4082865	-1.12	-0.22	1.37	0.47	0.06	0.20	-0.07	-0.20	-0.36	-0.17	-0.11	-0.03	-0.15	-0.74	0.54	-0.24	0.15	-1.47	-0.65	-0.96
13	**K-015-000**	HLC	642409	4082916	-1.95	0.52	1.93	0.50	0.74	0.95	0.13	-0.02	-0.09	-0.10	-0.08	0.25	0.18	-1.53	0.40	-0.16	0.58	0.02	0.06	-1.22
14	**K-T-3-635**	HLC	642694	4082932	0.99	0.70	2.70	1.71	0.31	0.60	0.12	-0.06	-0.51	0.41	0.54	-0.04	0.20	-0.57	0.42	-0.12	0.61	-0.98	-0.27	-0.33
15	**K-T-3-634**	HLC	642663	4082973	1.24	-0.10	0.93	1.28	0.04	0.05	-0.05	-0.17	-0.54	0.08	0.07	-0.15	-0.37	0.18	0.56	0.04	-0.01	-1.37	1.40	1.02
16	**K-T-3-633**	HLC	642804	4082807	1.21	0.24	0.43	1.06	-0.09	-0.14	-0.18	-0.09	-0.53	0.19	0.22	-0.32	-0.18	2.84	1.12	-0.08	-0.20	-0.82	0.12	0.57
17	**K-T-3-632**	HLC	642764	4082855	0.18	-0.33	1.10	1.44	0.22	1.01	-0.20	-0.22	-0.36	-0.27	-0.02	0.38	0.24	0.58	0.82	-0.72	0.78	0.09	0.73	0.27
18	**K-T-3-631**	HLC	642795	4082968	0.59	-0.25	0.37	1.16	-0.22	0.04	-0.23	-0.21	-0.60	-0.23	-0.12	-0.26	0.06	1.30	0.69	-0.54	0.09	-1.47	1.03	-0.30
19	**K-T-3-630**	HLC	642763	4082920	0.58	-0.09	1.10	1.17	-0.04	-0.07	-0.20	-0.21	-0.63	0.03	0.04	-0.83	-1.25	0.41	0.44	-0.34	0.00	-0.94	-0.23	0.22
20	**K-T-3-000**	HLC	642725	4082889	0.11	0.05	1.37	0.74	0.55	0.24	0.24	0.02	-0.14	0.14	0.20	-0.04	0.68	-0.29	0.23	0.37	-0.07	-0.60	-0.66	0.31
21	**K-39**	HLC	643071	4082508	-0.17	-0.71	0.00	1.33	-0.56	-0.02	-0.66	-0.61	-0.37	-0.52	-0.51	-0.11	0.85	-0.46	0.60	-1.30	0.60	1.41	0.49	-0.63
22	**K-37**	HLC	643718	4082070	-0.57	-1.03	-0.90	1.43	-0.64	0.49	-0.70	-0.67	-0.70	-0.81	-0.73	0.44	2.20	0.67	0.02	-1.16	0.63	1.70	1.47	-1.39
23	**K-R-621Y**	HLC	643940	4081750	-0.45	1.03	3.04	0.73	1.18	0.59	0.57	0.39	0.25	0.38	0.18	0.51	-0.66	-1.33	0.34	0.61	-0.22	0.22	0.08	0.11
24	**K-R-620**	HLC	643987	4082011	1.32	0.98	-0.07	1.34	-0.05	-0.51	-0.33	-0.29	-0.57	-0.21	-0.24	-0.39	-0.78	0.46	1.10	0.16	-0.41	-1.35	-1.10	0.73
25	**K-R-619**	HLC	643861	4081923	0.77	-0.17	-0.10	1.48	-0.11	0.19	-0.36	-0.44	-0.59	-0.35	-0.39	-1.00	-1.03	-0.55	0.42	-0.07	0.59	0.03	-0.56	0.84
26	**K-R-618**	HLC	644120	4081843	0.88	0.18	-0.57	1.26	-0.01	-0.61	-0.19	-0.17	-0.52	-0.06	-0.14	-0.99	-1.47	0.26	1.58	0.12	-0.46	-0.11	-0.55	0.07
27	**K-R-617**	HLC	644065	4081747	0.95	0.05	0.97	1.14	0.14	-0.35	0.07	-0.21	-0.54	0.07	0.10	-1.06	-0.05	-0.28	0.64	0.20	-0.43	-0.60	0.19	0.50
28	**K-R-028**	HLC	643751	4081904	1.45	0.22	0.23	1.68	-0.11	-0.56	-0.37	-0.36	-0.64	-0.36	-0.38	-0.90	-0.87	1.48	0.83	0.14	-0.48	-1.01	-0.77	1.54
29	**K-R-027**	HLC	643975	4081886	1.31	-0.22	0.33	1.39	-0.58	-0.59	-0.31	-0.44	-0.66	-0.44	-0.41	-0.80	1.72	1.29	0.89	-0.45	-0.47	1.33	-0.13	0.29
30	**K-R-026**	HLC	644100	4081976	1.16	0.34	-0.30	1.17	0.04	-0.42	-0.01	-0.23	-0.55	-0.16	-0.09	-0.88	0.59	0.26	1.39	0.04	-0.24	-1.47	-0.77	1.05
31	**K-R-024**	HLC	643871	4082002	0.89	0.07	0.77	0.85	-0.24	-0.51	-0.30	-0.30	-0.56	-0.21	-0.16	-0.80	-1.93	-0.02	0.94	-0.17	-0.31	0.01	-0.22	1.76
32	**K-42**	HLC	644494	4081634	-0.39	-0.86	-0.20	0.89	-0.73	0.17	-0.68	-0.74	-0.71	-0.87	-0.73	-0.33	-0.77	0.31	0.91	-0.42	0.87	-0.49	-0.57	1.22
33	**K-7**	**CLC**	642862	4083653	-0.11	-0.33	1.43	1.75	-0.44	0.11	-0.55	-0.50	-0.69	-0.26	-0.25	-0.64	-0.73	-0.16	0.90	-0.34	0.60	-0.90	-0.98	0.97

34	**K-38**	**CLC**	643387	4082903	0.26	-1.10	-1.24	1.01	-0.85	-0.50	-0.83	-0.76	-0.82	-0.91	-0.75	-1.06	-1.14	0.59	0.35	-0.42	0.25	0.07	-0.48	1.14
35	**K-36**	**CLC**	644081	4082513	0.65	-0.61	-1.77	0.87	-0.80	-0.68	-0.65	-0.42	-0.68	-0.70	-0.61	-0.60	-0.85	1.96	1.27	-0.05	-0.35	-1.47	-0.56	1.39

Supplementary Table 1 contuniued.

	ID	Type	X	Y	kcps	Si	S	Cl	K	Ca	Ti	Cr	Mn	Fe	Ni	Zn	As	Se	Br	Rb	Sr	Y	Zr	Pb
36	**K-43**	**CLC**	644872	4082142	-0.50	-0.57	-0.77	0.75	-0.31	0.45	-0.44	-0.33	-0.56	-0.36	-0.24	-0.29	-0.22	0.37	0.76	-0.21	0.64	1.21	-0.35	-0.39
37	**K-66**	**CLC**	645460	4081551	-1.83	-0.95	-0.54	0.69	-0.40	1.69	-0.75	-0.47	-0.60	-0.90	-0.65	-0.86	-0.85	-0.32	1.39	-1.06	2.22	-0.27	0.27	0.07
38	**K-65**	**CLC**	645875	4082013	-1.95	-1.17	-2.17	0.83	-0.39	3.28	-0.82	-0.29	0.03	-1.04	-0.92	-0.69	0.63	-0.77	0.54	-0.91	3.45	-0.51	-0.51	-1.21
39	**K-44**	**CLC**	645379	4082750	-0.40	0.64	1.10	-0.04	0.62	0.32	0.00	0.06	-0.38	0.30	0.28	0.37	-0.92	-0.54	0.11	-0.47	0.08	-0.70	0.92	0.02
40	**K-35**	**CLC**	644430	4082925	-0.08	-0.87	-0.37	0.74	-0.74	-0.03	-0.63	-0.52	-0.75	-0.62	-0.53	-0.38	-1.03	0.47	0.90	-0.57	0.46	-0.17	-0.07	1.18
41	**K-10**	**CLC**	643798	4083413	-0.18	-0.95	-0.03	1.11	-0.69	-0.29	-0.66	-0.60	-0.76	-0.44	-0.32	-0.42	-1.93	0.36	1.15	-0.27	-0.15	-0.70	-1.63	2.25
42	**K-6**	**CLC**	643321	4084181	0.01	-0.64	0.37	1.39	-0.47	-0.03	-0.46	-0.45	-0.68	-0.39	-0.30	-0.81	-0.80	0.29	0.86	-0.18	0.53	-0.55	-1.05	0.99
43	**K-41**	**CLC**	642996	4084726	0.34	-0.84	0.57	1.40	-0.50	-0.35	-0.52	-0.23	-0.68	-0.04	0.09	-0.48	-0.10	-0.01	0.67	-0.61	-0.02	-1.47	-0.45	0.25
44	**K-8**	**CLC**	643029	4085344	0.01	-1.03	-1.00	0.91	-0.82	0.16	-0.77	-0.32	-0.80	-0.67	-0.48	-0.93	-1.35	-0.01	0.80	0.19	0.56	-0.78	-0.88	1.72
45	**K-11**	**CLC**	644188	4084101	-0.06	-0.68	0.23	0.68	-0.65	-0.15	-0.51	-0.47	-0.69	-0.38	-0.26	-0.83	-0.91	0.61	0.48	-0.48	0.25	-1.43	-0.80	0.95
46	**K-34**	**CLC**	644873	4083484	-0.35	-0.79	0.10	0.47	-0.32	0.58	-0.51	-0.37	-0.64	-0.35	-0.22	-0.83	-0.28	-0.15	0.29	-0.75	0.87	-0.43	-0.73	-0.09
47	**K-45**	**CLC**	645775	4083244	-2.42	-0.22	-2.04	0.27	-0.02	4.40	-0.61	1.08	0.05	-0.84	-0.66	-0.21	-0.31	-1.65	-0.15	-1.32	2.59	0.36	-0.52	-1.01
48	**K-64**	**CLC**	646220	4082702	-1.19	0.02	1.17	0.11	0.12	1.90	-0.35	0.09	-0.26	-0.42	-0.20	-0.09	0.55	-0.18	-0.31	-0.66	1.18	0.11	-0.06	-1.72
49	**K-33**	**CLC**	645333	4084028	-1.55	-0.66	-1.30	-0.02	-0.18	2.96	-0.64	-0.08	-0.34	-0.78	-0.48	-0.93	-0.28	-1.32	1.49	-1.13	3.40	0.50	-0.35	-0.64
50	**K-12**	**CLC**	644828	4084650	-1.15	0.07	0.43	-0.09	0.23	0.85	0.02	1.08	0.31	0.24	0.41	0.15	0.28	-1.00	-0.32	-0.14	0.40	-0.62	0.06	-0.62
51	**K-32**	**CLC**	645786	4084749	-0.86	-0.52	-0.84	-0.37	-0.17	1.87	-0.49	-0.33	-0.34	-0.54	-0.30	-0.86	-0.99	-1.24	1.54	-0.34	2.89	-0.76	0.82	-0.05
52	**K-13**	**CLC**	645320	4085261	-3.77	-1.33	-0.34	-2.13	-1.74	-1.38	-1.26	-1.17	-0.98	-1.67	-1.48	-0.77	-1.93	-0.10	-0.90	-0.06	-0.68	1.63	0.23	1.24
53	**K-5**	**CLC**	644934	4085676	-1.01	-0.90	-0.37	-1.33	-1.04	-0.83	-0.90	-0.88	-0.76	-1.00	-0.96	-0.03	-1.30	0.28	-1.03	-0.13	-0.13	0.11	-1.05	0.18
54	**K-14**	**CLC**	645876	4085956	-3.40	-1.25	-1.04	-1.86	-1.61	-1.35	-1.22	-1.07	-0.90	-1.52	-1.35	-0.41	-1.93	0.30	-1.07	0.34	-1.16	1.84	-0.85	2.41
55	**K-31**	**CLC**	646267	4085354	-0.12	1.15	-0.64	-0.96	0.27	0.67	0.44	1.25	1.91	0.46	0.60	1.51	0.39	-0.91	0.35	-0.61	0.11	0.95	0.03	-0.89
56	**K-46**	**CLC**	647507	4085404	-1.02	0.21	-1.44	-0.69	0.17	0.68	0.03	0.16	1.18	0.18	0.17	0.91	2.17	-1.13	0.13	-0.53	0.74	0.70	1.22	-2.54
57	**K-30**	**CLC**	646970	4086044	1.11	-0.28	-0.50	-0.86	-0.49	-0.69	-0.33	-0.35	-0.34	-0.39	-0.39	-0.53	-0.09	1.38	-1.12	-0.25	-0.85	-0.74	-1.63	0.22
58	**K-15**	**CLC**	646450	4086636	0.75	-0.25	0.43	-0.27	-0.15	-0.69	-0.20	-0.46	-0.35	-0.15	-0.32	0.07	1.34	0.72	-0.58	0.12	-0.45	0.20	-0.70	-0.06
59	**K-3**	**CLC**	646262	4087710	0.76	0.07	0.03	-0.48	-0.08	-0.03	-0.16	-0.31	-0.49	-0.07	-0.09	0.72	0.20	0.32	-1.17	-0.66	0.05	-0.02	0.77	-0.17
60	**K-16**	**CLC**	646992	4087300	0.54	-0.87	-0.90	-0.98	-1.11	-1.02	-0.82	-0.54	-0.63	-0.98	-0.73	-0.53	-0.78	1.76	-0.64	0.14	-0.95	0.45	-1.63	2.35
61	**K-29**	**CLC**	647464	4086657	0.54	0.38	-0.10	-0.80	-0.22	-0.29	-0.09	0.21	0.45	0.26	0.26	0.00	-0.62	-0.42	-0.34	0.49	-0.42	1.57	1.17	0.60
62	**K-47**	**CLC**	648001	4086000	-1.43	0.53	0.10	-0.95	0.18	1.63	-0.02	1.06	0.62	-0.06	0.26	0.50	-0.17	-1.59	0.59	-0.24	1.50	1.54	1.42	-1.19
63	**K-63**	**CLC**	648601	4085443	-1.75	0.33	-1.34	-1.06	-0.18	3.00	-0.32	1.75	0.43	-0.39	-0.22	-0.12	0.70	-1.54	-0.59	-0.83	2.15	1.61	1.58	-1.92
64	**K-62**	**CLC**	649048	4085973	-1.64	0.91	-0.64	-1.08	0.20	0.86	0.34	1.85	1.54	0.54	0.79	0.47	-0.37	-2.00	-0.42	-0.39	0.68	0.34	1.16	-1.07
65	**K-48**	**CLC**	648447	4086580	0.47	-0.36	-0.40	-1.12	-0.45	-0.58	-0.10	0.03	0.55	0.12	0.35	-0.14	-0.26	0.16	1.47	-0.23	-0.52	2.51	0.91	-0.46
66	**K-67**	**CLC**	649761	4086044	0.05	2.53	0.17	-1.20	0.56	-0.02	1.33	2.23	1.72	1.93	2.77	1.23	1.08	-0.70	-1.10	-0.11	-0.27	1.19	0.56	-0.94
67	**K-61**	**CLC**	649544	4086587	0.85	-0.11	-0.30	-0.67	-0.10	-0.44	0.13	0.13	3.57	0.64	0.62	-0.03	-1.93	-1.31	1.61	0.70	-0.51	1.72	0.97	0.08
68	**K-49**	**CLC**	648992	4087228	0.38	1.26	-0.24	-1.03	0.23	-0.91	1.50	3.38	3.45	3.00	4.26	0.78	1.54	-1.11	-1.70	0.67	-1.30	-0.31	0.32	-1.33

69	**K-28**	**CLC**	648103	4087422	1.38	-0.33	0.43	-0.66	-0.86	-0.90	-0.42	-0.26	-0.34	-0.22	0.11	-0.97	-1.53	-0.06	-1.24	0.86	-1.11	2.23	0.89	0.98
70	**K-17**	**CLC**	647583	4088032	0.57	1.24	0.23	-0.88	0.29	-0.88	1.63	3.77	0.17	2.77	2.99	1.99	0.81	-0.87	-1.78	0.51	-1.26	-0.31	1.30	-0.89

Supplementary Table 1 contuniued.

	ID	Type	X	Y	kcps	Si	S	Cl	K	Ca	Ti	Cr	Mn	Fe	Ni	Zn	As	Se	Br	Rb	Sr	Y	Zr	Pb
71	**K-18**	**CLC**	648079	4088632	1.18	1.21	0.83	-0.71	0.37	-0.94	1.57	2.73	0.28	2.82	2.79	1.83	0.42	-0.61	-1.51	0.85	-1.27	1.07	1.68	-1.26
72	**K-27**	**CLC**	648616	4088021	0.49	1.48	-0.57	-1.07	0.11	-0.88	1.39	4.16	1.62	2.98	4.15	1.67	0.06	-1.50	-1.85	-0.02	-1.29	-1.25	1.31	-1.55
73	**K-50**	**CLC**	649472	4087826	0.44	3.53	-0.37	-1.34	0.72	-0.72	2.07	3.16	1.49	2.99	4.05	1.92	1.49	-0.68	-1.96	0.87	-1.26	1.16	1.32	-1.64
74	**K-68**	**CLC**	650723	4087255	-0.54	0.01	-1.94	-0.90	-0.09	0.29	0.34	1.53	3.61	0.56	0.61	0.89	0.53	-0.44	0.13	-0.73	-0.59	-1.07	-0.35	-0.29
75	**K-59**	**CLC**	650504	4087831	1.28	-0.44	-0.84	-0.78	-0.88	-0.89	-0.52	-0.60	-0.28	-0.59	-0.45	-0.65	-0.18	1.92	-0.27	0.25	-0.99	0.72	-0.66	0.89
76	**K-51**	**CLC**	650001	4088492	1.07	-0.75	-1.14	-0.61	-0.89	-0.91	-0.71	-0.70	-0.70	-0.91	-0.78	-0.41	0.72	0.93	-1.04	0.00	-1.03	0.42	-0.59	1.05
77	**K-26**	**CLC**	649064	4088587	0.84	1.18	2.00	-1.05	0.50	0.01	0.86	1.22	0.85	1.29	1.37	0.56	0.74	0.18	-0.78	0.94	0.05	0.06	2.29	-1.08
78	**K-19**	**CLC**	648575	4089249	-0.69	-0.22	0.57	-0.49	0.04	2.14	-0.12	0.72	0.48	0.00	0.40	-0.01	0.07	-2.15	-0.35	-0.39	2.12	0.00	1.24	-1.23
79	**K-2**	**CLC**	648150	4089979	0.49	-0.44	-0.37	-0.44	-0.47	-0.95	-0.17	-0.40	-0.25	-0.37	-0.36	0.41	1.40	0.58	-0.60	-0.53	-0.89	-1.47	-0.19	-0.66
80	**K-20**	**CLC**	649088	4089900	0.70	-0.76	-0.57	-0.58	-0.44	-0.39	-0.37	-0.68	-0.59	-0.55	-0.65	0.01	0.83	0.38	-0.80	-0.42	-0.37	0.34	0.02	-0.72
81	**K-25**	**CLC**	649609	4089254	0.95	-0.71	-0.84	-0.48	-0.70	-0.67	-0.66	-0.72	-0.73	-0.92	-0.81	-0.74	0.83	1.99	-0.36	-0.14	-0.90	0.18	-1.63	0.43
82	**K-52**	**CLC**	650482	4089108	1.15	-0.38	-0.90	-0.39	-0.67	-0.91	-0.66	-0.78	-0.61	-0.87	-0.70	-0.91	-0.64	2.03	-0.38	-0.69	-1.11	-0.76	-1.44	0.91
83	**K-58**	**CLC**	651018	4088464	0.71	-0.49	-0.90	-0.34	-0.63	-0.85	-0.52	-0.59	-0.42	-0.66	-0.53	0.09	1.12	1.82	-0.43	-0.32	-0.91	-0.96	-0.86	0.27
84	**K-69**	**CLC**	651220	4087886	0.53	-0.33	-0.03	-0.63	-0.17	-0.60	0.21	0.03	2.38	0.56	0.36	0.90	1.05	1.14	0.42	0.38	-0.81	-0.41	-0.44	0.31
85	**K-57**	**CLC**	651356	4089125	0.85	-0.75	-0.77	-0.59	-0.46	-0.64	-0.27	-0.50	-0.41	-0.25	-0.21	-0.55	0.48	0.09	-0.62	-0.25	-0.57	-0.87	-1.08	0.43
86	**K-24**	**CLC**	650173	4089890	0.23	0.67	0.97	-0.71	1.56	-1.16	2.51	0.29	0.16	1.85	0.45	1.95	1.78	0.89	-1.21	2.00	-1.30	-0.37	1.21	-0.53
87	**K-53**	**CLC**	650932	4089676	0.96	-0.76	-0.44	-0.39	-0.69	-0.90	-0.52	-0.60	-0.57	-0.67	-0.33	-1.06	0.07	1.15	-0.63	0.14	-1.11	-0.52	-0.89	0.77
88	**K-56**	**CLC**	651919	4089598	0.38	0.21	1.03	-0.91	0.58	-0.08	0.31	-0.28	-0.03	0.21	0.06	0.43	0.72	0.10	-0.53	0.18	0.03	1.19	0.15	-0.53
89	**K-70**	**CLC**	652739	4089574	-0.15	-0.52	-0.74	-1.18	0.30	0.23	-0.01	-0.52	0.08	-0.26	-0.49	-0.24	1.25	-0.42	-0.71	-0.21	0.51	-0.67	-0.62	-0.17
90	**K-74**	**CLC**	653614	4089248	0.16	-0.47	-0.03	-1.01	0.08	-0.05	-0.30	-0.44	0.41	-0.42	-0.45	-0.35	-0.77	0.13	-0.52	0.31	-0.12	-0.41	-0.74	0.73
91	**K-73**	**CLC**	653410	4089703	0.34	-0.36	-0.14	-0.97	-0.07	0.60	-0.42	-0.57	0.23	-0.46	-0.53	-0.17	-0.40	0.40	-0.57	-0.10	0.69	-1.47	-0.10	-0.48
92	**K-55**	**CLC**	652306	4090116	0.53	0.59	0.93	-0.98	0.15	-0.64	-0.13	-0.45	0.74	-0.12	-0.25	-0.10	1.25	1.04	-0.71	0.25	-0.66	-0.67	-0.94	0.40
93	**K-54**	**CLC**	651381	4090220	0.63	0.02	0.30	-0.90	0.49	-0.53	0.00	-0.47	-0.21	-0.20	-0.32	-0.86	1.10	-0.07	-0.90	0.05	-0.87	-0.41	-1.15	0.52
94	**K-23**	**CLC**	650589	4090434	0.72	-0.40	-1.17	-0.40	0.05	-0.49	-0.05	-0.49	-0.54	-0.16	-0.23	-0.35	-0.56	1.66	-0.64	0.38	-1.03	0.55	-1.35	1.17
95	**K-21**	**CLC**	649632	4090562	-0.44	2.22	-0.84	-1.11	2.73	-1.06	4.09	1.02	0.70	2.84	0.71	3.08	1.16	-0.69	-1.71	1.66	-1.27	0.32	2.05	-0.96
96	**K-1**	**CLC**	648955	4090607	0.70	-0.17	-0.37	-0.51	-0.37	-1.02	0.01	-0.56	-0.51	-0.41	-0.73	0.52	-0.29	1.80	-0.74	-0.51	-1.16	-1.33	-0.79	1.29
97	**K-22**	**CLC**	648280	4090888	0.35	0.16	0.10	-0.90	0.24	-1.03	0.38	-0.34	0.49	0.18	-0.31	1.14	-1.29	0.93	-0.72	0.45	-1.17	-0.19	-0.28	1.05
98	**K-75**	**CLC**	649456	4091218	-0.28	5.16	0.60	-1.15	3.85	-0.91	5.62	1.35	1.11	3.39	1.25	3.35	0.54	-0.99	-1.95	2.60	-1.25	0.93	3.24	-1.82
99	**K-76**	**CLC**	650035	4091048	-0.33	1.72	0.43	-0.15	2.11	-0.82	1.81	0.28	0.40	1.47	0.32	1.46	-0.53	-0.73	-0.95	1.42	-1.12	0.71	1.60	-0.52
100	**K-77**	**CLC**	650813	4090888	-0.49	-0.52	0.10	0.87	0.85	1.14	0.30	-0.53	-0.18	-0.03	-0.38	0.72	-1.40	-1.93	-0.56	0.62	0.28	0.01	0.29	-0.80
101	**K-78**	**CLC**	651312	4090737	0.22	3.21	-0.70	-1.51	6.84	-1.12	3.17	-0.44	4.08	2.04	-1.14	4.96	1.82	-0.76	-1.57	7.86	-1.29	1.39	3.11	-0.46
102	**K-79**	**CLC**	651919	4090534	-0.22	-0.55	-1.10	-1.20	0.60	0.28	-0.36	-0.74	0.14	-0.77	-0.95	0.23	2.26	0.13	-1.32	-0.79	0.62	2.53	1.38	-1.08
103	**K-80**	**CLC**	652488	4090455	0.89	-0.41	-1.04	-1.43	0.07	-0.04	-0.38	-0.78	0.61	-0.51	-0.71	-0.56	-0.20	1.00	-0.29	0.22	-0.08	-1.35	-0.71	0.31

104	**K-71**	**CLC**	653093	4090108	0.86	-0.28	-0.03	-1.06	0.11	-0.18	-0.37	-0.63	0.44	-0.39	-0.48	-0.64	-0.45	0.26	-1.15	0.38	0.31	-1.12	-1.01	0.65
105	**K-72**	**CLC**	653719	4089989	0.66	-0.20	0.17	-1.30	-0.07	-0.29	-0.22	-0.50	0.57	-0.30	-0.46	-0.29	-0.81	0.19	-0.58	0.69	-0.26	-0.52	-0.14	1.09

Supplementary Table 2. Standardized ITRAX analysis results for Dalyan channel cores.

	ID	Type	X	Y	kcps	Si	S	Cl	K	Ca	Ti	Cr	Mn	Fe	Ni	Zn	As	Se	Br	Rb	Sr	Y	Zr	Pb
1	**D-L-1**	CLC	645642	4080700	0.43	-1.82	-0.38	-0.70	-2.69	3.43	-3.14	-1.12	-1.41	-3.20	-2.36	-2.60	-1.93	1.19	2.18	-1.68	3.61	0.77	-1.57	1.14
2	**D-L-2**	CLC	645589	4079949	1.02	-1.62	-0.33	-0.66	-1.17	-0.52	-1.32	-0.95	-1.85	-1.45	-1.25	-1.24	-1.95	0.50	1.57	-1.25	0.65	1.80	0.88	2.05
3	**D-L-3**	CLC	645622	4079284	-0.76	0.90	-0.13	-0.73	1.35	0.03	0.70	-0.65	1.43	0.50	0.00	-0.43	-0.56	-0.46	-0.93	1.38	-0.53	-0.84	0.51	-0.37
4	**D-006-130**	CLC	645505	4079077	0.61	1.93	0.07	-0.08	1.49	0.00	0.89	-0.38	1.42	1.15	0.74	-0.12	-1.19	0.58	-1.31	1.29	-0.62	0.58	1.28	0.11
5	**D-006-133**	CLC	645460	4079062	1.22	1.53	-0.01	-0.18	1.90	-1.11	1.64	-1.04	0.22	1.21	-0.13	1.99	-0.11	0.54	1.05	1.79	-0.59	1.02	1.81	-0.22
6	**D-006-000**	HLC	645551	4079019	0.12	-1.18	-0.12	0.65	-1.29	-0.07	-0.23	0.22	0.40	0.00	0.60	-1.39	0.24	-0.31	0.32	0.01	-0.22	-0.34	-0.30	-1.29
7	**D-006-134**	CLC	645496	4079018	1.57	-0.15	1.61	0.59	1.00	-1.37	0.52	-0.98	1.62	0.49	-0.73	-0.48	1.24	0.74	1.45	0.34	-0.64	-0.98	-0.09	-1.16
8	**D-006-132**	CLC	645542	4078991	-1.07	-0.76	-0.88	2.08	0.78	0.93	-0.39	-0.75	-0.67	-1.08	-1.44	-0.06	0.73	-0.90	-0.04	-0.98	1.70	1.93	-1.21	-1.45
9	**D-006-138**	CLC	645578	4078952	-0.92	-1.53	0.05	1.41	-0.42	1.61	-1.70	-0.94	-0.60	-2.23	-2.02	0.06	-0.88	1.09	0.40	-1.28	2.41	-1.25	-1.07	-0.48
10	**D-006-137**	CLC	645522	4078943	0.81	1.13	0.27	1.20	1.52	0.13	0.84	-0.47	-0.08	0.11	-0.69	0.04	-0.22	0.37	0.00	1.44	0.06	-0.51	1.47	1.43
11	**D-005-139**	CLC	645650	4078782	0.30	0.34	-1.85	-1.81	-0.42	-0.27	0.20	-0.28	0.99	0.09	0.54	-0.45	-1.10	0.58	-0.22	-0.18	-0.42	0.76	0.49	0.90
12	**D-005-140**	CLC	645613	4078736	-0.54	0.88	0.83	-0.92	0.04	-0.27	0.67	0.28	-0.91	0.44	0.79	0.32	0.27	0.22	-1.11	-1.08	-0.30	-0.58	-0.72	0.68
13	**D-005-141**	CLC	645561	4078729	-0.48	0.04	-0.51	-0.01	-0.32	0.79	-0.42	1.15	-1.37	-0.22	-0.08	0.51	-1.11	-1.00	-0.49	0.82	0.08	1.54	0.87	1.56
14	**D-005-000**	HLC	645629	4078718	-1.28	0.73	-1.43	-0.70	-0.34	0.67	-0.45	0.62	-0.05	0.35	0.97	-0.70	1.87	-1.76	-1.00	-1.28	-0.32	-0.95	-0.88	-2.67
15	**D-005-142**	CLC	645594	4078690	-1.26	0.08	-0.01	0.27	-0.50	0.70	-0.66	1.59	-0.34	0.22	1.04	-0.56	1.45	-1.87	-1.41	-0.41	-0.32	-0.18	-0.98	0.00
16	**D-005-144**	CLC	645635	4078680	0.59	-1.22	-0.23	-0.68	-1.28	0.04	-0.85	0.06	0.66	-0.41	0.46	-0.59	0.45	0.33	-0.02	0.01	-0.20	-1.52	1.21	-0.62
17	**D-005-143**	CLC	645591	4078648	-0.97	-0.04	0.22	-0.44	-0.64	1.02	-0.66	1.24	-0.35	-0.06	0.83	-0.48	1.44	-0.78	-0.67	-1.62	0.26	-0.09	0.50	-0.58
18	**D-L-4**	CLC	645736	4078344	0.17	-0.36	2.18	0.05	-0.25	-0.91	0.46	-0.40	-1.30	0.06	-0.11	0.37	1.22	-0.30	-0.19	1.20	-0.38	0.55	-1.08	-0.40
19	**D-016-146**	CLC	645901	4078252	0.07	0.33	0.27	-0.70	0.20	-0.15	0.80	-0.31	0.61	0.32	0.19	1.36	0.99	0.58	-0.10	0.63	-0.25	-1.11	-0.21	-0.16
20	**D-016-145**	CLC	645825	4078250	-0.21	-1.36	-1.13	-0.55	-0.78	-0.26	-0.52	-0.43	-0.23	-0.51	-0.50	-0.51	0.18	1.50	0.06	-0.43	0.20	0.74	0.60	0.63
21	**D-016-147**	CLC	645882	4078189	0.21	1.13	2.18	-0.28	0.72	-0.65	1.04	-0.09	-1.22	0.61	0.52	-0.32	-0.38	0.04	-0.64	0.80	-0.51	0.88	0.80	0.49
22	**D-016-000**	HLC	645955	4078161	-0.34	0.39	-0.33	0.14	0.22	-0.03	0.47	0.14	0.86	0.42	0.50	0.35	-0.24	0.41	-0.65	0.03	-0.37	0.88	0.22	-0.67
23	**D-016-658**	CLC	645981	4078103	1.08	0.10	0.37	-0.62	0.50	-0.24	0.50	-0.12	0.81	0.41	0.04	0.69	-0.15	0.67	0.17	0.55	-0.14	0.36	-0.25	0.22
24	**D-016-148**	CLC	645926	4078102	0.06	-0.36	1.12	-0.37	-0.10	-0.79	-0.26	-0.45	-0.67	0.02	-0.23	0.37	0.18	-1.07	0.21	0.06	-0.32	-1.34	0.26	-0.32
25	**D-016-149**	CLC	645942	4078052	1.67	-0.99	-0.53	-0.17	-0.44	-0.84	-0.49	-0.97	1.37	-0.41	-1.01	-0.35	0.02	1.10	-0.02	0.37	-0.39	0.05	0.55	0.41
26	**D-016-150**	CLC	646012	4078027	0.68	0.21	0.37	-0.39	-0.11	-0.66	0.08	-0.10	-0.28	0.23	-0.04	0.14	0.24	-0.09	-0.17	-0.31	-0.28	-0.06	-0.63	0.10
27	**D-L-6**	CLC	646067	4077417	-2.88	0.67	-1.78	-0.55	0.22	0.73	0.95	3.33	-0.40	1.48	2.34	0.30	0.53	-1.26	-1.63	-0.95	-1.05	-0.75	-2.32	-0.41
28	**D-L-10**	CLC	645015	4076334	-0.21	0.44	0.67	2.80	0.70	-1.09	0.90	0.60	1.39	0.92	0.61	1.92	-0.13	1.33	1.78	-0.08	-0.62	-1.35	-0.45	0.44
29	**D-L-8**	CLC	645930	4076095	0.32	0.56	-0.63	1.38	0.10	-0.84	0.44	1.21	-0.05	0.54	0.43	1.85	-1.12	-2.01	1.40	0.80	-0.51	-0.02	0.32	0.63

Supplementary Table 3. Standardized ITRAX analysis results for Fethiye-Göcek bay cores.

	ID	Type	X	Y	kcps	Si	S	Cl	K	Ca	Ti	Cr	Mn	Fe	Ni	Zn	As	Se	Br	Rb	Sr	Y	Zr	Pb
1	**I-100**	HLC	675787	4066071	-1.40	-2.01	1.63	3.45	-0.98	3.10	-2.17	-0.58	-2.57	-2.56	-1.59	-2.61	-0.52	-0.69	-0.91	-2.58	3.65	-0.84	-1.13	-1.60
2	**I-103**	HLC	675803	4066045	-1.90	-2.26	3.70	2.47	-1.03	3.33	-2.09	-1.21	-2.39	-2.65	-1.72	-1.91	-1.17	-0.74	-0.58	-2.63	3.28	-1.97	-0.52	-1.25
3	**I-123**	HLC	675819	4066069	-2.03	-3.08	3.21	1.08	-1.51	5.50	-3.16	-1.15	-2.79	-3.29	-1.85	-3.51	-0.46	-2.96	-1.98	-3.06	4.11	0.65	-1.72	-1.67
4	**I-106**	HLC	675722	4066166	-2.38	-3.33	1.39	3.03	-1.78	3.43	-3.24	-0.88	-2.77	-2.45	-1.35	-2.80	-0.10	-0.06	-1.68	-2.68	1.86	-0.70	-1.56	-0.44
5	**I-122**	HLC	675744	4066234	-0.53	-0.65	1.63	0.02	-2.17	-0.21	-3.15	0.35	-1.08	1.10	2.95	-3.05	3.20	-3.41	-2.65	-1.68	-0.07	-1.76	-2.72	-2.10
6	**I-107**	HLC	675770	4066297	0.46	-1.84	1.75	1.36	-2.43	0.94	-3.36	0.11	-0.47	0.03	1.22	-2.92	1.73	0.19	-1.67	-2.32	0.70	-1.19	-2.16	-1.50
7	**I-111**	HLC	675811	4066096	-1.10	-0.12	0.54	0.07	-0.32	0.16	-0.26	-0.31	-0.76	-0.51	-0.16	-0.24	-0.21	-1.19	0.35	-0.58	1.83	-0.52	-0.36	-0.44
8	**I-126**	HLC	675848	4066058	-0.11	-0.59	0.66	0.36	-0.16	0.27	-0.17	-0.38	-0.73	-0.60	-0.34	0.70	0.30	-1.19	1.52	-0.84	2.99	-1.10	-0.14	-1.33
9	**I-114**	HLC	675878	4066055	-0.42	0.87	-0.31	-0.86	-0.81	0.44	-0.55	1.01	-0.22	0.07	0.47	-0.53	0.05	-0.74	-0.79	-1.36	1.89	-0.73	-0.61	-0.29
10	**I-125**	HLC	675868	4066089	-0.08	0.56	0.90	-0.99	-1.01	0.13	-0.37	1.19	0.16	0.30	0.67	-0.54	-1.23	-1.17	-1.02	-1.15	1.66	-0.71	-1.58	-0.23
11	**I-112**	HLC	675863	4066127	-0.24	0.56	0.17	-1.05	-1.10	0.36	-0.82	1.45	0.43	0.54	0.89	-0.78	0.18	-1.19	-1.27	-0.88	0.83	-1.10	-1.21	-0.54
12	**I-124**	HLC	675826	4066143	-0.26	0.05	-0.19	-0.30	-1.04	0.13	-0.47	2.07	0.45	0.46	0.82	-0.56	0.84	-0.58	-1.30	-1.27	1.25	-0.64	-1.38	-1.19
13	**I-115**	CLC	675794	4066195	0.34	1.04	0.36	-1.09	-1.25	-0.14	-0.81	1.57	0.43	1.16	1.40	-0.92	3.62	-0.40	-1.72	-1.40	0.04	-2.41	-1.98	-2.60
14	**I-120**	CLC	675849	4066189	0.47	1.57	-0.07	-1.46	-1.23	-0.40	-0.48	1.74	0.84	1.20	1.37	-0.09	0.32	-0.33	-1.06	-0.53	-0.17	-0.87	-0.93	-0.90
15	**I-109**	CLC	675925	4066101	0.46	-0.18	-0.25	0.09	-1.26	-0.64	-0.54	1.43	0.76	1.18	1.28	-0.59	0.25	-0.47	-0.74	-0.51	-0.41	-2.18	-0.93	0.27
16	**I-127**	CLC	675923	4066051	0.37	0.17	0.05	-1.08	-0.99	-0.54	-0.37	1.36	0.55	1.17	1.33	-0.62	0.59	-0.38	-0.75	-0.19	-0.18	-0.94	-1.33	-0.48
17	**I-135**	CLC	675938	4066008	1.25	-0.86	-0.56	-0.35	-1.12	-0.41	-0.15	1.77	1.23	1.65	1.68	0.01	1.31	-1.78	-1.14	0.09	-0.25	-0.73	-1.50	0.22
18	**I-110**	CLC	675968	4066030	0.61	0.05	-0.43	-0.64	-1.18	-0.66	-0.44	1.30	0.59	1.20	1.28	0.01	-0.48	-0.47	-0.92	-0.56	-0.50	-1.51	-0.15	0.22
19	**I-105**	CLC	675952	4065951	0.63	0.01	1.02	-0.01	-0.92	-0.60	-0.45	1.69	0.36	1.00	1.21	0.17	0.55	0.94	-0.88	-0.40	-0.25	0.19	-0.88	-0.29
20	**I-121**	CLC	675987	4066125	0.84	0.42	0.66	-1.20	-0.98	-0.65	0.03	1.32	0.78	1.46	1.51	-0.34	0.66	-0.76	-1.31	0.01	-0.53	-1.33	-1.20	-0.79
21	**I-113**	CLC	675938	4066182	0.33	0.58	-0.07	-1.53	-1.24	-0.69	-0.31	0.95	0.60	0.99	1.09	-0.21	0.11	-1.37	-0.55	-0.70	-0.53	-0.63	-0.92	-1.06
22	**I-116**	CLC	675869	4066262	0.57	1.57	-0.74	-1.71	-0.80	-0.60	0.59	1.28	0.73	1.28	1.15	0.25	-0.17	-1.67	-1.09	-0.35	-0.46	0.01	-0.74	-1.04
23	**I-133**	CLC	675774	4066397	0.73	0.19	0.90	0.16	-1.30	0.05	-0.79	1.13	0.33	1.10	1.35	-1.17	0.81	0.21	-1.26	-1.15	0.53	-2.01	-1.07	-1.06
24	**I-132**	CLC	675906	4066352	1.05	0.38	0.42	-0.41	-0.95	-0.52	0.59	1.76	1.36	1.60	1.34	0.26	-0.64	0.60	-1.55	-0.16	-0.29	-0.31	-1.04	-0.44
25	**I-131**	CLC	675971	4066261	1.11	-0.10	-1.35	-1.13	-1.16	-0.71	0.47	1.19	0.87	1.63	1.53	-0.01	0.94	-1.39	-0.96	-0.40	-0.54	-1.46	-1.05	-0.40
26	**I-130**	CLC	676045	4066186	1.20	-0.16	-0.31	-0.96	-1.28	-0.85	-0.21	1.09	0.62	1.48	1.66	-0.70	0.49	0.05	-0.84	-0.26	-0.63	-0.59	-1.36	-1.83
27	**I-129**	CLC	676008	4066072	0.55	0.13	0.66	-1.00	-0.91	-0.77	0.02	1.35	0.46	1.43	1.44	-0.27	-0.06	-0.10	-0.80	-0.18	-0.58	-0.48	-1.22	-0.01
28	**I-128**	CLC	676052	4065986	0.30	0.01	0.54	-0.95	-1.18	-0.78	-0.51	1.32	0.67	1.31	1.52	-0.43	0.40	0.39	-0.88	-0.16	-0.59	-1.40	-1.32	-0.44
29	**F-70**	CLC	672579	4065446	-0.37	-1.20	-0.61	1.14	0.51	0.61	-0.31	-0.54	-0.74	-0.84	-0.66	0.03	-0.74	0.31	0.46	-0.08	0.45	-0.87	-0.07	0.49
30	**F-63**	CLC	673395	4068021	-0.98	0.47	-1.70	-0.41	-0.91	-0.10	-0.65	1.57	0.66	0.33	0.37	0.51	0.88	-1.34	-0.93	-0.76	-0.10	-0.77	-1.05	-0.67
31	**F-64**	CLC	672902	4068383	-0.17	-0.28	-0.80	-0.02	-0.97	-0.03	-0.11	2.68	0.33	0.67	-0.18	-0.28	2.67	-0.28	-1.23	-0.92	-0.38	-2.04	-0.98	-2.14
32	**F-65**	CLC	672794	4067762	-1.35	-0.62	-0.21	0.88	-0.44	1.40	-0.61	0.50	-0.67	-0.55	-0.80	-0.88	0.98	1.49	-0.79	-1.25	0.64	0.05	-0.92	-1.18
33	**F-66**	CLC	672606	4067052	-0.83	-0.57	-0.31	0.62	0.46	0.20	0.13	-0.13	-0.65	-0.63	-0.78	0.72	-0.36	0.23	0.19	0.27	0.03	0.30	0.86	-0.12

34	**F-67**	CLC	672154	4066275	-0.11	-0.11	-1.10	0.69	0.95	0.08	0.63	-0.23	-0.96	-0.56	-0.80	0.08	-0.91	1.33	0.68	0.80	-0.07	1.29	0.19	0.40
35	**F-69**	CLC	671900	4065635	-0.29	-0.03	-1.00	0.29	0.95	0.50	0.36	-0.46	-0.70	-0.73	-0.81	0.84	-0.65	-1.02	0.62	0.41	0.16	1.22	0.28	1.10

Supplementary Table 3 continued.

	ID	**Type**	**X**	**Y**	**kcps**	**Si**	**S**	**Cl**	**K**	**Ca**	**Ti**	**Cr**	**Mn**	**Fe**	**Ni**	**Zn**	**As**	**Se**	**Br**	**Rb**	**Sr**	**Y**	**Zr**	**Pb**
36	**F-85**	CLC	673753	4067631	0.67	0.39	0.78	0.24	-0.78	-0.42	-0.56	0.62	1.01	0.50	1.02	-0.09	0.39	0.04	-0.34	-0.41	-0.35	0.02	-0.16	0.21
37	**F-62**	CLC	674501	4066666	0.03	0.55	-0.01	-1.03	-0.03	-0.57	0.13	0.11	0.23	0.18	0.54	0.60	-1.13	-1.02	-0.40	0.02	-0.43	-0.46	-0.85	0.34
38	**F-84**	CLC	674888	4066139	0.72	1.48	0.38	-1.29	-0.55	-0.43	-0.45	-0.29	0.86	0.58	0.96	-0.11	-0.25	-0.24	-0.63	-0.35	-0.33	-0.57	-0.17	0.19
39	**F-61**	CLC	676075	4065876	0.64	-0.06	1.08	-0.29	-1.42	-0.83	-0.80	1.23	0.51	0.88	1.31	-0.37	0.55	0.64	-0.51	-0.52	-0.60	-0.82	-1.13	-1.08
40	**F-60**	CLC	674636	4065442	-0.65	-0.65	-1.10	-0.14	-0.13	-0.37	-0.44	1.32	0.01	-0.30	-0.10	1.08	-0.65	0.17	0.44	-0.13	-0.41	0.76	0.44	1.32
41	**F-71**	CLC	673064	4065097	-1.58	-2.58	2.26	2.15	-0.22	2.56	-1.84	-0.94	-2.40	-2.22	-1.58	-3.00	-0.14	-1.81	2.99	-1.70	3.27	-0.18	-0.84	-0.84
42	**F-59**	CLC	673793	4064755	0.04	-0.08	-0.92	-0.30	0.47	-0.18	-0.12	0.07	0.03	-0.36	-0.30	1.08	-0.69	0.30	1.09	0.73	-0.17	-0.09	0.09	-0.05
43	**F-55**	CLC	674162	4063171	-0.28	-0.94	-0.80	0.12	0.81	-0.27	0.16	-0.99	-0.31	-0.70	-0.92	0.86	-0.44	1.80	1.44	0.80	-0.43	0.26	0.72	2.11
44	**F-54**	CLC	674871	4064254	-1.60	0.05	0.17	1.19	0.05	-0.20	0.20	1.57	1.75	-0.41	0.16	0.26	-1.19	-1.15	-0.53	-0.28	-0.56	-0.52	-0.49	-0.48
45	**F-53**	CLC	675750	4064933	-0.66	0.13	-1.29	-0.52	0.65	-0.44	0.47	0.02	0.01	-0.12	-0.20	0.89	-2.14	-0.24	0.53	0.90	-0.50	0.08	1.08	0.60
46	**F-83**	CLC	676498	4065157	1.21	0.64	0.78	-1.42	-0.51	-0.93	0.53	-0.64	1.07	0.84	0.82	-0.21	-0.18	0.74	-0.25	0.02	-0.62	0.99	-0.20	0.57
47	**F-52**	CLC	676183	4064459	-1.17	-0.36	-0.68	-0.93	-0.02	-0.58	-0.09	-0.10	-0.82	-0.22	-0.02	0.96	-1.03	0.57	0.50	0.36	-0.55	-0.17	-0.34	-0.36
48	**F-51**	CLC	675922	4063775	-1.05	-0.06	-0.56	-0.63	1.11	-0.19	0.67	-0.87	-0.81	-0.39	-0.63	1.03	-0.36	-0.26	0.45	0.96	-0.45	0.44	1.01	0.66
49	**F-50**	CLC	674894	4062595	-1.06	-0.67	-1.71	-0.17	1.13	0.08	0.51	-1.10	0.26	-0.55	-0.94	1.27	0.49	0.12	0.74	1.10	-0.28	0.95	1.01	1.43
50	**F-49**	CLC	674129	4061555	-0.91	-0.73	-0.74	1.29	0.82	0.69	-0.13	-0.93	2.77	-1.02	-1.11	-0.13	0.65	-0.81	-0.08	-0.55	0.80	0.88	-0.17	-0.25
51	**F-48**	CLC	675028	4060955	-1.25	-0.36	-1.41	0.46	1.33	0.69	-0.03	-1.45	-0.11	-1.10	-1.35	-0.72	-0.31	0.89	0.45	0.26	0.20	2.03	-0.24	0.53
52	**F-46**	CLC	677029	4063255	-0.11	0.48	-0.74	-0.01	0.85	-0.12	0.56	-0.54	1.41	-0.15	-0.44	0.97	-0.12	0.39	0.91	0.96	-0.42	0.95	1.11	0.66
53	**F-82**	CLC	677457	4064661	0.84	0.89	0.28	-0.96	0.42	-0.86	0.76	-0.73	1.02	0.59	0.57	0.46	0.07	1.10	-0.27	1.39	-0.64	0.50	1.53	1.66
54	**F-45**	CLC	677798	4063913	0.12	0.64	-0.25	-0.57	0.77	-0.35	0.88	0.04	0.47	0.26	0.18	1.16	0.14	-0.31	0.45	1.04	-0.55	0.70	0.40	0.06
55	**F-44**	CLC	676980	4061670	-0.37	-0.82	-1.04	0.67	0.98	0.06	0.14	-1.35	0.72	-0.89	-1.16	0.45	-0.73	0.44	1.27	0.74	-0.30	1.29	1.04	1.57
56	**F-43**	CLC	676003	4060805	-0.23	-0.45	-0.07	0.56	1.39	0.54	0.15	-1.48	1.85	-1.01	-1.22	1.40	0.61	1.12	1.22	0.61	-0.12	1.18	0.70	0.56
57	**F-42**	CLC	676705	4060313	-0.01	-1.41	-0.01	1.22	1.31	0.18	0.13	-1.59	0.16	-1.01	-1.37	0.17	0.25	0.30	1.33	0.64	-0.22	-0.17	0.72	1.78
58	**F-41**	CLC	677700	4061345	0.34	-1.43	-1.35	1.28	0.86	0.15	0.13	-1.34	1.19	-1.07	-1.18	0.44	0.69	0.53	1.31	1.48	-0.09	0.69	0.61	0.31
59	**F-40**	CLC	677976	4062819	0.00	0.83	-0.31	0.38	0.84	0.16	0.42	-0.37	0.20	-0.28	-0.38	0.39	0.55	1.52	0.19	0.66	-0.28	0.37	0.55	0.14
60	**F-39**	CLC	678685	4063745	0.33	0.29	-0.19	-0.25	0.95	-0.38	0.55	0.30	0.40	0.29	0.32	1.11	0.17	1.07	0.21	0.96	-0.56	0.17	0.95	0.45
61	**F-38**	CLC	679251	4064155	0.79	0.25	-0.68	0.09	0.05	-0.65	0.23	0.35	0.40	0.43	0.58	0.36	-0.06	-0.15	1.03	0.72	-0.68	-0.91	0.61	0.99
62	**F-81**	CLC	680053	4064611	2.15	-0.03	0.18	-0.56	-1.40	-1.52	-0.70	-0.56	0.91	2.13	2.12	-0.07	0.55	-0.36	-0.33	0.34	-0.74	-1.02	-0.13	-0.99
63	**F-37**	CLC	678793	4062439	0.26	0.87	-0.92	-0.20	1.03	0.05	0.69	-0.23	-0.56	-0.06	-0.06	1.08	-0.92	0.39	0.39	0.82	-0.19	0.97	0.85	0.72
64	**F-36**	CLC	679773	4063445	0.90	0.52	-0.68	0.14	0.61	-0.44	0.73	-0.04	0.25	0.31	0.22	0.92	0.67	1.09	0.49	1.08	-0.56	0.28	1.10	-0.19
65	**F-35**	CLC	679600	4062065	1.03	1.04	-0.80	0.11	1.02	-0.03	1.03	-0.25	-0.45	0.05	-0.22	0.55	-0.19	-0.29	0.16	0.71	-0.24	-0.06	0.89	0.22
66	**F-34**	CLC	678659	4060908	0.28	1.18	-0.56	0.50	1.26	0.87	0.60	-0.79	-0.84	-0.70	-0.75	0.80	-0.81	-0.33	-0.02	0.24	0.42	1.75	1.49	-0.17
67	**F-33**	CLC	677723	4059825	0.84	0.62	0.90	0.70	1.52	0.68	0.91	-1.01	-0.62	-0.63	-0.88	1.21	-0.73	-1.33	0.46	0.55	0.12	1.75	1.14	2.76
68	**F-32**	CLC	678667	4059442	-0.96	0.69	-1.22	0.15	1.27	0.94	0.23	-1.15	-1.31	-0.96	-1.16	-0.83	0.60	-0.33	0.33	0.18	0.28	0.14	-0.03	-0.19

69	**F-31**	CLC	679543	4060525	-1.19	0.75	-0.43	-0.06	1.47	0.40	0.69	-1.05	-1.46	-0.86	-0.96	0.32	-1.17	-1.42	0.16	0.78	0.58	1.78	0.68	-0.83
70	**F-30**	CLC	680315	4061729	-1.21	1.51	0.05	-1.66	1.19	-0.29	1.46	-0.65	-0.52	-0.18	-0.64	0.64	-0.75	0.30	-0.10	1.61	-0.63	0.01	0.97	1.10

Supplementary Table 3 continued.

	ID	Type	X	Y	kcps	Si	S	Cl	K	Ca	Ti	Cr	Mn	Fe	Ni	Zn	As	Se	Br	Rb	Sr	Y	Zr	Pb
71	**F-80**	CLC	681072	4063573	0.08	1.01	1.08	-0.34	2.53	-0.48	2.70	-0.95	0.01	-0.27	-0.78	1.41	-1.18	0.82	0.22	2.22	-0.88	1.55	2.52	0.99
72	**F-29**	CLC	680862	4062964	-0.67	0.29	0.42	-0.86	0.38	-0.63	0.52	-0.74	-1.05	-0.67	-0.76	0.10	-1.55	0.35	0.96	0.71	-0.83	0.65	0.50	-0.21
73	**F-28**	CLC	680903	4061463	-1.46	0.29	-0.92	-1.04	0.72	-0.44	1.08	-0.55	-0.60	-0.47	-0.80	0.44	-0.37	0.69	0.34	1.13	-0.62	0.61	0.87	0.18
74	**F-27**	CLC	681579	4062136	-1.28	1.43	-0.74	-1.28	0.08	-0.38	0.41	-0.55	-0.87	-0.60	-0.60	-0.43	-0.71	-1.35	-0.18	0.50	-0.85	-0.55	0.05	1.26
75	**F-26**	CLC	682323	4061719	-0.99	1.73	0.05	-1.08	0.46	-0.39	1.28	-0.24	-0.61	-0.45	-0.73	0.01	-1.47	1.39	-0.91	0.73	-0.88	0.69	0.78	-0.13
76	**F-25**	CLC	681554	4061164	-0.40	0.87	-0.68	-1.00	2.00	-0.68	2.29	-0.76	-1.13	0.07	-0.89	1.43	-1.28	1.03	0.07	2.44	-0.76	1.29	1.13	-0.01
77	**F-24**	CLC	680482	4060097	-1.14	0.34	-1.22	-0.23	0.80	0.46	0.29	-0.82	-1.28	-1.02	-0.78	-0.27	-0.82	-0.62	-0.02	-0.11	0.57	0.31	0.12	-1.62
78	**F-23**	CLC	679671	4059085	-1.70	-1.06	-0.31	-0.12	0.67	0.17	-0.02	-1.47	0.18	-1.17	-1.29	-0.53	1.08	0.48	0.48	0.10	-0.17	1.78	0.14	-0.52
79	**F-22**	CLC	680736	4058572	0.24	-1.02	0.42	0.77	0.71	-0.19	0.03	-1.37	0.54	-0.87	-1.00	0.51	0.40	0.53	1.34	1.01	-0.40	1.15	0.19	0.83
80	**F-21**	CLC	682368	4060784	-0.99	0.87	-1.10	-0.62	1.54	-0.41	1.61	-0.35	-0.39	0.15	-0.53	0.26	0.43	-0.22	-0.24	0.75	-0.43	0.28	0.78	-1.31
81	**F-19**	CLC	683306	4060356	-0.32	0.42	0.17	-0.64	0.61	-0.43	1.12	-0.50	-0.86	-0.15	-0.66	0.45	-0.56	-0.42	0.29	1.06	-0.75	1.18	0.95	0.18
82	**F-18**	CLC	681776	4058139	-0.18	-0.28	-0.19	-0.01	0.79	-0.58	0.75	-0.55	1.83	0.10	0.09	0.77	-1.68	1.57	0.72	0.44	-0.52	0.72	1.35	0.91
83	**F-17**	CLC	682873	4057768	-0.83	0.13	-0.68	-0.57	0.80	-0.04	0.35	-1.09	-0.41	-0.54	-0.46	-0.27	-2.50	0.39	0.31	0.46	-0.41	0.15	0.50	0.68
84	**F-16**	CLC	684254	4059913	0.12	0.95	0.66	-0.56	0.45	-0.33	0.70	-0.53	-0.85	-0.13	-0.55	0.53	-0.43	-0.17	0.45	0.62	-0.60	0.22	0.67	0.91
85	**F-15**	CLC	684122	4060834	0.50	1.41	-0.19	0.00	0.29	-0.18	1.01	0.12	-0.04	-0.07	-0.50	0.14	0.42	0.53	-0.17	0.23	-0.73	2.00	1.50	0.41
86	**F-14**	CLC	685241	4060507	0.78	0.83	0.29	0.02	0.15	-0.11	0.65	-0.06	-0.67	0.07	-0.39	-0.24	0.00	1.98	0.40	0.27	-0.61	0.19	0.87	1.57
87	**F-13**	CLC	685292	4059431	0.66	0.73	-0.56	-0.26	0.17	-0.19	0.61	-0.23	-0.08	0.11	-0.31	0.96	1.02	1.23	0.29	0.27	-0.48	0.56	0.52	0.51
88	**F-12**	CLC	684102	4058485	0.92	0.50	2.36	0.28	0.14	-0.59	0.84	0.61	1.66	1.05	0.69	0.07	0.19	0.71	-0.37	0.09	-0.48	-1.12	-0.15	-0.01
89	**F-11**	CLC	683750	4057461	-0.26	-0.03	-1.16	0.55	0.28	-0.08	0.33	-0.54	0.02	-0.45	-0.49	0.07	0.70	1.71	0.35	-0.38	0.09	-0.06	-0.34	0.18
90	**F-10**	CLC	684523	4057009	-0.43	-0.34	0.29	0.14	0.47	0.15	0.28	-0.90	0.09	-0.53	-0.42	0.40	-0.68	0.14	1.10	0.35	-0.18	1.36	0.32	0.95
91	**F-9**	CLC	685095	4058061	0.39	-0.06	-0.37	0.84	0.13	0.21	-0.24	0.31	-0.28	-0.08	-0.05	-0.09	0.37	0.89	0.12	-0.30	0.22	0.15	0.24	0.29
92	**F-8**	CLC	686399	4058994	1.18	0.83	-0.56	0.00	0.26	-0.13	0.36	-0.12	0.07	0.32	-0.10	0.55	1.94	0.35	0.25	0.29	-0.42	0.37	0.15	-0.36
93	**F-7**	CLC	686293	4060059	0.77	0.75	0.29	0.31	0.16	-0.14	0.49	-0.08	-0.01	0.27	-0.23	-0.09	1.18	0.26	1.05	-0.19	-0.50	0.37	0.28	0.10
94	**F-6**	CLC	686644	4058081	1.96	0.17	0.54	1.91	0.26	-0.34	0.30	-0.31	1.37	0.69	0.15	0.45	0.63	0.12	2.13	0.23	-0.33	-0.09	0.25	1.37
95	**F-5**	CLC	687413	4059172	0.90	0.64	0.29	0.26	-0.52	0.20	-0.41	0.98	-0.26	0.33	-0.28	-0.64	1.28	0.14	-0.68	-1.18	0.09	0.79	0.87	0.10
96	**F-4**	CLC	688268	4057693	2.73	-0.32	0.29	0.19	-0.39	-1.08	-0.07	0.14	0.62	1.46	1.20	-0.42	-0.49	0.24	1.02	0.37	-0.72	-0.59	0.92	-0.05
97	**F-3**	CLC	688386	4056817	1.67	-1.02	-0.07	0.72	-0.30	-0.53	-0.24	-0.49	0.26	0.92	0.09	0.04	0.55	1.84	0.42	-0.01	-0.30	0.33	1.89	-0.59
98	**F-2**	CLC	688363	4056177	2.14	-2.01	0.78	1.85	-0.64	-1.12	-0.52	-0.71	-0.54	0.43	0.30	0.58	-1.26	1.03	2.34	0.24	-0.67	-0.31	0.65	1.26
99	**F-1**	CLC	687939	4055601	1.97	-1.84	2.24	2.00	-0.55	-1.06	-0.57	-0.76	0.27	0.67	0.40	1.27	-0.78	0.76	2.24	0.37	-0.58	0.19	0.89	1.93